Doctoral Dissertation

# Development of a molecular reel for mechanical manipulation of single-molecule DNA

(DNA を巻き取る「分子リール」の開発：DNA の曲げを操る新手法)

Huijuan You

September 2012

Graduate School of Engineering,
Osaka University

工研15-948

Doctoral Dissertation

# Development of a molecular reel for mechanical manipulation of single-molecule DNA

(DNA を巻き取る「分子リール」の開発: DNA の曲げを操る新手法)

Huijuan You

September 2012

Graduate School of Engineering,
Osaka University

# Table of Contents

## Abbreviations

| | |
|---|---|
| AFM | atom force microscopy |
| ATP | adenosine 5'-triphosphate |
| BM(PEG)2 | 1,8-bismaleimido-diethyleneglycol |
| BSA | albumin bovine serum |
| DIG | digoxigenin |
| DIG-11-dUTP | digoxigenin-3-O-methylcarbonyl-ε-aminocaproyl-[5-(3-aminoallyl)-2-deoxy-uridine-5'-triphosphate] |
| dsDNA | double stranded deoxyribonucleic acid |
| DTT | dichiothreitol |
| EM | electron microscopy |
| FJC model | freely-jointed chain model |
| fps | frame per second |
| FRET | Förster resonance energy transfer |
| HPLC | high pressure liquid chromatography |
| KWLC model | kinkable worm-like chain model |
| LDAO | lauryldimethylamine oxide |
| LDH | lactate dehydrogenase |
| LSEC model | linear sub-elastic chain model |
| MOPS | 3-[N-morpholino]propanesulfonic acid |
| NADH | nicotinamide adenine dinucleotide (reduced form) |
| NHS | N-Hydroxysuccinimide-esters |
| Ni-NTA | nichel nitrilotriacetic acid |
| PCR | polymerase chain reaction |
| PK | pyruvate kinase |
| rps | revolutions per second |
| SDS-PAGE | sodium dodecyl sulfate polyacrylamide gel electrophoresis |
| SPDP | succinimidyl 3-(2-pyridyldithio)propionate |
| WLC model | worm-like chain model |

# 1. Chapter 1 Introduction

## 1.1 Overview

The discovery of the double helix structure of DNA by Watson and Crick (1) in 1953 was one of the most important discoveries of the 20$^{th}$ century. This structure elucidated the basic mechanism of how genome information is stored in base pairs and copied in all living cells. In Watson and Crick's structure, two DNA strands are held together by hydrogen bonds and base pair stacking effects. The base pair stacking effects and the electrostatic repulsions between the negatively charged phosphate backbones of DNA lend it unusually high stiffness. Unlike other synthesized or natural polymers such as single-stranded DNA (ssDNA), which are flexible polymers, double-stranded DNA (dsDNA) is resistant to bending, containing over 100 base pairs.

The symmetric and highly regular structure of DNA in crystals is not really seen in DNA in the cell. Inside the cell, the DNA molecule is subject to many different types of mechanical forces: (1) Thermal force: DNA in solution is continually changing conformation due to thermal vibration and collisions with water. (2) Protein-DNA interactions: The interaction between DNA and protein also changes the conformation of the DNA molecule. Mechanical forces cause numerous deformations of DNA including bending, twisting and compression. In fact, DNA deformations control how DNA can be packaged and regulated in the cell.

The mechanical properties of DNA are important for its function inside the cell. Bending stiffness is especially important because many cellular processes such as DNA packaging and transcriptional regulation require tight bending of DNA.

This thesis focuses on the study of DNA bending stiffness in tightly bent conditions. The worm-like chain (WLC) model describes DNA properties in small bending conditions very well. However, the behavior of DNA in tightly bent conditions is still unclear. Several experiments under tight bending conditions suggest the presence of non-harmonic elastic energy. The WLC model suggests that bending energy has classic harmonic potential. One of the goals in this study was to distinguish the models of DNA micromechanics in tightly bent conditions. Another goal was to directly measure the magnitude of force required for bending DNA.

Before introducing this thesis in detail, two points must be mentioned to clarify the discussion.

First, we focus on DNA mechanical properties at equilibrium. The bent DNA structures have static bends, or kinks or dynamic isotropic and anisotropic flexibility. Most experimental methods measure the average conformation of populations of molecules and cannot distinguish between static and dynamic states. If the measurement were carried out slowly, we consider that the system remains in **quasi-static equilibrium**.

Second, particular sequences of DNA molecules have a preferred bend direction (anisotropic bending). For example, an A-tract sequence motif, which contains runs of four or more adenine residues in a row, adopts an intrinsic curve of DNA (2). The intrinsic curve, or permanent bendedness, is a structural property of DNA. In contrast, bendability is a dynamic mechanical property. It is difficult to distinguish bendedness and bendability experimentally; thus, this thesis will simply refer to the bending property as **bendability**.

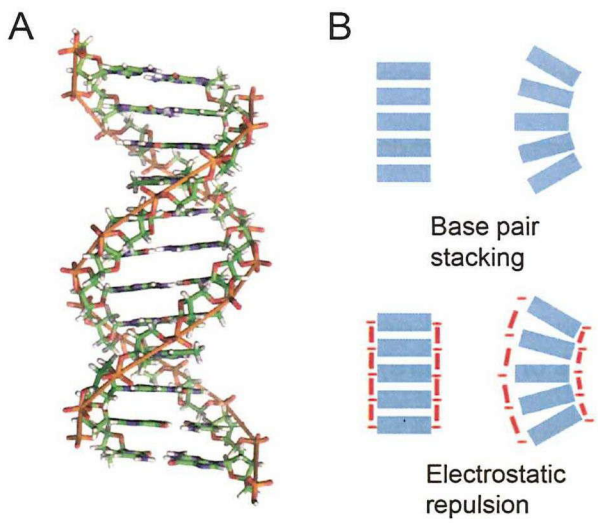


**Figure 1-1 DNA structure.** (A) Double helix structure of DNA. (B) Two interactions contribute to the stiffness of DNA bending. One is base pair stacking effects due to the hydrophobic effects. Bending will increase the exposure of the polar and non-polar surfaces to solvents. The other is the electrostatic repulsion between the negatively charged phosphate backbones.

## 1.2 Polymer mechanics of DNA

Biological polymers such as nucleic acids, actin and microtubes are semi-flexible; at small length scales, the chain behaves as a rigid rod, and at large length scales, the chain appears flexible.

In this section, the classic elasticity theory will be introduced first, since the bending elasticity is important for biological polymers. A simplified slender rod model is used for describing the bending of dsDNA. A slender rod is where the length is much greater than the diameter. The bending of a slender rod is calculated based on **Hooke's law**. Later, the statistic mechanics theory of the polymer, the **worm-like chain model** (WLC model), will be introduced. This model describes the behaviors of polymers in solution undergoing thermal fluctuation.

### 1.2.1 Bending of a slender rod

At small length scales, dsDNA behaves as a rigid rod. In mechanics and material physics, the bending of a slender rod is described by **beam theory** (also known as the elastic curve equation)(3). Suppose we apply a force (*F*) to the free end of a slender rod that is fixed at the other end (**Fig. 1-2**). In the small-angle deflection, the curvature of the bend 1/*R* (*R* is the radius of curvature) will be in proportion to the bending moment, *M*.

$$M = \frac{\kappa}{R} \qquad [1]$$

The bending moment (*M*) equals force (*F*) times the distance ($x$).The constant $\kappa$ is called bending stiffness or flexural rigidity. **Beam equation is an analogue to Hooke's law.**

Beam equation can be used to calculate the shape of a beam. All the information about the shape of the rod is contained in the tangent angle $\theta(s)$. For small angles and arc length, $\frac{1}{R} = \frac{d\theta}{ds} = \frac{d^2y}{dx^2}$, if we know the bending moment at each point, as well as the boundary condition, we can calculate the deflections of a beam and tangent angle θ(s).

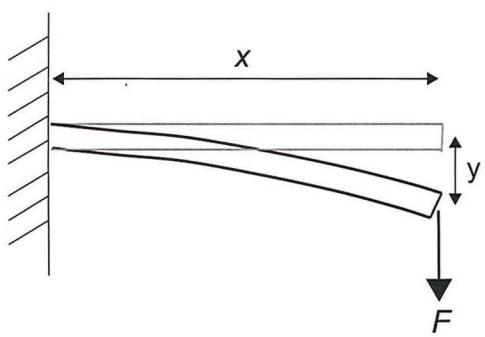


**Figure 1-2 Bending of a cantilevered beam.** For the small angle and arc length, $\frac{d\theta}{ds} = \frac{d^2y}{dx^2} = \frac{1}{R}$, y is the deflection of the beam, *s* is the arc length, and $\theta(s)$ is the tangent angle at each position *s*.

The beam equation can also be used to calculate the **bending energy** of a beam. Consider a slender rod of length *L*, where the shape of the rod is specified by the tangent angle $\theta(s)$ at each position s along the arc length of the rod ($0 < s < L$). Using the beam equation, the bending energy per unit length is calculated as $\frac{dU}{ds} = \frac{1}{2}\kappa(\frac{d\theta}{ds})^2$, where $\kappa$ is the bending stiffness and $\frac{d\theta}{ds} = \frac{1}{R}$ is the curvature of the arc. This equation is analogous to the energy stored in a spring $U = \frac{1}{2}\kappa x^2$, where *k* is the spring constant and *x* is the displacement. The total energy *U* required to bend a segment of DNA of length *L* through an angle θ is expressed as

$$U = \frac{1}{2}\kappa \int_0^L ds\,(\frac{d\theta}{ds})^2 = \frac{k}{2L}\theta^2 \qquad \textbf{[2]}$$

If a rod is of isotropic homogenous material, the bending stiffness can be separated into two terms: $\kappa = EI$. *E* is the Young's modulus, which is a property of material, and *I* is the second moment of inertia of the cross-section. For the bending of DNA, however, the molecular structure is not isotropic. *E* and *I* have not independent significances.

### 1.2.2 The worm-like chain model

At large length scales, dsDNA behaves as a flexible polymer. Like other polymers, DNA resists being straightened because of the thermal fluctuation. The entropic stiffness of DNA is remarkably great. The concept of entropic stiffness was introduced by the freely-jointed chain model (FJC model), which was the first and the simplest mechanical model for polymers. The FJC model was developed independently in the 1930s, by Kuhn, Guth, and Mark (3-5). However, the more recent WLC model is more often used for describing the mechanical properties of DNA. The WLC model was first proposed by

Kratky and Porod (6) in 1949 and first treated numerically by Fixman and Kovac (7) in 1973.

The FJC model treats polymers as a chain composed of *n* statically independent segments of length *b* (Kuhn length) with flexible connection (**Fig. 1-3A**). In an FJC chain, the interaction among the segments can be neglected, thus the orientation of a specific link is **uncorrelated** with the other links.

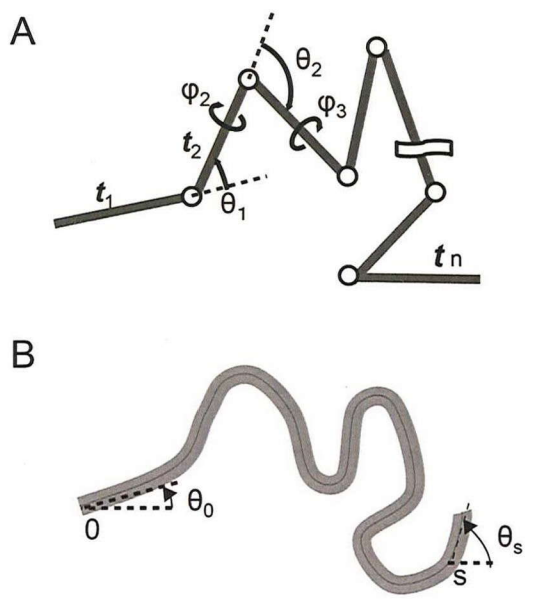


**Figure 1-3 FJC model and WLC model. (A) Freely-jointed chain.** A filament composed of *n* segments of the same length. **(B) Worm-like chain.** A filament in 2 dimensions, the tangent angles at the 2 ends *θ(s)* and *θ(0)* become uncorrelated as the arc length increases. *t*(s) is the tangent vector at point s.

In contrast to the FJC model, the WLC model treats the chain as a continuum elastic rod, by allowing the segment length *b* to go to 0, and the number of segments *n* to infinity (**Fig.1-3B**). The WLC model suggests that the bending of small fragments of the chain obeys Hooke's elasticity. **The orientation correlation function** of a WLC reveals exponential decay (equation [3]). Figure 1-2B depicts the time average of the

cosine of $\theta(s) - \theta(0)$ decreasing exponentially as the arc length s increases. The characteristic distance $L_p$ is **persistence length** which describes the resistance of DNA to thermal bending. Persistence length ($L_p$) is the most important parameter in the WLC model. The stiffer the polymer; the longer the persistence length. If the length of a filament is much greater than the $L_p$, the tangent angle at the two ends *θ(s)* and *θ(0)* will be uncorrelated.

$$\langle cos_{3D}[\theta(s) - \theta(0)]\rangle = \exp(-\frac{s}{L_p}) \qquad [3]$$

From this definition, the **mean-square end-to-end distance** calculated from the WLC is

$$\langle R^2\rangle = 2{L_p}^2\left[\exp\left(-\frac{L_0}{L_p}\right) - 1 + \frac{L_0}{L_p}\right] \qquad [4]$$

When the counter length $L_0$ is much greater than $L_p$, $\langle R^2\rangle = 2L_pL_0$.

Additionally, the **force-extension relationship** can be derived from WLC model. The complete treatment for describe the force-extension relationship of DNA was achieved by Marko and Sigia (8) in 1995 and reported by Bustamante et al (9) in 1994. For more detail description please refer to (3-5). The detail of force-extension curve of WLC model will discussed in Chapter 1.3.2.

***Persistence length and bending stiffness***

**The WLC model assumes that the local bending of a polymer has classical harmonic bending energy.** Using equation [3], $U = \frac{1}{2}\kappa\int_0^L ds\,(\frac{d\theta}{ds})^2 = \frac{k}{2L}\theta^2$, and the equipartition of energy $\langle U\rangle = k_BT$, the orientation correlation function can be derived as

$$\langle cos[\theta(s) - \theta(0)]\rangle = \exp(\frac{k_BTs}{k}) \qquad [5]$$

By comparing with equation [3], we can obtain

$$L_p = \frac{\kappa}{k_B T} \quad [6]$$

**Thus, $L_p$ is directly proportional to the bending stiffness $\kappa$ of the chain $L_p = \frac{\kappa}{k_B T}$** (deviation is shown in Appendix 2). The bending energy of a segment of length *L* bent through angle *θ* can be also expressed as

$$U(\theta) = \frac{L_p k_B T}{2L}\theta^2 \quad [7]$$

## 1.3 Measurements of DNA persistence length

In this chapter, both biochemical bulk measurements and single-molecule stretching experiments for measuring the DNA persistence length will be introduced.

### 1.3.1 Ensemble methods (Bulk assay)

Early studies used various methods to measure the persistence length of dsDNA, including optical methods to monitor the overall conformation of DNA in solution, electron microscopy to observe the image of DNA, and the ligase-mediated cyclization method (**Table 1**). The common point of bulk assays is that they sample large amounts of DNA and analyze the average properties of molecules. Hagerman have reviewed these bulk assays (10).

The bulk assay for measuring the persistence of DNA has several fundamental limitations. First, bulk assays probe the average behavior of many molecules, and rare events such as sharp bending conditions cannot be resolved. Second, the elastic parameters are not directly observed in these measurements. Therefore, although a great deal of mechanical information about DNA is studied using bulk assays, these limitations hinder the further applications of these methods.

**Table 1: Experiments for measuring DNA persistence length**

| Methods | Parameters for determining $L_p$ | Persistence length ($L_p$) | Reference |
|---|---|---|---|
| **Measurements based on the global properties of DNA** | | | |
| -Light scattering | Scattering angle and intensity<br>Rotation diffusion constant $D_{rot}$ | 66 ± 6 nm | D. Jolly et al (11) |
| -Hydrodynamic methods | Sedimentation velocity | 60 ± 10 nm | J.B.Hays(12) |
| | Intrinsic viscosity $\eta$ | 57.5 nm | Kovacic(13) |
| -Transient electric birefringence (TEB) | Rotation diffusion constant $D_{rot}$ | ~60 nm (in 1 mM $Na^+$) | P.J.Hagerman(14) |
| -Transient electric dichroism (TED) | Rotation diffusion constant $D_{rot}$ | | |
| **Measurements based on images of DNA** | | | |
| -Electron microscopy (EM) | $\langle cos\theta \rangle = \exp(-s/2L_p)$ (2D) | 54 ± 5 nm (0.3-0.5 M ammonium acetate) | Bettini and Frontali (15,16) |
| -Atom force microscopy(AFM) | $\langle cos\theta \rangle = \exp(-s/2L_p)$ (2D) | | |
| -Scan force microscopy (SFM) | $\langle cos\theta \rangle = \exp(-s/2L_p)$ (2D) | $L_{p\ (2D)}$ = 106 nm<br>$L_{p\ (3D)}$ = 53 nm | Rivetti (17) |
| **Measurements based on ligase mediated cyclization** | $j_{WLC} \equiv \frac{32\pi^3 {L_p}^3}{N_A {L_0}^6} \exp(-\frac{2\pi L_p}{L_0} + \frac{0.257 L_0}{L_P})$ | $L_p$ = 50.7 nm<br>(Torsional stiffness of DNA $C$ = 2.4~3.0×$10^{-19}$ erg·cm =240~300 pN·$nm^2$) | Shore(18) |

***Measurements based on the overall conformation of DNA***

Several methods including gel analysis, light scattering, hydrodynamic methods, and electro-optics are based on the overall conformation of DNA to calculate its persistence length. Physical properties such as viscosity coefficients and rotational diffusion coefficient which are measured in those methods can provide information about the overall conformation of the chain. In practice, these macromolecule properties of are difficult to measure directly. Therefore, the usual approach is combined with measurement of the molecular weight. From the following equation, the persistence length can be estimated from the mean-squared end-to-end length $\langle R^2 \rangle$ and molecule weight.

$$\langle R^2 \rangle = 2{L_P}^2 \left[ \exp\left( -\frac{L_0}{L_p} \right) - 1 + \frac{L_0}{L_p} \right] \qquad \textbf{[8]}$$

,where $L_0$ is contour length, which relates to the molecule weight.

The methods used in preliminary studies were as follows:

**(1) Rayleigh scattering method**: The quantitative measurement of DNA flexibility was first obtained by measuring the intensity of Rayleigh scattering of DNA in solution. A persistence length of 66 ± 10 nm was estimated (11). Visible light was used because light in this wavelength provides information about the global conformation of DNA ($<R^2>$). Subsequently, the angular dependence of scattering intensity was also used to measure the persistence length. The rotation diffusion coefficient of DNA, $D_{rot}$, was measured and then used to derive the radius of gyration $R_g$ ($R_g = <R^2>^{1/2}$). The persistence length could be calculated from the value of $R_g/L_0$, where $L_0$ is the contour length of DNA (19).

**(2) Hydrodynamic methods** are based on the measurements of intrinsic sedimentation and viscosity coefficient η of DNA molecules in a solution as a function of molecular weight. By fitting results to a relevant theoretical model, a persistence length of 60 ± 10 nm was determined(12). A later measurement obtained a value of 57.5 nm(13).

**(3) Electrooptic methods** such as the transient electric birefringence (TBE) or transient electric dichroism (TED) methods are based on the measurement of the rotational diffusion coefficient $D_{rot}$. In the TBE method, a short electric pulse (several microseconds) introduces optical anisotropy in the sample and gives rise to birefringence. After the field is switched off, the characteristic relaxation time of induced birefringence is measured. By fitting to an appropriate model, this relaxation time can be used to measure the rotational diffusion coefficient and persistence length of DNA. Using this approach an $L_p$ of approximately 50 nm was determined (14). Moreover, by using this method, the $L_p$ was shown to have a weak dependence on monovalent ion concentrations above 1 mM.

***Measurements based on the local image of DNA***

Electron microscopy (EM) and atomic force microscopy (AFM) can produce highly magnified images of DNA molecules on 2-dimensional (2D) substrates. Tracing the contours and using orientation correlation functions, enables estimation of the 2D persistence length of DNA. By using the EM method, Frontali et al (15) reported a persistence length of 54 ± 5 nm.

The assumptions embodied in this approach were that (a) the 2D contour on the grid is obtained by re-equilibration of the contour as the DNA is laid down on the

grid, not by projection of the 3D contour onto the grid. (b) The interactions between DNA and other materials do not influence the intrinsic flexibility of the DNA.

Despite the concerns pointed out above, EM and AFM approaches have several advantages: These approaches analyze individual molecules and allow observation of the behavior of DNA on a small length scale. Recently, Nelson and colleagues demonstrated that high resolution AFM can be used to visualize the curvature of DNA molecules over distances as short as 5 nm (20).

***Measurements based on DNA associating proteins***

DNA associating proteins have also been used to study the mechanical properties of DNA (21). Two methods, ligase-catalyzed cyclization and lac repressor-mediated DNA looping, will be discussed here.

Shore et al (18) carried out ligase-catalyzed cyclization experiments to determine the persistence length of DNA. This method is based on analysis of the ratio of monomeric circles versus linearly-ligated species by native polyacrylamide gel electrophoresis. This ratio is also known as the *j* factor. Determination of the *j* factor as a function of length allows estimation of persistence length. The kinetics scheme of cyclization is proposed in **Figure 1-4A**.

The cyclization reaction converts a linear DNA molecule (L) with cohesive termini into a circular substrate (Sc) for DNA ligase (E). When both E and S are less than $10^{-9}$ M, formation of the ES complex is slow compared to the dissociation rate of the cohesive ends. This condition can be considered a rapid pre-equilibrium condition. The *j* factor is determined as the ratio of the amounts of circular monomers, denoted

by $C(t)$, and linear and circular dimer, denoted by $D(t)$, formed during the early stages of fragment ligation:

$$j = 2\mathrm{M}_0 \lim_{t\to 0} \frac{C(t)}{D(t)} \qquad [9]$$

, where $M_o$ is the initial concentration of the fragments.

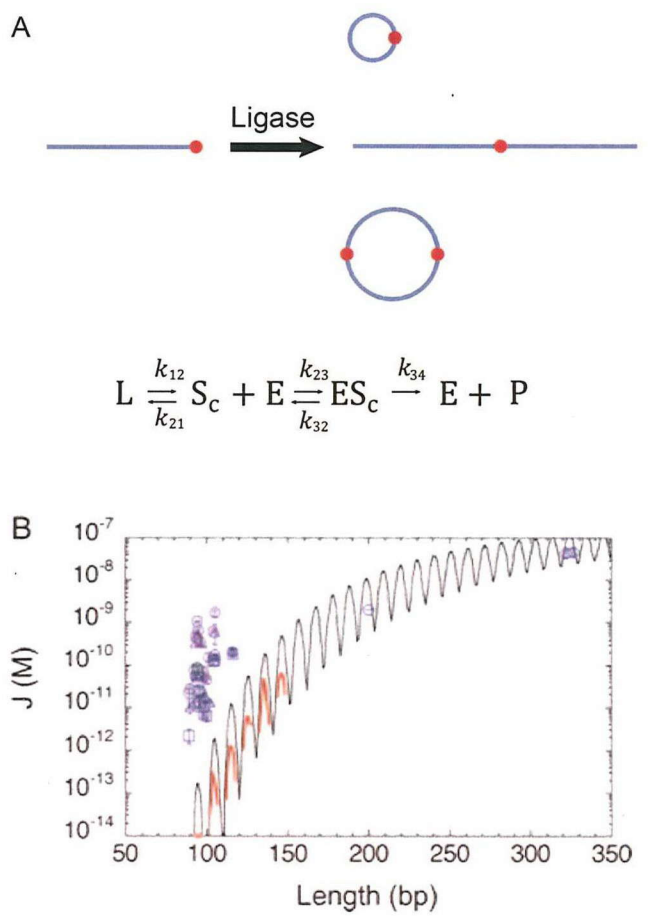


**Figure 1-4** (**A**) Cyclization reaction and the kinetic scheme. (**B**) Cyclization efficiency *j* factor versus DNA length. The black line is the simulation curve predicted from the WLC model with persistence length $L_p$ = 51 nm and torsional stiffness $C = 2.4 \times 10^{-19}$ erg·cm. Under sharp bend conditions, the *j* factor was 3 orders higher than predicted by the WLC model. Figure 1-4B was adapted from reference (22).

The concern that should be addressed in cyclization studies is that the rapid pre-equilibrilium conditions are required. Careful cyclization experiments require that the fraction of each substrate type must be small and of high purity.

The theoretical calculation of the *j* factor treated with the WLC model was presented by Shimida & Yamakawa (23). **Figure 1-4B** illustrates the simulation curve of the *j* factor. The *j* factor oscillates for every ~10 bp of increased length due to DNA torsional inflexibility. Practically, the *j* factor can be separated into the components $j_{WLC}$ and $j_{TW}$. Component $j_{WLC}$ reflects the bending energy of DNA and persistence length can be calculated by using an interpolation formula (equation [10]). This formula yields very accurate results for DNA fragments 150–250 bp in length (24).

$$j_{WLC} \equiv \frac{32\pi^3 {L_p}^3}{N_A {L_0}^6} \exp\left(-\frac{2\pi L_p}{L_0} + \frac{0.257 L_0}{L_P}\right) \qquad [10]$$

Compound $j_{TW}$ reflects the requirement of torsional alignment of the fragment ends for DNA ligation (24). From the $j_{TW}$ value the torsional stiffness of DNA was estimated as 240 pN $nm^2$ (25).

The cyclization experiment provided a powerful tool for the study of DNA elasticity. The cyclization efficiency is sensitive to strong bent conformations. Therefore, this method was applied to analyze the bending stiffness of DNA in sharp bend conditions(26). However, the results remain controversial(27). Details pertaining to this point will be discussed in chapter 1.3.4.

**The Lac repressor-based method** provided not only an *in vitro* method but also an *in vivo* assay to measure the transcription process dependent on DNA flexibility (21). The bending and twisting flexibilities of DNA *in vivo* may be influenced by supercoiling, DNA-binding proteins, and ionic and osmotic conditions. Thus, analyzing how the *in vivo* results differ from the *in vitro* WLC model might help us understand the detail of gene regulation inside the cell.

### 1.3.2 Single-molecule methods

Single-molecule methods have in many cases replaced bulk assays and have become the main methods of DNA mechanics over the past 20 years. Single-molecule techniques allowed the application of force to individual DNA molecules and measurement of the extension (**Table 2**). Using these techniques, the mechanical properties of DNA can be studied directly. More detail about single-molecule stretching DNA experiments is provided in (28,29).

**Table 2: Single-molecule manipulation methods and measurement of the force–extension relationship of DNA**

| Methods | Range of applicable force | Minimum displacement | Reference |
|---|---|---|---|
| Hydrodynamic drag | 0.1~1000 pN | 10 nm | M. Yanagida et al., (30) |
| Magnetic tweezers | 0.01~100 pN | 10 nm | S.B. Smith et al., (31) |
| Optical tweezers | 0.1~100 pN | 1 nm* | S.B. Smith et al., (32) |
| Glass needle | 0~500 pN | 1 nm | Wang et al., Cluzel,P. et al., (33) |
| AFM (atomic force microsopy) | 10~10000 pN | 0.1 nm | (34) |

* Recently, Block's lab reported the sub-nanometer precision of optical tweezers.

The force-extension relationship was first measured by Bustamante and colleagues using magnets and fluid flow (31). They first analyzed the force–extension curve by the FJC model, as it was the only known analytical solution for the force–extension relationship at that time. However, the data deviated greatly from the FJC model and implied that the DNA was locally largely curved (**Fig.1-5**).

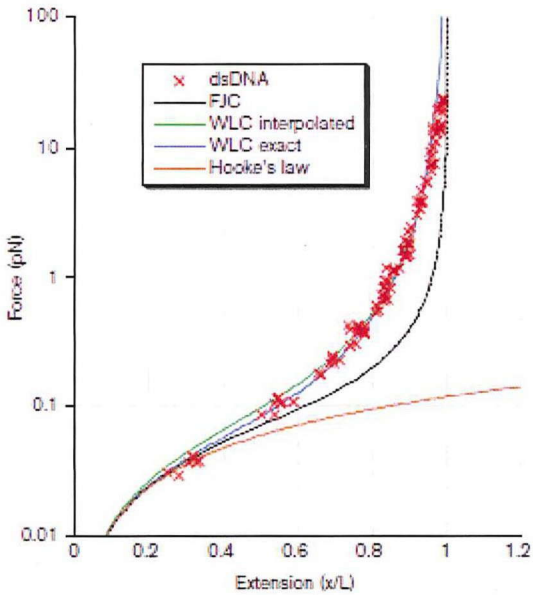


**Figure 1-5 Force–extension curve of dsDNA.** Red crosses are data from λ phage dsDNA (48,502 bp). (Adapted from (20)).

Marko and Sigia presented the first analytical treatment of the force-extension relationship of DNA using the WLC model (8). The approximation formula for the force-extension curve was also the most commonly used (derivation in Appendix 2).

$$F = \left(\frac{k_B T}{L_p}\right)\left[\frac{1}{4\left(1-\frac{z}{L_0}\right)^2} - \frac{1}{4} + \frac{z}{L_0}\right] \qquad \textbf{[11]}$$

In this formula, DNA is treated as an purely entropic chain with fixed contour length. The inextensible WLC model fits data at forces of **up to 10 pN**. Fitting data with high-force regime will lead to a small overestimate in the value of $L_p$.

For stretching forces above 10 pN, the enthalpic extension of DNA will cause the deviation from equation [11]. By introducing a parameter called the elastic modulus, $K_o$, Odijk proposed the modified WLC model combining both entropic and enthalpic theory.

$$z = L_0[1 - \frac{1}{2}\left(\frac{k_B T}{F L_p}\right)^{\frac{1}{2}} + \frac{F}{K_0}] \quad \textbf{[12]}$$

The corrected equation [11] becomes:

$$F = (\frac{k_B T}{L_p})[\frac{1}{4\left(1 - \frac{z}{L_0} + \frac{F}{K_0}\right)^2} - \frac{1}{4} + \frac{z}{L_0} - \frac{F}{K_0}] \quad \textbf{[13]}$$

$K_0$ equals approximately 1000 pN in 150 mM $Na^+$. This formula is applicable at large force regime.

Assuming DNA behaves like a cylindrical rod of homogeneous elasticity, the elastic modulus $K_0$ actually relates to Young's modulus $E$. In the WLC model, $E$ is related to the persistence length $L_p k_B T = EI$. Thus, the quantities $K_0$ and $L_p$ are related through Young's modulus $E$ and the rod diameter $d$.

$$K_0 = \frac{\pi}{4} d^2 E = 16 k_B T L_p d^{-2} \quad \textbf{[14]}$$

The diameter of DNA is 2 nm; $K_0$ is 40 nm; from equation [14], the **intrinsic persistence length** of DNA can be estimated. This value agrees with the value obtained from the entropic elasticity measurements. It means that this idealization model might be a realistic. Even though the persistence length is related to experiment conditions such as ion strength, the intrinsic persistence length yields a lower limit.

Other single-molecule techniques, such as hydrodynamic drag flow, magnetic tweezers, optical tweezers and AFM have been used to stretch single molecule DNA. The results and methods are summarized in the following table.

***Summary***

The persistence length of dsDNA ranges from 50–60 nm in solutions of low ionic strength and decreases to ~45 nm in solutions containing 100 mM $Na^+$ or low concentrations of $Mg^{2+}$ ions.

## 1.4 Mechanics of tightly bent DNA

The experiments introduced in Chapter 1.3, such as free DNA in solution and the force–extension curve, agreed well with the WLC model; however, these experiments could not reveal the micromechanics of tightly bent DNA. Stretching experiments typically measure the ensemble-averaged stiffness over a long DNA strand, in which small fragments may experience many small bending events influenced by thermal energy. As thermal energy supplies only low forces of the order of ~0.1 pN (28), it is rarely possible to induce sharp bending of DNA with a nanometer–range curvature radius in DNA stretch experiments. Therefore, methodology that controls the bending curvature of DNA is required to explore the micromechanics of tightly bent DNA and its physiological role.

The micromechanics of tightly bent DNA are very important for its cellular function and remain unclear. In this section, I will first introduce several examples of tightly bent DNA in the cell and in engineering. Following this, several studies that described the fundamental mechanical features of tightly bent DNA will be introduced. Based on these results, alternative models of DNA bending are proposed. However, none of these experiments produced a final conclusion about tightly bent DNA.

### 1.4.1 The role of tightly bent DNA in the cell

Many significant protein–DNA interactions involve sharp bending and looping of dsDNA with a curvature radius of 2–20 nm (35) (**Fig.1-6**).

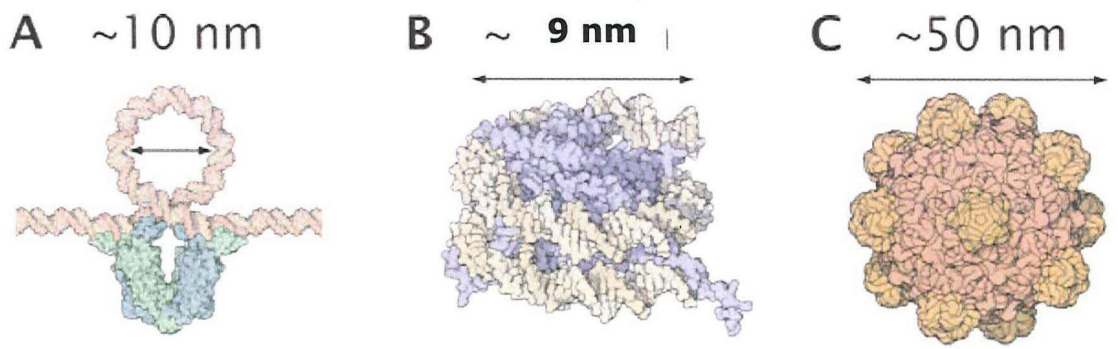


**Figure 1-6 Tightly bent DNA inside cell.** (A) Transcription factor lac repressor-mediated DNA looping, (B) DNA packing in the nucleosome, (C) DNA packing in bacterial viruses. (Modified from et al (35)). The original figure used 8.5 nm for nucleosome. We used 9 nm to represent the curvature diameter of nucleosome DNA. The diameter of nucleosome is about 11 nm and the diameter of DNA is 2 nm.

***-DNA packing in the nucleosome***

In eukaryotic cells, chromosomal DNA is sharply bent and packed in the nucleosome. The nucleosome core consists of four core histone proteins (36) and a 147 bp DNA(37). The DNA is wrapped in 147 bp segments, roughly $1\frac{3}{4}$ times around the histone octamer on this charged ramp (**Fig. 1-6B**). The curvature diameter of DNA wrapped around the histone is only 9 nm, which is much smaller than the persistence length. Simply by invoking equation [7] applicable to circular loops of diameter *D*, the elastic energy is yielded by

$$U = 2L_{\mathrm{p}}k_{\mathrm{B}}\mathrm{T}/D \qquad \textbf{[15]}$$

The energetic cost of bent DNA in the nucleosome can be calculated as 38 $k_{\mathrm{B}}$T. The contacts between positively charged residues on the histones and the negative charges

on the DNA phosphate backbone are considered essential to overcoming this energetic barrier.

It was suggested that the sequence dependence of bending energy might affect the localization of nucleosomes, thus affecting the gene expression (38). Whether a DNA sequence affects its bending stiffness, which influences nucleosome positioning and gene expression, is an important question in biophysics. Several experimental and theoretical studies have attempted to solve this problem; the details will be introduced in Chapter 5.1. However, to answer this question quantitatively, a novel method is still needed for precise measurement of DNA bending energy in tightly bent conditions.

***-DNA packing inside viruses***

DNA packaging in extremely small viral capsids (radius of 15–50 nm) is another example of extensive winding or bending of DNA (39). Since the genome DNA of viruses typically has a length in excess of 10 μm, DNA must be tightly bent to fit inside a small protein capsid.

The packaging of DNA inside a virus is supplied by portal motors that consume ATP. The force generated by the motor of bacteriophage ϕ29 has been directly measured using optical tweezers to pull the end of the DNA as it was packaged, and the value obtained was 57 pN (40).

Calculating the bending energy of tightly bent DNA and analyzing the force required to bend DNA tightly is important for understanding how DNA packing motor function. Considering only the bending energy, inserting a DNA segment of length $L$ into a capsid, will require a force of:

$$F = \frac{2\kappa}{D^2} = \frac{2L_p k_B T}{D^2} \quad [16]$$

At R = 3 nm, a force of 12 pN is required. This is a high force; therefore, a strong molecular motor is required simply to overcome the bending energy of the DNA. In fact, the energy of the DNA compressed within the capsid has two components: the bending energy and DNA–DNA repulsive interaction. This can explain why motor proteins generate forces ~50 pN.

***-DNA bending in transcriptional regulation***

Transcriptional regulation of gene expression is carried out by a variety of DNA-associating proteins known as transcription factors. Many transcription factors that mediate transcriptional control bind at two sites on the DNA simultaneously, looping the intervening DNA. For example, lactose repressor protein modulates transcription of the *Escherichia coli* lactose operon by looping DNA in a ~8 nm diameter loop. Garcia et al summarized some of the best known examples of transcription regulation involving DNA looping (35) (**Table 3**). In most cases, the relevant loops have lengths that are comparable to or smaller than the persistence length. This bending or looping of DNA plays an important role in the regulation of gene expression.

Measuring of the free energy of DNA loop formation *in vitro* is necessary for understanding DNA looping *in vivo*. The free energy of loop formation has been measured by single-molecule methods such as tethered particle motion (41). However, in these approaches, the free energy reflects not only the mechanical properties of DNA, but also the effect of protein flexibility and the binding energy exerted by protein. A new method capable of generating tightly bent DNA without DNA-associating proteins is required.

**Table 3 DNA looping in transcriptional regulation.**

| Molecule or locus | Mode of action | Wild type loop lengths (bp) |
|---|---|---|
| Lac repressor | Repression | 92, 401 |
| AraC | Repression and activation | 210 |
| Gal repressor | Repression | 115 |
| Deo repressor | Repression | 270, 599, 869 |
| Nag repressor | Repression | 93 |
| NtrC | Activation | 110–140 |
| λ repressor | Repression and activation | ~2400 |
| XylR | Activation | ~150 |
| PapI | Activation | ~100 |
| β-globin locus | Activation | 40,000–60,000 |
| RXR | Activation | 30–500 |
| SpGCF1 | Activation, domain intercommunication | 50–2500 |
| HSTF | Activation | 23 |
| P53 | Repression and activation | 50–3000 |
| Sp1 | Activation | ~1800 |
| c-Myb and C/EBP | Activation | ~80 |

* Adapted from reference (35).

### 1.4.2 Tightly bent DNA in engineering

Measurement of DNA bending stiffness is also important for designing of DNA–based nano-devices. The DNA molecule has become a popular material in nano-engineering. DNA has been used as self-assembling materials (42), actuators (43), and even programmable motors (44).

An important issue in nano-engineering is mechanical control of nano-meter scale devices. The distinct mechanical properties of single and double DNA strands can be utilized for this purpose. The elastic energy of a dsDNA molecule wound into a circle

is approximately 50 times higher than that of ssDNA. Simply annealing complement ssDNA, allows active mechanical control of nano-devices.

The **DNA spring** is one of such device. **Figure1-7** depicts the DNA spring using the elastic energy of bent dsDNA to exert tension on enzyme molecules and modulate catalytic activity (45). However, the lack of quantitative information regarding the mechanics of DNA molecules under high bending forces limits the application of dsDNA as a molecular spring in nano-engineering.

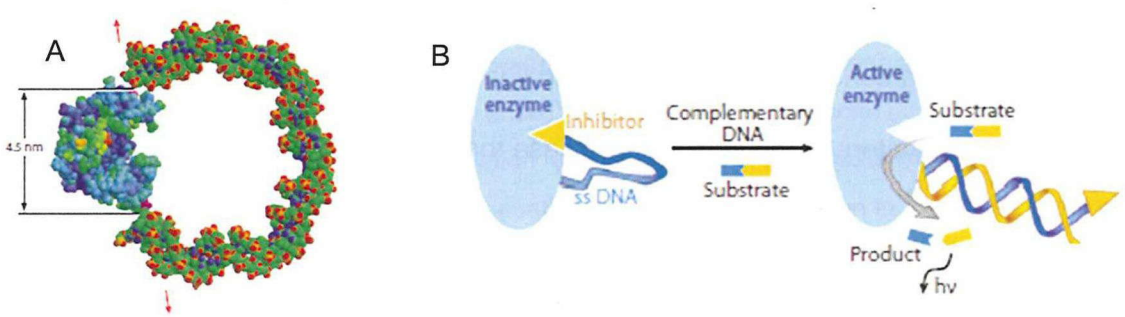


**Figure 1-7 DNA spring** (A). Mechanical control of the enzyme guanylate kinase by the DNA spring. The distance between the attachment points of the DNA spring on the protein is 4.5 nm. In the double-stranded form, the DNA spring exerts a stress on the protein that tends to pull the attachment points apart. (B). Hybridization of the complementary strand to the DNA arm stiffens the molecular spring, which removes the inhibitor from the active site, activating the enzyme. (Adapted from reference (45)).

### 1.4.3 Previous measurements in tightly bent conditions

As introduced in Chapter 1.3, all previous measurements were based on the thermal bending of DNA, for which the tightly bent conformation is energetically unfavorable.

The Ligase-mediated cyclization method overcomes this difficulty by circular ligation of short dsDNA to synthesize a sharply bent DNA loop. Recently, a short 94bp DNA fragment was reported to have demonstrated unexpectedly higher flexibility than predicted by the WLC model (26). The cyclization efficiency, *j* factor, measured in this

study was several orders higher than predicted by the WLC model (**Fig 1-4B**). However, Vologodskii and colleagues claim that the cyclization of the short DNA fragment agreed with the WLC model, but with a smaller persistence length ($L_p$ = 47 nm) than that found in other experiments ($L_p$ = 53 nm) (22). It seems plausible that the WLC model fails to explain several results (20,22,26). Further investigation into this issue is still necessary.

Moreover, as introduced in Chapter1.3.2, this method is not at equilibrium condition, and cyclization efficiency could be enhanced by the ligase binding and the chemical potential of ATP hydrolysis. In addition, the rapid pre-equilibrium conditions require low starting concentrations of DNA and ligase. Decreasing the size of DNA and increasing the curvature of the loop will decrease the yields of looped DNA.

Another way to overcome this difficulty is by using an AFM image to measure the distribution of dsDNA bending angles directly. By sampling a large amount of bending angles on a small length scale, the rare event of sharp bending can also be observed. By using this approach, Wiggins and colleagues estimated the bending energy of dsDNA on a short length scale (20). They found the number of highly bent segments was much higher than predicted by the WLC model. In principle, EM or AFM methods can be used to detect differences in $L_p$ for various DNA molecule regions. However, this study analyzed the average of a large amount of DNA, thus the deviation of the distribution of the WLC model may have been caused by the sequence deference of flexibility. Moreover, the immobilization of DNA on a surface for AFM imaging may have biased the populations of individual DNA forms.

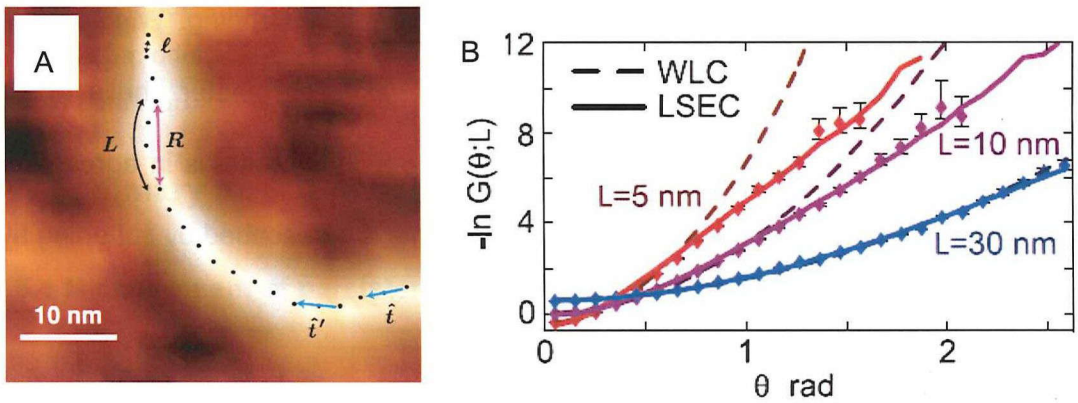


**Figure 1-8 (A)** AFM image of DNA on mica with 12 mM $Mg^{2+}$. **(B)** The chain of points was determined by AFM. The angle distribution $-\ln G(\theta, L)$ is the probability distribution of angles between tangents (blue arrows) separated by $L$. Negative logarithm of the probability distribution function $-\ln G(\theta, L)$ for the angle $\theta$ between tangents separated by contour length $L$, for $L$ = 5 nm (orange), 10 nm (purple) and 30 nm (blue). The dots are experimental data. Solid curves are the Monte Carlo evaluation of this correlation function in a linear sub-elastic chain (LSEC) model. Dashed curves were the Monte Carlo evaluation of the same correlation in the WLC model with persistence length $L_p$ = 54 nm. (Adapted from reference (20)).

### 1.4.4 WLC model vs. nonharmonic model

Previous studies such as ligase-catalyzed cyclization (26) and AFM studies (20) suggested the bending energy in tightly bent conditions is lower than predicted by the WLC model. The WLC model might fail when applying large force to dsDNA at the elastic limit. This is similar to macroscopic materials: beyond the elastic limit, permanent deformation will occur and Hooke's law will fail in high-force regions.

The WLC model suggested a harmonic bending energy function (equation [7]). In contrast, several nonharmonic models were developed to describe the results that differed from the WLC model.

**The kinkable WLC model (KWLC model)**: Several models have been proposed to clarify the high cyclization efficiency of short DNA fragments (**Fig. 1-4**), including a

local melting bubble (46) or kink (47) formation during sharp bending. Wiggins and colleagues characterized the kinking behavior with a single parameter, the average number of kinks per unit length. At low curvatures, the KWLC model is in agreement with the WLC. At high curvatures, cyclization experiments are described by softening by kink formation.

**The linear sub-elastic chain model (LSEC model)**: By observing the 2D image of DNA on a short length scale by AFM, Wiggins and colleagues also showed that it understates the prevalence of large-angle bends (**Fig. 1-8**) (48). The energy potential cannot be clarified by the KWLC model. Thus, they developed the LSEC model to clarify these results (49).

The bending energy of LSEC model is derived as

$$U_{\mathrm{LSEC}}(\theta) = \alpha|\theta|k_{\mathrm{B}}T \qquad [17]$$

The LSEC model also adequately describes force–extension, solution scattering, and long counter length cyclization experiments.

**Figure 1-9** illustrates the energy potential of all three models discussed in this thesis. In Chapter 4, we will analyze our data with these models.

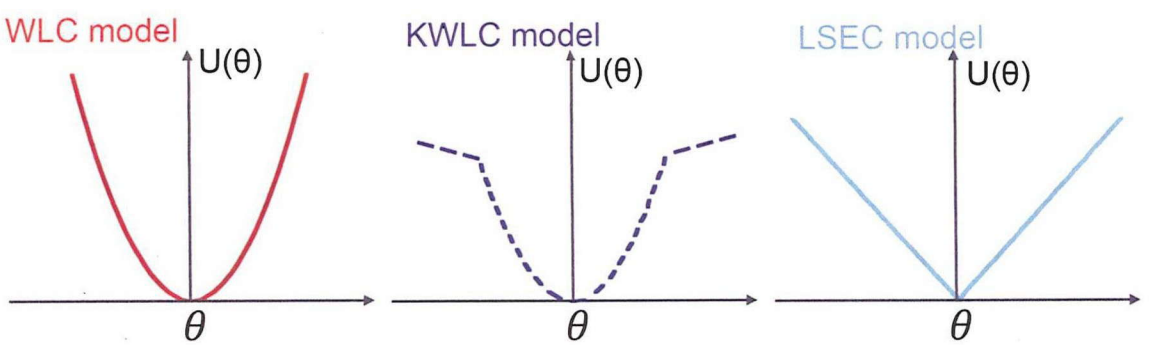

**Figure 1-9 Models for DNA bending energy.** The WLC model has harmonic energy potential. The KWLC model suggests DNA breakage at a critical angle. The LSEC model suggests linear energy potential.

## 1.5 Summary and motivation of this study

### 1.5.1 Measurement of persistence length of tightly bent DNA

The most important issue discussed in this thesis is determining whether the bending energy of tightly bent dsDNA follows the WLC model. Focusing the study on this problem was hindered by the difficulties of generating tightly bent dsDNA. All previous measurements were based on thermal bending. The average force for thermal bending is in the order of 0.1 pN; thus tight bending is a rare event. In ligase-catalyzed cyclization experiments, synthesis of a dsDNA loop less than $L_p$ in circumference is nontrivial because of the formation of such loops is energetically unfavorable. In this study, our goal was to develop a new method to directly generate tightly bent DNA by external force and to measure the persistence length in tightly bent conditions.

### 1.5.2 Measurement of force required to bend DNA

Another issue is that the magnitude of force required to bend DNA is still unknown. Previous study showed that the affinity of a transcription factor (TBP) for its binding site was 300-fold higher (equivalent to a free energy change of 3.4 kcal $mol^{-1}$) when the sequence was pre-bent in the same direction as TBP-induced bending. Many studies have demonstrated that mechanical force can modulate enzyme activities (50). It was reasonable to assume that the tension of looped DNA applied to DNA-associating proteins might modulate the proteins activity. Quantitatively characterization of the magnitude of force is important for revealing the details of the mechanics between DNA and DNA-associating proteins.

A lack of methods to measure the forces inside a nanometer-sized DNA loop is the main problem. Conventional force-measurement technologies such as optical tweezers and AFM are well suited for measuring tensile forces and are also better suited for DNA molecules on a large length scale.

To our knowledge, the only experiment to measure the mechanical force inside a DNA loop was by Shoff and colleagues (51,52). They used a ssDNA as a molecular force sensor, both ends of which were linked to the ends of bent dsDNA (**Fig. 1-10**). The force applied to the ssDNA ends was calibrated by single-molecule Förster resonance energy transfer (FRET). By varying the length of the loop and the proportion of dsDNA, they modulated the internal force from 1 pN to >20 pN. In the smallest loop they measured (57-base DNA), the internal force exceeded the range of force that could be measured by this method. The problem with this method is that the precision of the force determination suffered from the intrinsic noise and nonlinearity of the FRET signal, and the range of force that could be measured was also limited by the small dynamic range of the FRET signal. Additionally, the mismatch between oligonucleotide also made it difficult to determine the shape and actual curvature of the DNA loop.

To overcome the measurement difficulties, we will apply force actively to generate sharply bent DNA. Our solution is to manipulate DNA mechanically by using a small molecular reel (Chapter 4). By winding DNA, we would measure the tensile force instead of the contraction force inside a DNA loop; thus we can use optical tweezers to apply force precisely and over a wide range. The curvature of the wound DNA can also be measured precisely from the position of the trapped bead.

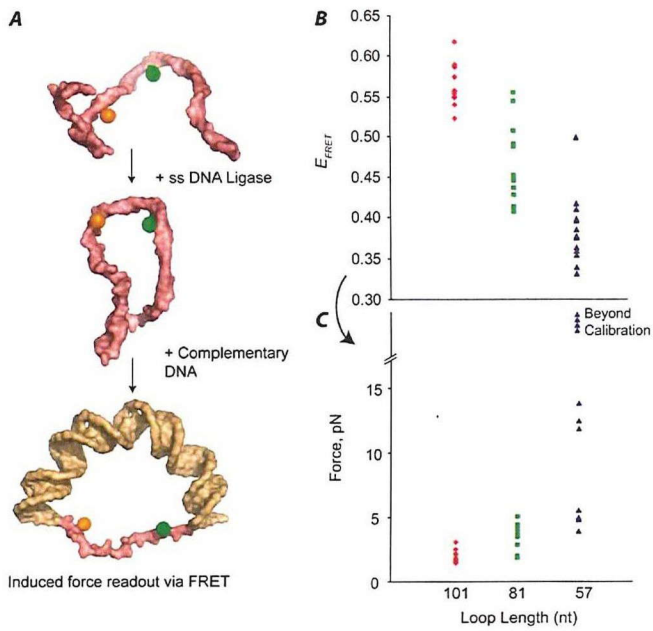


**Figure 1-10 Measurement of mechanical forces inside short DNA loops by FRET** (A) Experimental schematic. ssDNA oligos containing force sensors are circularized with a single-stranded ligase. Variation of internal force is achieved by annealing different lengths of complementary DNA to the loops. (B) FRET for 3 different loop lengths, annealed to a variety of complement lengths. Each point corresponds to a distinct construct. (C) Forces corresponding to the data in B after correction for differences in Ro between constructs. The forces for the indicated 57-mer data points are beyond the upper boundary because the corresponding $E_{FRET}$ values were below the calibration range of the FRET force sensor. (Adapted from reference (52)).

# 2. Chapter 2 Material and methods

Previous mechanical manipulations of DNA molecules were limited to large-scale attempts, such as stretching or twisting dsDNA. In this thesis, I will introduce a novel method to manipulate the local curvature of DNA. The uniqueness of our construction is that the rotary motor protein $F_1$-ATPase was used as a molecular reel to wind dsDNA (**Fig. 2-1** please refer to Chapter 4 for details). This chapter focuses on the construction of the experimental system. First, the rotary motor protein, $F_1$-ATPase, will be introduced. Later, optical tweezers for applying force to DNA will be introduced. Finally, I will introduce the assembly techniques. Both the optical and magnetic tweezers used in our system require the attachment of micron-sized beads to the molecule. The assembly of DNA, $F_1$, and beads on a glass surface is the most difficult part of this construction.

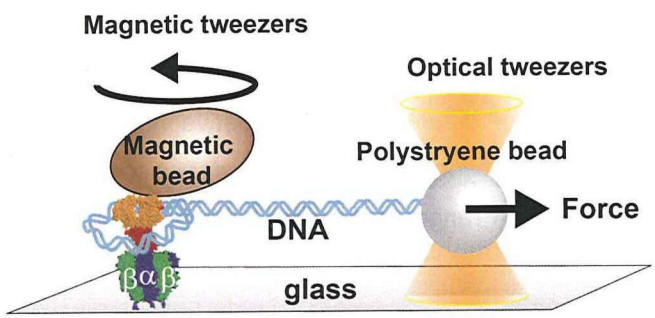


**Figure 2-1 Experimental setup for winding DNA.** One end of the DNA is wound around the rotor of the rotary motor protein $F_1$-ATPase. The other end of the DNA is connected to a polystyrene bead and stretched by optical tweezers. Please refer to Figure 4-1 for details.

## 2.1 Introduction: A molecular reel made of $F_1$-ATPase

### 2.1.1 $F_oF_1$ ATP synthase

$F_oF_1$ ATP synthase is an enzyme that synthesizes ATP from ADP and phosphate by using the energy of a downhill proton flow across the membranes of mitochondria,

chloroplast and bacteria. $F_oF_1$ ATP synthase composes two parts, a membrane embedded portion called $F_o$ and membrane-extrinsic portion called $F_1$. $F_o$ is a rotary motor driven by the proton motive force and $F_1$ is another rotary motor driven by ATP hydrolysis (**Fig. 2-2**). The two motors have a common rotary shaft. In living cells, the proton motive force is generally large, and the $F_o$ motor rotates the common shaft and forcibly rotates $F_1$ to synthase ATP.

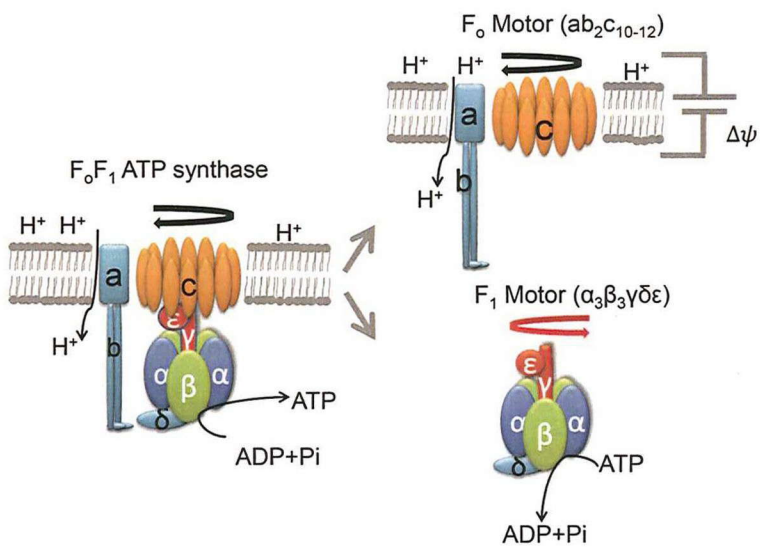


**Figure 2-2 Schematic images of $F_oF_1$ ATP synthase.** ATP synthase composes two rotary motors. $F_o$ (upper right) is embedded in the cell membrane and rotates with the translocation of protons, driven by the proton motive force. The proton motive force is formed by the difference in proton concentration ($\Delta$pH) and membrane potential ($\Delta\psi$) across the membrane. $F_1$ (lower right) rotates with ATP hydrolysis. The subunit composition of bacterial $F_o$ is $ab_2c_{10\text{-}15}$. $F_o$ is embedded in the cell membrane and rotates the c-ring against the $ab_2$ stator, driven by passive proton translocation along the proton electrochemical potential that comprises the proton concentration and membrane voltage across the membrane. Bacterial $F_1$ is composed of $\alpha_3\beta_3\gamma\delta\varepsilon$ and is an ATP-driven rotary motor in which the $\gamma$ subunit rotates against the $\alpha_3\beta_3$ cylinder. The $\varepsilon$ subunit binds to the protruding part of the $\gamma$ subunit. The $\delta$ binds to the bottom of the $\alpha_3\beta_3$ ring.

The first crystal structure of $F_1$-ATPase was determined from bovine mitochondria by Walker and colleagues in 1994 (53). The complex, with the minimum

stability and functionality as an ATPase, is an $\alpha_3\beta_3\gamma$ sub-complex. The crystal structure showed that three α subunits and 3 three subunits are arranged alternately, forming a cylinder $(\alpha\beta)_3$. The central γ subunit forms an asymmetric coiled-coil structure. All α subunits are bound to the ATP analogue AMP-PNP and exhibit near-identical conformation. However, three β subunits have different conformations: The $\beta_E$ (empty) has an open conformation; $\beta_{TP}$ (bound ATP analogue AMP-PNP) and $\beta_{DP}$ (bound ADP) have close conformation. (**Fig.2-3**). The crystal structure supported "binding change mechanism" of ATP synthase proposed by Boyer (54).

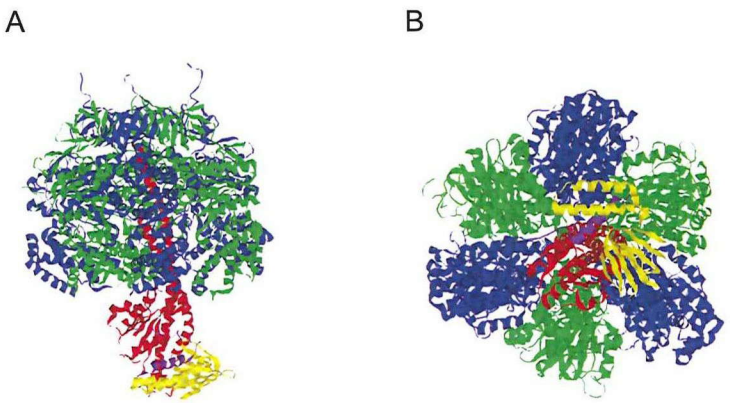


**Figure 2-3. Crystal structure of mitochondrial $F_1$-ATPase.** Side view (A) and top view (B) of $F_1$-ATPase from bovine heart mitochondria (PDB: 1E79) (Blue: α, green: β, red: γ, yellow: δ, purple: ε).

### 2.1.2 Single molecule manipulation of $F_1$ by magnetic tweezers

#### *-Single molecule observation of $F_1$ rotation*

The rotation of the γ subunit in a single $F_1$ was directly visualized by optical microscopy in the laboratories of Yoshida and Kinosita (55). $F_1$ molecules from a thermophilic bacterium (*Bacillus* strain PS3) were fixed on the Ni-nitrilotriacetric acid modified glass surface, and a large marker, a fluorescently labeled actin filament, was attached to the γ

subunit. Instead of an actin filament, latex beads have often be used as rotational probe in recent experiments.

***-Single molecule manipulation of $F_1$ by magnetic tweezers***

Single-molecule techniques not only allow observation of the rotation of $F_1$, but also the direct manipulate $F_1$. Using magnetic tweezers, Hirono-Hara, et al demonstrated that external force can mechanically activate pausing of the $F_1$ motor (56). Later, magnetic tweezers were used to reveal the coupling between gamma rotation and synthesis of ATP (57). Recently, Watanabe and colleagues demonstrated that the catalysis of $F_1$-ATPase substates can by enhanced by mechanical manipulation (58).

**2.1.3 Molecular reel**

Many efforts have been devoted to designing controllable nano-machines to miniaturize macroscopic mechanical devices such as gears, bearings and motors. However, applications for artificial nano-devices are limited due to the lack of force-exerting capabilities and the difficulties in motion control.

As a molecular reel, $F_1$ has an ideal size and good force-exerting capabilities and advantages in manipulation of the rotation on a glass surface. The radius of the central shaft of the $\gamma$ subunit is ~1 nm and that of the $\alpha_3\beta_3$ stator ring is ~5 nm. The $F_1$ motor is powered by ATP hydrolysis and it is easy to manipulate the rotation of $F_1$ with magnetic tweezers.

As a molecular reel, the torsional stiffness of $F_1$ is well characterized. Previous study has shown that the torsional stiffness ($\kappa^{torsion}$) of $F_1$ crosslinked between the rotor and stator is 72 pN·nm/radian (59). The elastic energy ($\kappa^{torsion}\ \theta^2/2$) stored in twisted

streptavidin and $F_1$ was estimated to be 358 $k_BT$ per turn, which was much higher than the elastic energy stored in wound dsDNA (approximately 30 $k_BT$).

## 2.2 Optical tweezers

### 2.2.1 Introduction of optical tweezers

Ashkin and colleagues reported the first 3D optical tweezers or optical trap in 1986 (60). Optical tweezers use a focused laser beam to exert force on dielectric particles such as a glass or polystyrene bead. The particle usually has diameter of 0.5~2 μm. Recently, optical tweezers have become a very powerful tool that is widely used in biology, to manipulate single cells, DNA, or proteins such as single motor proteins. For more details on the recent advanced optical tweezers system, please refer to Block (61) and Bustamante (62).

The full theory of optical tweezers is quite complex. Here, I will illustrate the theory in a simple manner with two cases(63).

1. When the dimension of the dielectric particle is much larger than the wave length of light ($d \gg \lambda$), the particle acts as a positive lens and refracts light. The interaction of the radiation can be described using simple ray optics (**Fig. 2-4A**). In the actual case of a Gaussian laser beam, the intensity profile of the laser beam in a plane perpendicular to the direction of propagation is a 2D Gaussian beam.

$$\boldsymbol{F} = -\Delta\frac{d\boldsymbol{P}}{dt} \qquad \textbf{[18]}$$

, where $d\boldsymbol{P}$ represents the change in momentum.

This equation can be used to calculate the restoring force of optical tweezers by $d\boldsymbol{P}$ from the intensity of light (W). W can be directly measured with a photodetector.

$$F_x = \frac{n_L}{c} \sum W_i \sin\theta_i,\ F_y = \frac{n}{c} \sum W_i (1 - \cos\theta_i) \quad \textbf{[19]}$$

, where c is the speed of light, $\theta$ is the deflection angle, n is the refractive index of liquid and W is the intensity of light.

**2.** When the dimension of the dielectric particle is very small compared to the wavelength of light ($d \ll \lambda$), the particle can be treated as a Rayleigh scatter (**Fig. 2-4B**). The force can be approximated as a dipole that feels a Lorentz force due to the gradient in the electric field. The attraction force toward the focus is

$$\boldsymbol{F} = \frac{\alpha}{2} \nabla \langle \boldsymbol{E}^2 \rangle \quad \textbf{[20]}$$

, where $\alpha$ is the polarizability, $\boldsymbol{E}$ is the electric field. As $\alpha$ is proportional to the particle volume, the force holding the particle in the trap is proportional to the particle size, as well as the beam intensity gradient.

It is difficult to calculate the restoring force of optical tweezers from current theory, since the optical forces are sensitive to small perturbations in geometry. By measuring the changes in light momentum flux based on equation [23], Bustamante's lab developed a method for calculating the trap force. However, the more commonly used method is assuming a linear-spring restoring force and pre-calibration of trap stiffness experimentally. We will introduce the detail of calibration trap stiffness in Chapter 2.2.3.

$$F = \kappa \Delta x$$

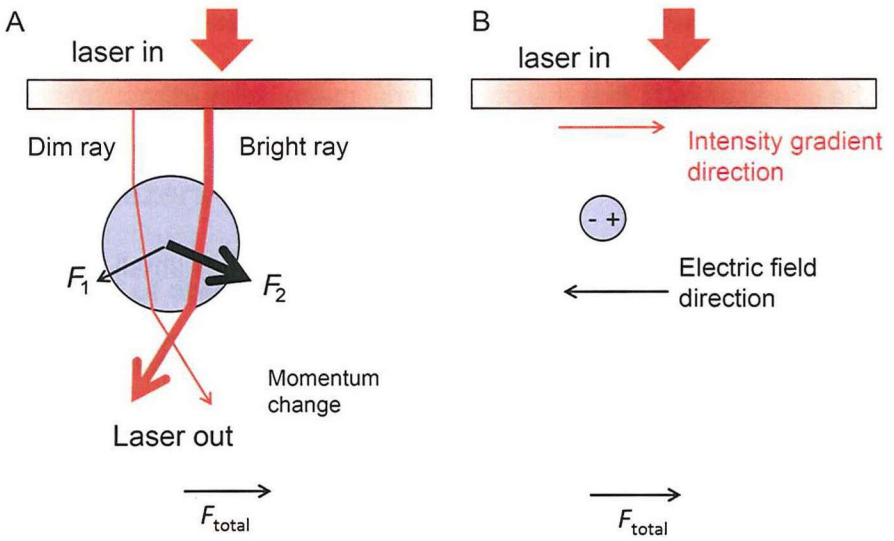


**Figure 2-4 Tapping theory (A) A simple ray optics diagram.** A parallel beam of light with a gradient in intensity shines through a transparent sphere. The brighter ray conveys more force than the dimmer ray. The sum of all rays in the beam tends to pull the sphere towards the right. **(B) Small particles experience a Lorentz force.** Dielectric particles much smaller than the wavelength of light can be considered as perfect dipoles. The gradient in intensity exerts a Lorentz force on the particle directed towards the laser focus.

### 2.2.2 Construction of optical tweezers

Our single-beam gradient optical tweezers consisted of a tightly focused laser beam, a sample manipulating system and an imaging system. The design is illustrated in **Figure 2-5.**

An infrared laser (1047 nm, Nd:YLF, 1 W, IPG Photonics, USA) was used to reduce the photo damage to the sample. A high NA objective lens (PlanSAPO 100×, NA1.3, Olympus, Japan) was used. When the N.A of the lens increased, the dimension of the focal spot decreased and the gradient strength increased. The laser power was controlled by a 1/2 λ waveplate and a polarizing beam splitter. By rotating the 1/2 λ waveplate, the polarization of the input light could be controlled, and some of the laser power can be divert into a beam block with the polarizing beam splitter.

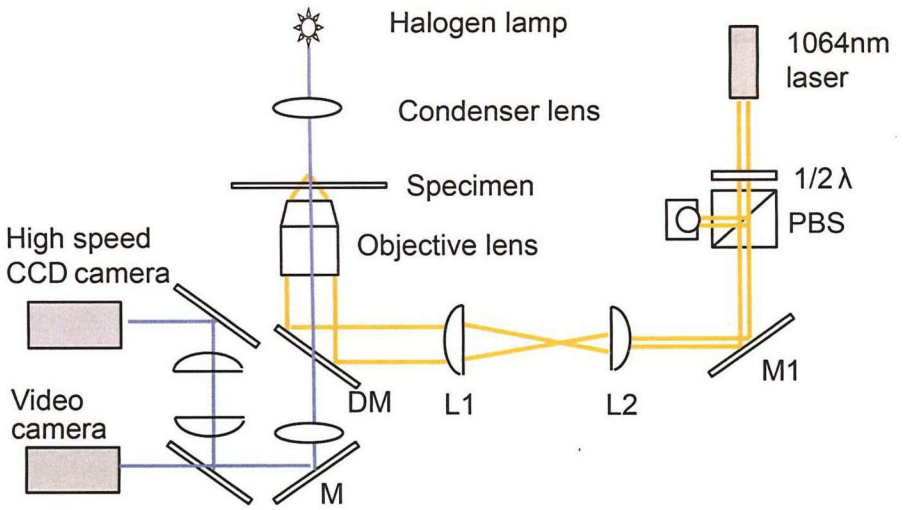


**Figure 2-5 Optics of single-beam optical tweezers.** DM: Dichroic mirror; L: lens; M: mirror; Objective lens, PlanSApo 100×; PBS: polarizing beam splitter.

The manipulation was carried out by translating the sample using a stepping motor controlled stage. The *x*- and *y*- movements of the sample stage were manipulated using stepping motors (SGSP-13ACTR, Sigma Koki, Japan) controlled by custom-made software (ActOperator, Sigma Koki).

The quadrant photodiode (QPD) or position sensitive detector (PSD) was usually used to record the bead position due to the high frequency and nanometer-size precisions required. However, this setup required a high-NA condenser lens to be placed in the back focal plane. It was very difficult to combine this setup with the magnetic tweezers placed above the sample. Thus, a high speed CCD camera was used instead of a QPD or PSD. Bead position was measured as the centroid of the bright field image by Image J (National Institutes of Health, USA) and custom-made plug-ins (K. Adachi, Gakushuin University, Japan).

### 2.2.3 Calibration of optical tweezers stiffness

The easiest method for calibrating the trap stiffness, $\kappa$, is based on the equipartition theorem:

$$\kappa = \frac{k_B T}{\langle x^2 \rangle} \quad \textbf{[21]}$$

, where $k_B T$ is Boltzmann's constant multiplied by the absolute temperature. $\langle x^2 \rangle$ is the standard deviation of the bead position. This method requires accurate distance measurement at high bandwidth. Therefore, a high-speed camera, QPD or PSD is needed.

The other method of stiffness calibration applies a viscous drag force to the trapped bead. The drag force exerted on the trapped bead was calculated using Stokes' law:

$$F = 6\pi\eta r v \quad \textbf{[22]}$$

, where $F$ is the drag force, $\eta$ is the viscosity of water, which is approximately $10^{-3}$ N S/m$^2$, $r$ is the radius of the sphere, and $v$ is the velocity of stage movement. For a 500 nm diameter bead, the drag force at 200 μm/s is approximately 0.9 pN. In our experimental setup, the nearer the trapped bead is to near the coverslip, the higher the drag coefficient increases. The drag force method was performed far from the glass surface where viscous coupling to the glass surface was essentially negligible.

In our study, both these methods were used to calibrate the trap stiffness. First, the position of a bead undergoing thermal Brownian motion around the trap center was captured using a high-speed camera (FASTCAM-1024PCI, Photron, USA) at 27,000 frames/s. Stiffness was determined from the data of bead trapping at 0.5 and 1.0 μm

from the glass surface. The 2 values of the stiffness coincided to within ±10%. The stiffness of the DNA-coated polystyrene bead in BSA buffer and the polystyrene bead in distilled water also coincided to within ±10%. Second, the drag force method was performed using polystyrene beads in distilled water by trapping at a height of 1.0 μm The microscope stage was moved using a stepping motor (SGSP-13ACTR, Sigma Koki) at a speed of 200 μm/sec. Images of the bead were captured at 250 frame/s using the same high-speed camera. The results of both measurements are summarized in **Figure 2-6** where stiffness was plotted against the laser power of the optical tweezers. The linear fit of the data points for the 2 measurements coincided to within ±5%.

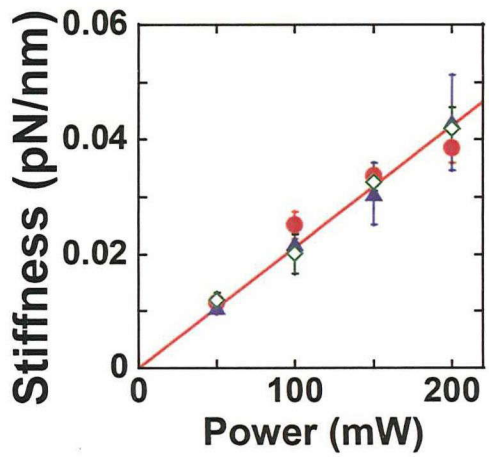


**Figure 2-6 Optical tweezers stiffness versus laser power**. The trap stiffness of a 0.5-μm polystyrene bead coated with 8.7-kbp dsDNA was measured using the Brownian motion method at h = 0.5 μm (h: height from the glass surface, red circles) and at h = 1.0 μm (green rhombuses), respectively. The trap stiffness of a 0.5-μm polystyrene bead was also measured using the drag force method at h = 1.0 μm (blue triangles). Laser power was measured before the objective lens. Slopes of the linear fitting for 3 different methods coincided to within ±5%. The red line represents the linear fitting of the data shown by the red circles (Brownian motion method, h = 0.5 μm). This line was used to determine the trap stiffness in the winding and stretching experiments.

## 2.3 Assembly of $F_1$, DNA, and beads

In this section, a general introduction about bioconjugation techniques of proteins and DNA, including covalent methods and non-covalent methods, will be stretched. Later, the assembly process for $F_1$-DNA-beads construction on a glass surface will be introduced.

### 2.3.1 Introduction of bioconjugation methods

***-Covalent conjugation methods***

Covalent methods can be used to directly crosslink proteins and DNA or to label a special group among the target molecules. A crosslinking or labeling reaction depends on the availability of particular chemicals that are capable of reacting with the specific groups existing in proteins or DNA. Many commercial crosslinkers are available for linking specific functional groups (64).

**Proteins**

All proteins comprise 20 amino acids; thus only 4 functional groups in proteins are commonly used in a crosslinking reaction. There are primary amine groups (-NH2), carboxyl groups (-COOH), sulfhydryl groups (-SH) and carbonyl groups (-CHO). Most common used crosslinkers react with these groups (**Fig. 2-7**). Primary amine groups exist at the N-terminus of each polypeptide chain and in the side chain of lysine and arginine residues. Carboxyl groups exist at the C-terminus of each polypeptide chain and the side chains of aspartic acid and glutamic acid. Sulfhydryl groups exist in the side chain of cysteine. Carbonyl groups can be created by oxidizing carbohydrate groups in glycoproteins. Amine groups and carboxylate groups are widely used for non-specific modifying proteins, because one protein contains many amine and

carboxylate groups. The cysteine residue is the most commonly used target for special labeling of an amino acid, because the number of cysteine residues in wild-type proteins is limited and those residues are usually in oxidized form (S–S).

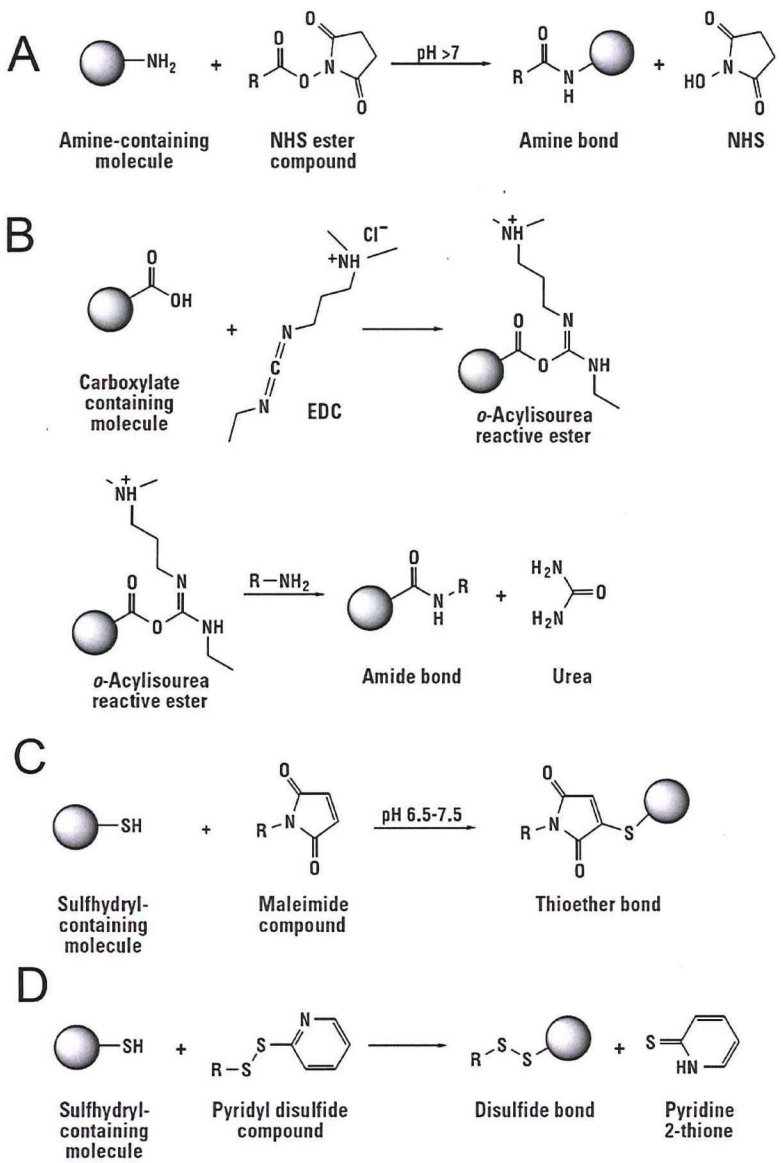


**Figure 2-7 Most commonly used reaction schemes for modifying proteins.** (A) Amine and NHS-ester reaction. (B) EDC coupling reaction. (**C**) Sulfhydryl and maleimide reaction. (D) Sulfhydryl and pyridyl disulfide reaction. Modified form Crosslinking Reagents Technical Handbook, Thermo Scientific Pierce.

The following should be considered for crosslink reaction: (1) Micromolar concentrations of proteins and DNA are required. (2) A proper molar ratio is required. (3) Proper pH conditions are required as the reaction generally takes place in water solution. (4) Accessibility of the crosslink reagent to the specific target is important. (5) If amine or carboxylase groups are used as reaction targets, the excess reagent should be removed or typical blocking reagents used to preserve the activity of the proteins. (6) The activity of nucleophilic reactions for those residues is $R\text{-}S^- > R\text{-}NH^2 > R\text{-}COO^- = R\text{-}O^-$.

To specifically label proteins *in vivo*, special amino acid sequences such as SNAP-tag, CLIP-tag, GST tag or avi-tag are introduced to the target protein (65). These tags can be recognized by enzyme *in vivo* or *in vitro* and be labeled specifically. They might also be used in single-molecule experiments.

**Nucleotide**

The targets of nucleotide modification could be the sugar portion, the base residues, or the 5' phosphate groups. In this thesis, the end of the dsDNA to wind was specifically labeled by digoxigenin (DIG).

At least 3 methods were used to introduce the special group at the end of the DNA:

**PCR methods using 5' labeled primers:** Using different 5' labeled primers (**Fig 2-8A**) (oligonucleotides) in PCR reaction, it was easy to introduce digoxigenin, biotin, thiol or other groups to the end of long dsDNA. Many commercial labeled primers are available. This method can be applied to DNA lengths ranging from 200 bp to 30 kbp. For long DNA, the yield is limited by the polymerase activities.

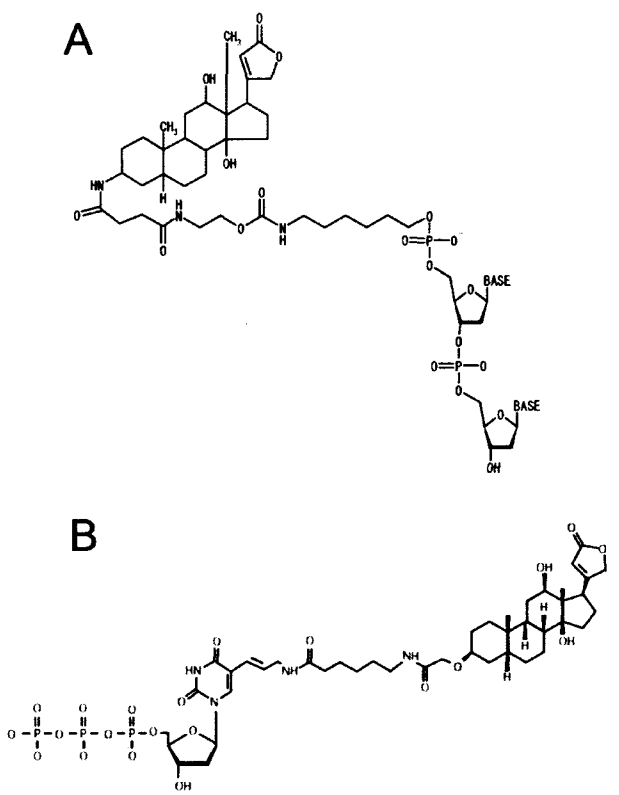


**Figure 2-8 Modifying a nucleotide with digoxigenin.** A. 5' Digoxigenin labeled oligonucleotide (Sigma). B. Dig-11-dUTP, (Roche # 11 093 088 910)

**3' Labeling of DNA using T4 DNA polymerase:** T4 DNA polymerase has 3' → 5' exonuclease activity in the absence of dNTP and polymerase activity in the presence of dNTP. By utilizing these properties, DNA can be labeled with two steps reaction. First, DNA is incubated with T4 DNA polymerase alone. The 3' base will be removed. Second, digoxigenin-11-dUTP (**Fig 2-8B**) is added into the reaction mix. Then, the 3' thymine will be replaced by digoxigenin-11-dUTP. This method can introduce multiple labels in one DNA molecule and can be applied to various lengths of linear DNA. The number of digoxigenin introduced to the end of the DNA depends on the reaction time and enzyme concentration. By using dATP dCTP and dGTP instead of a dNTP mixture, it is also possible to introduce a single label at the 3' end to replace the

first thymine with digoxigenin-11-dUTP. with this method, both 3' ends of one DNA molecule are labeled with the same group.

**Ligation of labeled fragments with unlabeled central fragment**: The labeled short fragments can be generated by PCR using digoxigenin-11-dUTP or by using a complementary oligonucleotide with 5' labeled digoxigenin. For bacteriophage λ DNA (48,502 bp), the 12-base sticky end can be used for labeling.

***-Non-covalent conjugation methods***

Non-covalent conjugation by small ligands and protein receptors such as the antibody and antigen connection (Dig and anti-dig), avidin and biotin system, and His-tag and Ni-NTA interaction has been widely used. Non-covalent conjugation methods are very highly efficient and specific even when substrate concentrations are very low. Moreover, the binding affinity is not sensitive to buffer conditions. Therefore, **non-covalent conjugation methods were used for assembly of the target complex under microscopy in this study.**

**The biotin and avidin system** is the most useful ligand interaction. The extraordinary affinity of avidin for biotin (dissociation constant $K_d$ = $10^{-15}$ M) is the strongest known non-covalent interaction of a protein and ligand. Biotin, also known as vitamin $B_7$, is a small molecule (MW = 244.3) that is present in all living cells. Avidin is a tetrameric protein. The labeling of protein or DNA with biotin, also called biotinylation, is used as an important laboratory technique. Many commercial biotinylation chemical compounds are available.

**Digoxigenin and anti-digoxigenin antibody system:** Digoxigenin (DIG) is a hapten, a small molecule with high immunogenicity. Digoxigenin is found exclusively in

only a few plants cells in nature, so it is usually introduced chemically into a biomolecule. The dissociation constant of antibody for DIG depends on the antibody, but is usually around several nano-molars.

**Ni-NTA and $His_6$ system**: His-tag or polyhistidine-tag is an amino acid motif in protein that consists of at least 5 histidines. His-tag is widely used in the purification of proteins. The dissociation constant of single NTA to His-tag has been determined as 3 ± 1 μM. In single-molecule observation of $F_1$ rotation, His-tag is used to immobilize $F_1$ proteins. However, a high concentration of free $Ni^{2+}$ ions reduced the enzyme activity (our data, not shown here) and the release of $Ni^{2+}$ ions will cause the dissociation of protein to an NTA labeled surface.

In contrast with the covalent bonds that usually cannot break, non-covalent bonds are not stable, especially when force is applied. The stability of a non-covalent interaction is important for single-molecule mechanical manipulation. The energy landscapes of receptor-ligand bonds and the dynamic strength of molecular adhesion bonds have been studied by measuring the rupture force at different loading rates by using AFM or optical tweezers. General information about the non-covalent bonds used in this study is summarized in **Table 4.**

The theory about the dynamic properties of non-covalent bonds was described by Bell (66)using Kramers' transition state theory. The lifetime of non-covalent bonds exponentially decreases when force is applied:

$$\tau\,(\mathrm{F}) = \tau\,(0) * \exp(-\frac{FIr}{k_{\mathrm{B}}T}) \qquad \textbf{[23]}$$

, where *F* is applied force, *lr* is the effective bond length and $\tau(F)$ is the lifetime at the given force. $\tau(0) = {k_{off}}^{-1}$. Another important conclusion from this model is that the distribution of rupture forces depends on the loading rate. **Figure 2-9** showed one example of the measurement of biotin-stretpavidin strength.

**Table 4 Non-covalent interactions used in single-molecule conjugation**

| | **Biotin-avidin** | **Dig-anti dig** | **Ni-NTA $His_6$-tag** |
|---|---|---|---|
| $K_d$ | $10^{-13}$-$10^{-15}$M | $10^{-7}$-$10^{-11}$ M | $(3 \pm 1)\times 10^{-6}$ M |
| $k_{off}$ | N/A | 0.015 $s^{-1}$, 4.56 $s^{-1}$ | 0.067 $s^{-1}$ |
| Energy barrier width | 0.5 nm, 0.12 nm | 1.15 nm, 0.35 nm | 0.19 nm |
| Lifetime (force) | N/A | 67 s (zero force) | 15 s (zero force)<br>17 ms (150 pN) |
| Unbinding force*<br>(loading rate) | 170 pN (~100 nN/s) | 30 pN (0.1 nN/s)<br>90 pN (63 nN/s) | 150 pN (4.5 nN/s)<br>194 pN (70 nN/s) |
| Reference | (67) | (68) | (69,70) |

***The unbinding force represents the most probable rupture force.**

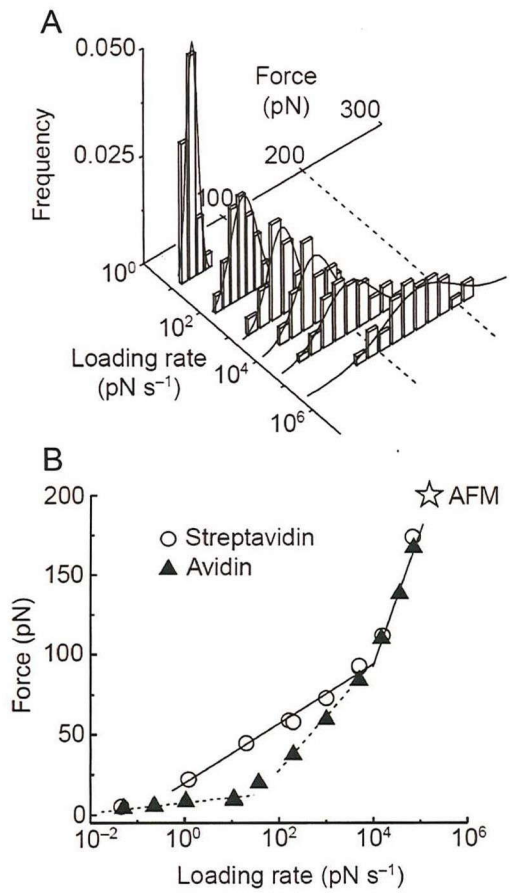


**Figure 2-9 Biotin-streptavidin bond strengths. (**A) Histogram of rupture force of single biotin-streptavidin bond. The peak location shifts to higher forces and increases in width with the rising loading rate. (B) Rupture force *F** plotted against loading rate. (Adapted from reference (67))

### 2.3.2 Crosslink of DNA to $F_1$ by digoxigenin-antibody connection

#### *-Crosslink of $F_1$ to anti-Dig antibody for DNA anchoring*

In our winding experiment, the end of the DNA was connected to the rotor of $F_1$-ATPase (gamma subunit). To anchor of 5' digoxiginin labeled DNA to $F_1$, an anti-digoxigenin Fab fragment was crosslinked to the gamma subunit of $F_1$-ATPase. The amino groups of the Fab fragment were used for both biotinylation and the crosslink reaction. The Fab fragment was activated by the crosslinker SPDP and then reacted with the cysteine residue at the gamma subunit (**Fig. 2-10**). A mutant of the $\alpha_3\beta_3\gamma$ subcomplex of

$F_1$-ATPase from the thermophilic *Bacillus* PS3, $\alpha(His_6$ in N-terminus/C193S$)_3$ $\beta(His_{10}$ in N-terminus$)_3$ $\gamma$(S108C/I211C) was used. The cross-linked product was confirmed by SDS-PAGE (**Fig 2-11**).

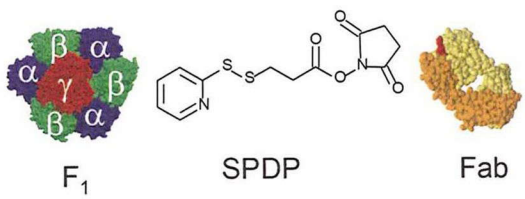


**Figure 2-10** Cross-linking reaction with SPDP

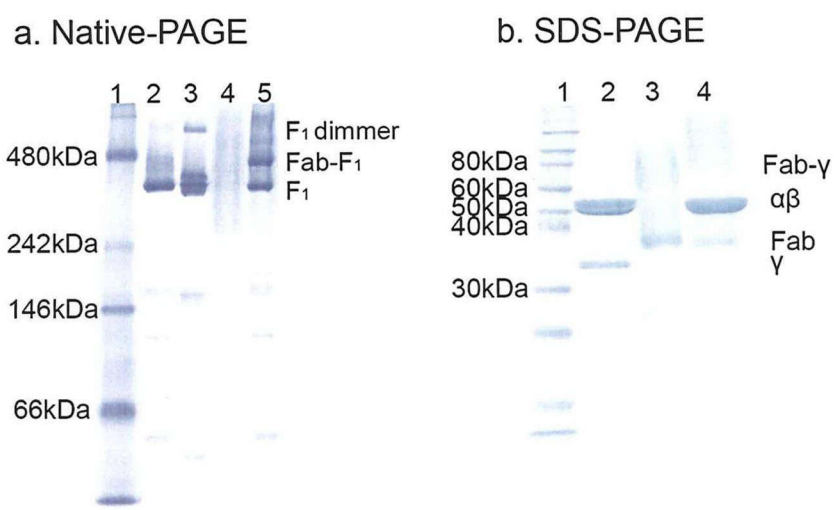


**Figure 2-11** Cross-linking reaction of Fab fragment and $F_1$ analysed by polyacrylamide gel electrophoresis (PAGE).(a) Native-PAGE: Lane 1, marker; Lane 2, $F_1$; Lane 3, oxidized $F_1$ forming a dimer; Lane 4, anti-DIG Fab fragment; Lane 5, anti-DIG Fab-$F_1$ cross-linked sample. (b) SDS-PAGE: Lane 1, maker; Lane 2, purified $F_1$; Lane 3, anti-DIG Fab fragment; Lane 4, anti-DIG Fab-$F_1$ cross-linked sample. SDS-PAGE was conducted under non-reducing conditions to avoid cleavage of the Fab-γ cross-linking.

***-DNA construction***

The 8,688-bp dsDNA was prepared by PCR using Ex-Taq DNA polymerase (TaKaRa, Japan) and the pRA100 plasmid as the template (71). The 5'-biotin primer and the 5'-digoxigenin primer (Sigma Genosys, USA) were used in the PCR reaction. PCR products were purified using the Wizard PCR Clean-Up System (Promega, USA).

Purified DNA (12.5 μg) was incubated with 100 μL streptavidin-coated polystyrene beads (0.5 μm diameter, 1%, Bangs Laboratories, USA) suspension overnight, and unbound DNA was removed by washing several times using buffer (100 mM KPi, pH 7.0). The number of dsDNA strands bound to each bead was $1.7 \times 10^2$.

***-Assembly of magnetic beads, DNA coated beads and $F_1$ on glass.***

The binding efficiency of magnetic beads and DNA coated beads to $F_1$ molecules are very critical for assembly of the experimental constructs. First, we confirmed that even at low $F_1$ molecule density on a glass surface (0.028 molecules per $\mu m^2$), we were able to find rotating magnetic beads which attached on the γ subunit of $F_1$. The density of $F_1$ molecule on glass surface was estimated by using fluorescent labeled $F_1$ (**Fig. 2-12**). Second, the connection of DNA-coated beads to the anti-digoxigenin antibody was confirmed (**Fig. 2-13**). **Table 5** lists the number of Cy3-labeled $F_1$ molecules, magnetic beads and DNA coated bead. The number of $F_1$ molecules was much higher than that of the magnetic beads and DNA coated beads, indicating that the binding efficiency is not high (less than 10%).

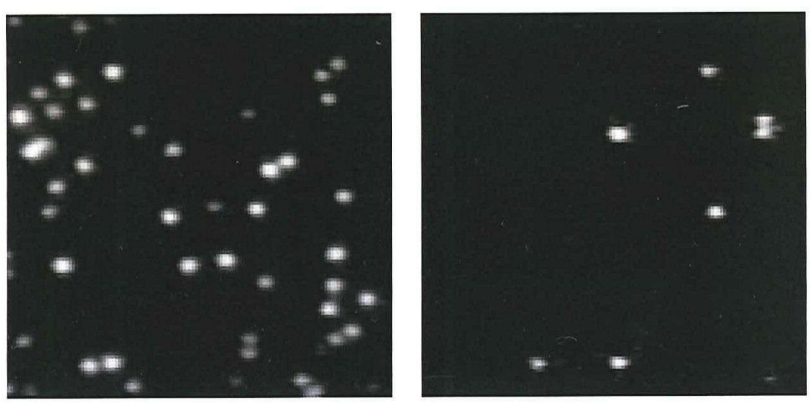

**Figure 2-12 Controlling the density of $F_1$ molecules on a glass surface.** Left : 50 pM $F_1$-Fab (Cy3), Right: 10 pM $F_1$-Fab (Cy3) ROI size 10 um × 10 um. The density of the anti-DIG Fab-$F_1$ complex immobilized on the glass surface was determined using Cy3-labled Fab-$F_1$. When 5 pM Fab-$F_1$ was infused into the flow chamber, the density was 0.028 molecules per $\mu m^2$.

The probability of neighboring Fab-$F_1$ molecules existing within 1 μm from the center of the rotating magnetic bead was 4% based on the Poisson distribution $P = 1\text{-}exp(-\rho\pi r)^2$; $\rho$ is the density of the Fab-$F_1$ complex; $r$ = 1 μm. DNA bead was rarely attached on the surface at the position over 1 μm away from the rotation center of the magnetic bead. Such data was omitted from analysis.

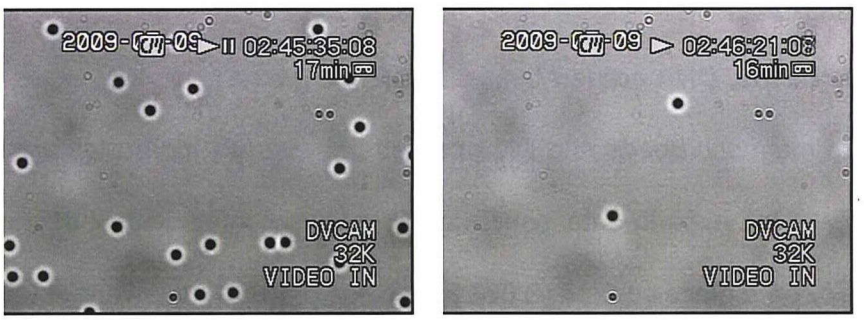


**Figure 2-13 DNA-coated beads can bind to $F_1$-Fab.** 1 nM $F_1$-Fab, 50 pM $F_1$-Fab ROI size 64 μm ×48 μm.

**Table 5 $F_1$ density, and number of rotating beads and DNA-coated beads at different $F_1$ concentrations.**

| $F_1$ concentration | Fab (Cy3)-$F_1$ | Magnetic beads Rotating/attached | DNA coated beads |
|---|---|---|---|
| 10 pM | 258 | 5/28 | 1~2 |
| 100 pM | 750 | 14/136 | 22 |
| 1 nM | N/A | 1/219* | 119 |

ROI size was 64×48μm$^2$. $F_1$ was incubated for 15 min and washed with BSA buffer. Magnetic beads and DNA-coated beads incubated for 1 hour. *At 1nM $F_1$ concentration, almost all magnetic beads were attached to the glass. The low number of rotating beads might due to multiple-binding.

Due to the low binding efficiency, it was extremely difficult to connect 2 beads to the same $F_1$ molecule by diffusion. Therefore, a DNA-coated bead was trapped by optical tweezers and moved close to a rotating magnetic bead to enhance the connection to the specific rotating $F_1$ molecule (**Fig. 2-14**). We examined the enhancement of the DNA-coated beads and found that the attachment probability was

improved (**Fig. 2-15A**). The trapped DNA coated bead could attach to the target $F_1$ molecule 0.8 μm away from the trap center (**Fig. 2-15B**).

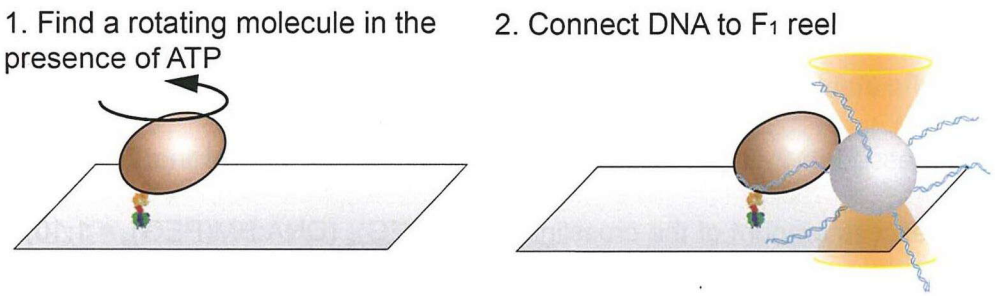


**Figure 2-14 Assembly of magnetic bead and DNA-coated bead to $F_1$**

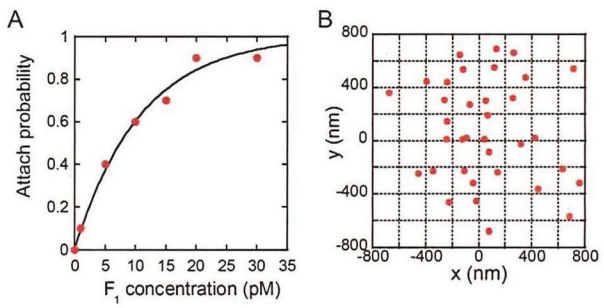


**Figure 2-15 (A) Probability of trapped DNA beads attaching on the glass.** DNA coated beads 6kb were trapped for 1 min. The probability was calculated from 20 trails. **(B) Distance between the trap center and anchor point.** 6kb DNA were used.

### 2.3.3 Crosslink of DNA to $F_1$ by covalent bond

Covalent cross-linking of a DNA handle to protein was used to study the folding and refolding process of RNase H (72). The protocol was presented by Cecconi et al (73). We used the same approach to connect 0.46-kbp, 1.5-kbp, 6.3-kbp, 8.7-kbp DNA to $F_1$ molecules. The connection efficiencies were assessed and the yield was very low for DNA longer than 1.5 kbp. Moreover, the efficiency of finding a rotating $F_1$ molecule was very low. Thus, we did not use this approach in the final construction for winding DNA. I present this method and results here in the event this approach might be used for other purposes.

***-Crosslink of $F_1$ to sulfhydryl modified DNA***

A cysteine mutant of $F_1$ was connect to sulfhydryl-modified DNA by a homobifunctional, maleimide crosslinker $BM(PEO)_2$. A sulfhydryl reacting to the maleimide group results in the formation of a stable thioether linkage. To improve the connection efficiency, this reaction was processed in 2 steps. First, the sulfhydryl modified end of the DNA was modified with an excess amount of the crosslinker, $BM(PEG)_2$ (DNA:$BM(PEG)_2$ = 1:10). As there was excess of crosslinker, the formation of DNA dimmer could be ignored. Then, the free crosslinker was removed by the size exclusion column Nap5. Second, $F_1$ was mixed with the crosslinker-activated DNA. Finally, free $F_1$ was removed by the superpose 6 gel filtration column.

***-Estimation of the crosslink efficiency***

DNA and $F_1$ could be separated by gel filtration using a superpose 6 column. The first peak was DNA and $F_1$-DNA complex and the second was free $F_1$. First, we analyzed the ATPase activity of the DNA fraction. The results showed that the DNA fraction contained $F_1$ molecules. Most probably, it was due to the connection of $F_1$ to DNA. For further confirmation of the connection of $F_1$ and DNA, we also analyzed the DNA fraction by SDS-PAGE and AFM.

**ATPase activity**

The ATPase activity at high ATP concentration (2 mM) of the $F_1$-DNA complex was measured using biochemical assay. Using the ATP hydrolysis rate of $F_1$ measured earlier, the $F_1$ concentration in the DNA fraction could be calculated. If all $F_1$ in the DNA fraction were connected to DNA, the conjugation efficiency of $F_1$ to 0.46-kbp DNA would be estimated as 16%.

## SDS-PAGE

The DNA fraction was analyzed by SDS-PAGE (**Fig. 2-16**). Two bands represent the original DNA and β+DNA complex, respectively. When the density of these two bands was compared, the conjugation efficiency of $F_1$ to 457-bp DNA was measured as 46% (analyzed by ImageJ). SDS-PAGE was stained by CBB protein stain.


**Figure 2-16 $F_1$-DNA conjugation was confirmed by SDS-PAGE.** $F_1$ was conjugated to 457 bp DNA and after HPLC the fraction was analyzed by SDS-PAGE. (a) SDS-PAGE stained by SYBR Safe DNA stain. The DNA fraction displayed 2 bands after HPLC: the bottom band is original DNA and the top band is the DNA+ β complex. When the density of these 2 bands was compared, the conjugation efficiency of $F_1$ to 457-bp DNA was measured as 46% (analyzed by ImageJ). (b) SDS-PAGE stained by CBB protein stain. Lane 1 and lane 4 contain $F_1$ and β monomer which was used as a control. Lane 2 contains the DNA fraction after HPLC and lane 3 contains the $F_1$ fraction. In lane 2, a new band appears which is the DNA+β complex.

## AFM

The DNA fraction was analyzed by AFM image (**Fig. 2-17**). The length and height of the filaments corresponded with the 0.46-kbp DNA molecules. The average height of 74 $F_1$ molecules in the AFM image was 4.55 nm±1.13 nm, while the height of the DNA was <0.5 nm. We counted the total number of $F_1$ and DNA molecules in the AFM image. The conjugation efficiency derived was 7.7% (74 $F_1$ molecules and 691 DNA molecules,).

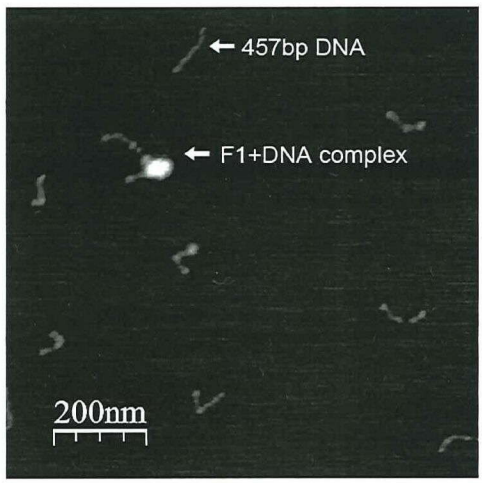


**Figure 2-17 Example of AFM image**. The AFM image show some filaments and spots on the surface. The length and height of the filaments correspond with that of 0.46-kbp DNA molecules. The spots are connected with DNA filaments and the height of the spots corresponds to the $F_1$ molecule (10 nm). In total 74 spots were measured, and the average height of $F_1$ molecules in the AFM image is 4.55 nm $\pm$ 1.13 nm, where the height of DNA is <0.5 nm.

**Table 6: Conjugation efficiency of 0.46-kbp DNA**

| | ATPase | SDS-PAGE | AFM |
|---|---|---|---|
| **[$F_1$]/[DNA]** | 16% | 43% | 7.7% |

The conjugation efficiency of the 3 methods is summarized in **Table 6**. SDS-PAGE analyzed the β-DNA complex, while the AFM and ATPase methods analyzed the $F_1$-DNA complex. After purification, the $F_1$ complex may dissociate into α, β, and γ subunits. Thus, the SDS-PAGE result might be an overestimation of the active $F_1$. The preparation of the AFM sample may cause further dissociation of the $F_1$ complex. Thus, the AFM result might be underestimation of the conjugation efficiency. ATPase activity analysis yielded the correct estimation of conjugation efficiency.

***-Rotation assay of DNA-$F_1$ complex***

Simultaneous observation of DNA by fluorescence image and bead by bright field imaging showed that some DNA and rotating beads were colocalized on the glass

surface, indicating that the DNA and beads connected to the same $F_1$ molecule. For 1.5-kbp DNA, 23 rotating beads were found and in 16 cases, DNA was located in the same position as the rotating beads (about 70%). However, as DNA length increases (6.3 and 8.7-kbp DNA) the frequency of finding rotating beads bound with DNA decreased (**Table 7**). The steric effect of DNA might have reduced the binding of magnetic beads to $F_1$. Furthermore, many beads that had co-localized with DNA did not exhibit rotation. It might also have because of the steric effect of long DNA on bead rotation.

**Table 7 Ratio of rotating beads with DNA on coverglass**

| Ratio | 1.5-kbp DNA | 6.3-kbp DNA | 8.7-kbp DNA |
|---|---|---|---|
| Rotating beads with DNA | 70% (16/23) | 21% (8/39) | 9% (1/11) |

# 3. Chapter 3 Persistence length of DNA measured by stretching experiment

In this chapter, the force–extension curve for single-molecules DNA was measured. The persistence length of DNA at small bending condition was measured based on the fit of force-extension curve. Verification of the experimental system was one purpose of this experiment, since the persistence length was sensitive to buffer conditions such as ion strength and $Mg^{2+}$ concentration. Another purpose was to correct the extension of wound DNA (Chapter 4).

## 3.1 Experimental procedures

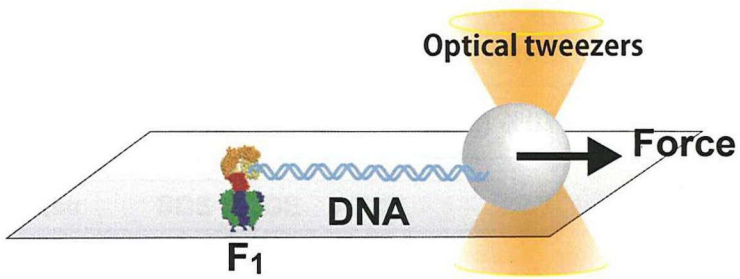


**Figure 3-1** Experimental setup.

The experimental geometry is presented in **Figure 3-1**. One end of the dsDNA was attached to a coverglass through an anti-DIG Fab-$F_1$. The other end was attached to a polystyrene bead trapped in an optical trap. The density of Fab-$F_1$ was controlled by the Fab-$F_1$ concentration. The DNA was subsequently stretched by moving the coverglass with in relation to the trap using a stepping motor-controlled microscope stage. The anchoring point of DNA on the glass was roughly estimated as the center of the Brownian motion of the beads before they were trapped with optical tweezers (precision of ± 0.3 μm). The extension was measured as the distance between the trapped bead and anchoring point, accounting for the movement of the stage. The strain exerted on

the DNA strand was calculated as bead displacement from the trap center times trap stiffness.

## 3.2 Results

### 3.2.1 Fit of force-extension curve with WLC model

As introduced in Chapter 1.3.2, the most commonly used WLC model is equation [11], $F = (\frac{k_B T}{L_p})[\frac{1}{4\left(1-\frac{z}{L_0}\right)^2} - \frac{1}{4} + \frac{z}{L_0}]$. In a low-force regime, force ($F$) grows linearly with extension ($z$) with a slope of $3k_B T/L_p L_0$, whereas in a high force regime, the force diverges as $k_B T/L_p[(1-\frac{z}{L_0})^2]^{-1}$. For moderate extensions, a crossover occurs between these 2 regimes. Comparisons of the force–extension curve with equation [11] have been limited to the low-force regime. Equation [11] correctly describes the experimental data by Smith et al in a 10-mM salt buffer. The interpolation formula is less accurate in the crossover regime. The error is typically of the order of 5%, but will actually depend on the range of extension spanned and the statistical error of each point (31,74).

The force-extension curve obtained by our measurement is shown in **Figure 3-2**. The experimental data points from 0 pN to 5 pN were fitted according to the Marko and Siggia WLC model (equation [11]). The counter length ($L_0$) was set as a constant value of 2950 nm assuming 0.34 nm per base pair. The fitting was sensitive to the noise of the bead positions, which come from Brownian motion. The equilibrium positions of the beads are calculated from time averages of over 2 sec. We obtained a persistence length of 48 nm. This value was consistent with that of a previous study. The black solid

line represents the fitting curve. The dashed line represented the calculated curve with $L_p$ = 38 nm and $L_p$ = 58 nm for comparison.

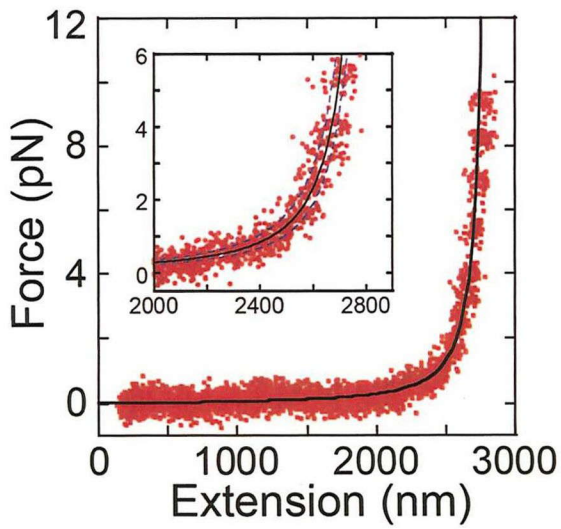


**Figure 3-2 Force-extension curve of 8.7-kbp DNA.** One end of the dsDNA was attached to a coverglass through an anti-DIG Fab-F1. The other end was attached to a polystyrene bead trapped in an optical trap. DNA was stretched by moving the microscope stage. The anchoring point of DNA on the glass was roughly estimated as the center of the Brownian motion of the beads before they were trapped with optical tweezers (precision of ± 0.3 μm). The extension was measured as the distance between the trapped bead and anchoring point, accounting for the movement of the stage. The strain exerted on the DNA strand was calculated as bead displacement from the trap center times trap stiffness. The experimental data points from 0 pN to 5 pN were fitted according to the Marko and Siggia WLC model (equation [11]). The counter length ($L_0$) was set as a constant value of 2950 nm assuming 0.34 nm per base pair. The error in the anchoring point of DNA was also set as a fitting parameter to obtain the best fit with $L_0$. The persistence length for the stretching experiment was determined to be 48 nm. The inset represents the data point from 0.1-6 pN. The black solid line represents the fitting curve. The dashed line represents the calculated curve with $L_p$ = 38 nm and $L_p$ = 58 nm for comparison.

# 4. Chapter 4 Persistence length of DNA measured by winding experiment

## 4.1 Experimental procedures and results

### 4.1.1 Construction of reel system

The designed architecture of the molecular reel is shown in **Fig. 4-1**. An $F_1$ molecule was used as a passive bearing to wind dsDNA. The molecular reel was built using $F_1$, a magnetic bead, and the Fab fragment (radius of ~2.5 nm) of the anti-digoxigenin (DIG) antibody. The anti-DIG antibody was covalently cross-linked to the $\gamma$ subunit of $F_1$ and connected to the magnetic bead through biotin-streptavidin interaction. The complex of the $\gamma$ subunit, anti-DIG Fab fragment, and the magnetic bead acted as a rotor while the $\alpha_3\beta_3$ stator was immobilized on the glass surface. DNA molecules of 8.7 kb labelled with DIG and biotin at distal 5' ends were grabbed through the anti-DIG Fab fragment of the reel and a streptavidin-coated polystyrene bead that was trapped using optical tweezers.

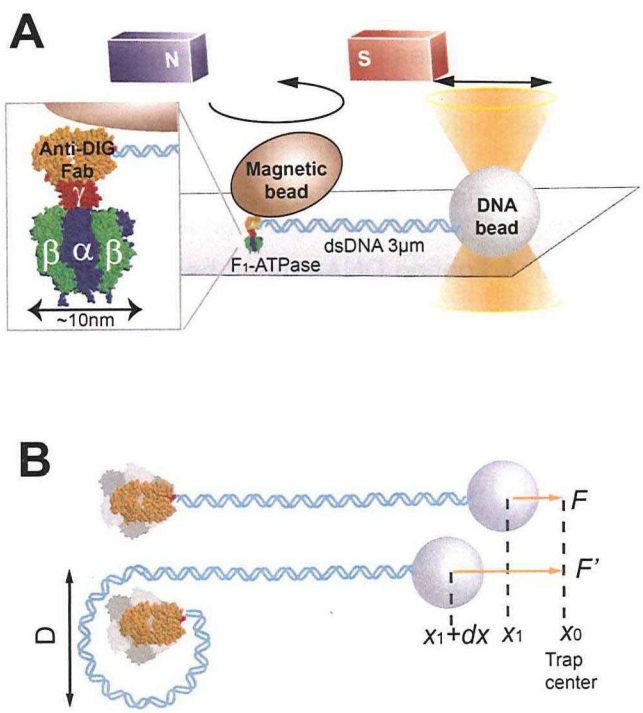

**Figure 4-1 Experimental setup.** The molecular reel was constructed of $F_1$, a magnetic bead, and the Fab fragment on Ni-NTA glass. A biotinylated anti-DIG Fab fragment (orange) specifically linked the γ subunit (red) of $F_1$-ATPase and the streptavidin-coated magnetic bead. A dsDNA molecule (8.7 kbp) was bridged between the anti-DIG Fab fragment and a streptavidin-coated polystyrene bead trapped using optical tweezers. The dsDNA was wound by rotating the magnetic bead using the magnetic tweezers. The stretching force was nearly parallel to the glass surface; the angle of the DNA strand against the coverglass was less than 10 degrees. (**B**) The diameter of the wound DNA ($D$) was calculated from the total length of wound dsDNA ($L$) and the number of revolutions ($n$) as $D = L/n\pi$. The $x_0$ represents the center of the optical trap; $x_1$ and $x_1+dx$ are the bead positions before and after winding. The length ($L$) of the wound dsDNA corresponds to the sum of the bead displacement ($dx$) and the increase of tethered dsDNA's extension (Supplementary data). The winding tension ($F$) equals $k \cdot dx$ where $\kappa$ is the trap stiffness. Experiments were carried out at a low revolution rate (0.1 rps).

Procedures for constructing the system were carried out as follows. First, reel complexes were built by infusing the anti-DIG Fab-$F_1$ complex and magnetic beads solutions into a flow cell. The density of $F_1$ on the glass surface was maintained at less than 0.03 molecules per $\mu m^2$. Some reel complexes showed continuous rotation at rotation speed faster than 5 revolutions per second (rps) in the presence of ATP (2 mM), indicating that the magnetic bead was tightly bound to the rotor γ subunit of a single $F_1$ molecule. Next, DNA-coated polystyrene beads, which made of streptavidin-coated polystyrene beads and 5'-biotin and 5'-DIG labelled DNA molecules, were also introduced into the flow cell. A floating DNA-coated bead nearby a rotating $F_1$ molecule was captured and moved towards the rotating magnetic bead using optical tweezers until the DNA-coated bead inhibited the rotation of $F_1$ through steric hindrance. For establishing a connection between the 5'-DIG end of DNA and the anti-DIG Fab fragment on the rotor, the bead was held adjacent to the reel complex for 5-30min. More than 340 experimental trials were conducted. Only 44 cases showed the connection of the DNA bead to a rotating $F_1$ molecule. The connection was confirmed by observing

that $F_1$ rotation was stalled when the stretching tension was exerted on DNA strand trapped with optical tweezers. In the most of failure cases, the DNA bead was simply not connected. In some failure cases, the DNA bead was anchored on a glass surface but at apparently distant point from the rotation centre of the magnetic bead. These cases were omitted from analysis. The experiment was often terminated by the detachment of the magnetic bead from glass surface, probably due to the detachment of His-tag or the dissociation of the $\gamma$ subunit from the $\alpha_3\beta_3$ stator ring. The released magnetic bead always accompanied the DNA-coated bead, which ensured the connection of the reel complex to DNA-coated bead.

### 4.1.2 Winding DNA by magnetic tweezers

After establishing the connection, the DNA molecule was stretched by horizontally moving the microscope stage using a stepping motor, and then an arbitrary level of tension was applied to the DNA strand to stall the ATP-driven rotation of $F_1$ (**Fig. 4-2**). To minimize stage drift, the system was held for several seconds after applying the tension. Stage drift was typically within 10 nm per minute, which was measured using the polystyrene bead non-specifically attached to the glass in the same observation field or from the centroid of the rotating magnetic bead. Data exhibiting large drift were omitted from analysis. After holding the stage, the magnetic bead was rotated at 0.1 rps in a counterclockwise direction using the magnetic tweezers to wind the DNA. Upon winding, the polystyrene bead in the optical trap moved towards the rotating magnetic bead. In most cases, experiments were terminated due to detachment of the magnetic bead from glass surface as described before due to the developed tension. At detachment, the trapping force immediately decreased to zero (asterisk in **Fig. 4-2A** and **B**).

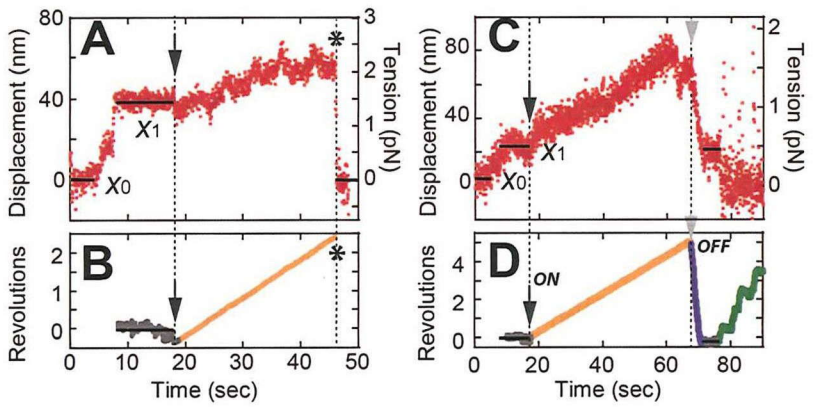


**Figure 4-2 Time courses of winding experiments.** An example of the time course of the displacement of an optically trapped polystyrene bead during the winding procedure. Trap stiffness was 0.040 pN/nm. dsDNA was stretched at around 1.5 pN force for 8–18.5 s. (B) Time course of magnetic bead rotation during the winding experiment for (A). The magnetic bead was rotated from 18.5 s at 0.1 rps (orange line). The optically trapped bead was moved concomitantly with the magnetic bead rotation. After 2.5 revolutions, the magnetic bead detached from the glass surface (showed by asterisk). The optically trapped bead immediately returned to the trap center ($x_0$). (C), (D) Time course of another winding experiment. Trap stiffness was 0.022 pN/nm. The magnetic bead was forcibly rotated for 5 revolutions. The optically trapped bead was constantly pulled toward the rotating magnetic bead. The sudden decrease at 63 s occurred for unknown reason; it might be due to structural relaxation of the DNA wound up around the molecular reel. The magnetic field was turned off at 66 sec (gray arrowheads), and then, beads showed backward rotation (blue part). At 75s, after reducing the tension exerted on DNA by moving stage, $F_1$ resumed ATP-driven rotation (green line).

In some cases, the system was able to withstand the stretching. When the magnetic tweezers were turned off (grey arrowheads in **Fig. 4-2C** and **D**), the magnetic bead exhibited fast backward rotation, turning the same number of rotations as was observed in the forcible wind up process. The speed of this backward rotation was 0.4–1.7 rps (n = 3). When the tension exerted on the molecular reel complex was completely removed by moving stage, $F_1$ showed ATP-driven rotation (green data point in **Fig. 4-2D**) indicating $F_1$ molecules were still active after manipulation. In some cases, F1 did not resume ATP-driven rotation, likely due to the exposure of $F_1$ to infrared light for

optical trapping. However, inactivated $F_1$ molecules still acted as a molecular bearing; the magnetic beads showed rotational Brownian motion after the experiment (data not shown).

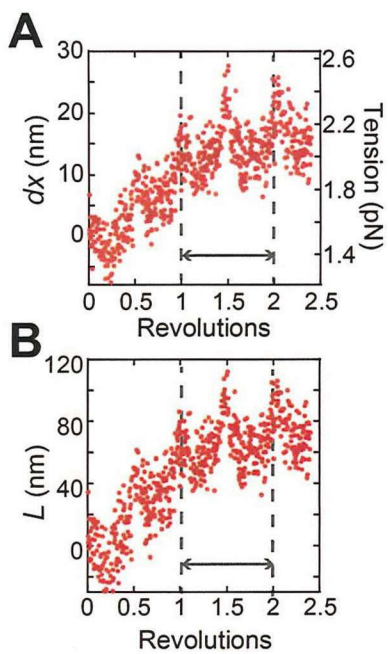


**Figure 4-3 Wound DNA length versus revolutions.** (A) Displacement of optically trapped bead (*dx*) versus revolutions (*n*). (B) Total length of wound dsDNA (*L*) versus revolutions (*n*). *L* was determined from *dx* and the force-extension curve of the same dsDNA. Considering the precision of *dx* determination or steric interaction with other wound DNA region, the data points between 1.0 and 2.0 revolutions were subjected to the data analysis (indicated by grey dashed line and arrow).

### 4.1.3 Analysing tension and diameter

To draw a curve of winding tension (*F*) versus curvature diameter (*D*) of wound DNA, we determined the tension exerted on the DNA and the length of the DNA wound around the reel complex (*L*). Force was determined based on the displacement of the DNA bead from the trap center of the optical tweezers. The stiffness of the optical tweezers used was 0.01−0.05 pN/nm. The diameter of wound DNA was calculated using $D = L/n\pi$; where *n* is the number of forced rotations. Because the displacement of the DNA bead upon winding was partly compensated by the extension of the trapped DNA strand (extension/*L* = 31%-88%), total length of the DNA wound around the reel complex (*L*) is represented as the sum of displacement of DNA-bead (*dx*) and DNA extension. Here, DNA extension was determined based on the force applied on the DNA in winding

experiment, and the force-extension curve of the same DNA obtained from the stretching experiment (**Fig. 4-3A** before correction, **Fig. 4-3B** after correction). For precise measurement, only the data points from 1.0 to 2.0 revolutions were analysed; data points of less than 1.0 or greater than 2.0 revolutions did not provide reproducible values, likely due to the low precision of diameter estimation for less than 1.0 revolution and steric interactions between wound DNA strands for greater than 2.0 revolutions.

### 4.1.4 Fit of force-diameter data with WLC model

**Fig. 4-4** shows the results of 8 independent winding experiments represented by different colors, with winding tension ranging from 0.9 pN to 6.0 pN and curvature diameters ranging from 21.4 nm to 8.5 nm. Diameters were larger than the size of nano-reel (~5 nm). Thus, this value represents the mechanical property of dsDNA without steric interaction with the reel. Based on the WLC model, the relationship between winding tension and loop diameter of dsDNA can be expressed as follows:

$$F = \frac{2\kappa}{D^2} = \frac{2L_p k_B T}{D^2} \qquad \textbf{[24]}$$

where $F$ is the winding tension, $D$ is the curvature diameter of DNA loop, $\kappa$ is the bending stiffness of dsDNA (also referred to as flexural rigidity), $k_BT$ is thermal energy (4.1 pN·nm at room temperature), and $L_p$ is the persistence length of dsDNA. By fitting the averaged data points of individual experiments (open squares in Fig. 4a and 4b), persistence length $L_p$ of highly bent DNA was determined to be 54 ± 9 nm (mean ± standard deviation; correlation coefficient R = 0.93). This value agrees well with previously reported persistence length from stretching experiments (~50 nm)(75). This agreement suggests that sharply bent dsDNA retains the same mechanical properties

as dsDNA in the relaxed state, implying that deformation of dsDNA, such as local melting or kinking, does not occur in the present condition.

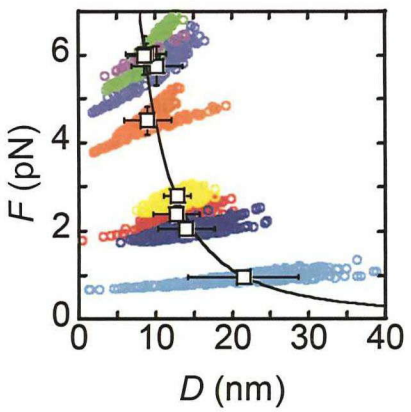


**Figure 4-4 Winding tension (*F*) versus wound DNA diameter (*D*).** Data points (n = 2027) were derived from 8 individual measurements represented by different colors (open circles). Open squares represent the averaged values of each experimental trial, where the coefficient of variation (standard deviation/mean) for *F* was 4−13%, and for D was 14−35%. Black solid line is a fit of averaged data points with WLC model with Equation (1) and the fit parameter was *L*p = 54 ± 9 nm (mean ± standard deviation).

# 5. Chapter 5 General conclusions

## 5.1 Discussion and conclusions

The bendability of double-stranded DNA (dsDNA) on a small length scale (5–100 nm) is important for understanding genomic DNA packaging, transcriptional regulation, and the fabrication of DNA nanostructures. In terms of mechanical properties, the classical worm-like chain (WLC) model describes DNA as a rod that is smoothly bent by thermal energy. The persistence length ($L_p$, 40–50 nm) has been used to characterize DNA bending stiffness. However, the WLC model is refuted when DNA is tightly bent and its curvature diameter is smaller than the $L_p$. Recent experiments have suggested that the breakdown of the WLC model for tightly bent dsDNA might be caused by deformations such as kinks or melting bubbles, but those findings are still controversial.

This thesis described a novel method for winding single dsDNA molecules and to study the bending stiffness of dsDNA. In our experimental system, a rotary motor protein $F_1$-ATPase was used as a unique protein reel. By combination with an optical tweezers and magnetic tweezers system, dsDNA was wound around the molecular reel. The bending stiffness of dsDNA was determined from the winding tension (0.9–6.0 pN) and the diameter of the wound loop (21.4–8.5 nm). Our results were in good agreement with the conventional WLC model and a persistence length of 54 ± 9 nm was estimated. This molecular reel system offers a new platform for single-molecule study of the micromechanics of sharply bent DNA molecules and is expected to be applicable to the elucidation of the molecular mechanism of DNA-associating proteins on sharply bent DNA strands.

### 5.1.1 Comparison of WLC model and non-harmonic models

The SEC model assumes the curvature diameter to be inversely proportional to the tension, while the WLC model assumes the square of the curvature diameter to be inversely proportional to the tension as represented by the equation [25]. To test which model is consistent to the present results, the observed curvature radius was plotted against the inverse of tension (**Fig. 5-1A** and **5-1B**). As results, $D^2$ versus $1/F$ plot (**Fig. 5-1A**) showed better linearity than $D$ versus $1/F$ plot (**Fig. 5-1B**). Thus, it is evident that the WLC model well fits with the present data over the SEC model.

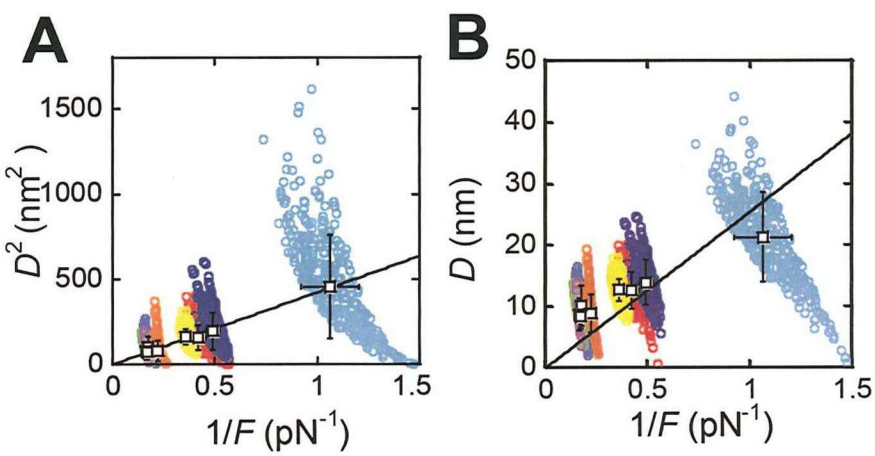


**Figure 5-1 Comparison of the WLC model and the SEC model. (A)** The linear fit of $D^2$ versus $1/F$, corresponding to the WLC model. Same data shown in Fig4-4 was analyzed. **(B)** The linear fits of $D$ versus $1/F$ corresponding to the SEC model.

### 5.1.2 Explanations: sequence dependence of DNA flexibility

To explain this discrepancy, various factors can affect the DNA flexibility, including ion strength, $Mg^{2+}$ concentration, temperature, and sequence of DNA. We will mainly discuss the effects of sequence on the DNA flexibility in this section. In Cloutier and Widom's report, several verifications of 94bp DNA sequence showed lower cyclization efficiency than 94 bp DNA, indicating that sequence may affect the DNA persistence

length. Use a small value of persistence length ~ 40 nm can explain Cloutier and Widom's results. Recent cyclization experiment reported different persistence length of different sequences(24). Thus, some sequences of DNA may have higher cyclization efficiency than calculated from the average persistence length. Moreover, recently theoretical study based on dynamic simulations showed sequence might influence DNA's ability of forming kinks (76). Four DNA segments were analyzed, and only one segment of DNA showed the breakdown of harmonic elasticity model at sharply bent condition. Therefore, it is possible that different sequence required higher energy to form kinks than calculated from Cloutier and Widom's results ($11k_BT$).

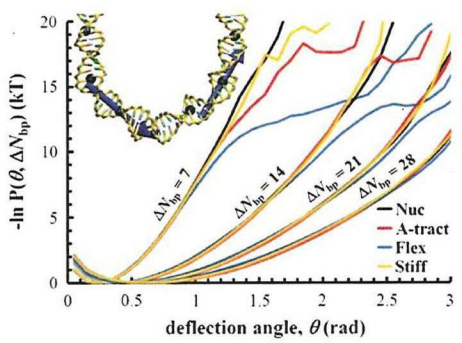


**Figure 5-2 Sequence effects on the DNA flexibility analysed by coarse-grained model.** Four segments of DNA were analysed: Nuc, A-tract, Flex, and Stiff. Negative logarithm of the observed probability distribution function $P(\theta, \Delta N_{bp})$ of angles between tangents separated by $\Delta N_{bp}$. For $\Delta N_{bp}$= 7 bp, the Flex and A-tract sequences exhibit a proclivity to form tight bends ($\theta$ > 1.2 rad), whereas Nuc and Stiff do not. The difference between sequence are disappear when $\Delta N_{bp}$ increased.

## 5.2 Future work

### 5.2.1 Sequence dependence of DNA flexibility

#### Sequence dependence and nucleosome positioning

Eukaryotic genomes are packaged into the nucleosomes that regulate the access of other proteins to DNA, thus regulating gene expression. Special sequence motifs such as AA-TT-TA have been shown to be more likely to form nucleosomes (77) (**Fig.5-3**). The sequence dependence of DNA bending stiffness is vital for understanding nucleosome positioning. The affinity of histones for different DNA sequences is differ by as much as 100–1000 fold (>4 kcal/mol in free energy) (38). The crystal structures of nucleosomes indicate no contacts between DNA bases and histones (37), leading to the proposal that the sequence could influence nucleosome positioning indirectly by facilitating the tight bending required to wrap DNA around histones.

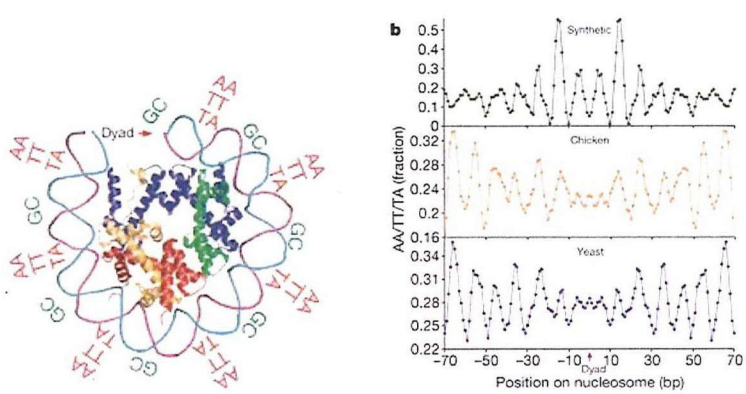


**Figure 5-3 AA-TT-TA bp steps are more likely to be found at the DNA-histone interface.** (Adapted from reference (77)).

In Chapter 4.2.2, we discussed the effects of sequence on the DNA bending stiffness in that it might explain the difference between our data and previous measurement. The fact is, whether a DNA sequence affects its mechanical properties is

a central question in biophysics. Our experimental system might offer a tool to measure DNA bending stiffness of different sequences.

To analyze the sequence dependence of bending stiffness, candidate sequences that might have different bending stiffness are required. In collaboration with Prof. Maeshima at the National Institute of Genetics, we prepared two other types of DNA: GC (with high GC content) and AT-track (with high AT content). The AT-track sequence form a scaffold-attachment region (SAR) sequence.

**Construction of force-clamp optical-tweezers**

In the present study, an error in the estimation of the DNA extension could largely impair the precision of measurement of the diameter of the wound DNA. The precision can be improved by introducing a feedback control system to apply constant force to the DNA strand.

Force-clamp optical-tweezers can be accomplished by beam deflection, stage movement or intensity modulation (**Fig. 5-4**). Several reviews have presented the design and construction of a feedback system (78). However, these optical tweezers require expensive equipment such as a computer-controlled acousto-optical deflector (AOD).

Here, we developed a piezo controlled sample stage to construct feedback system. The program diagram is presented in **Figure 5-5**. We tested the response of the feedback system by using a stepping motor to move the stage and increase the force applied to the DNA (**Fig. 5-6**). Our results demonstrated the response time for this system was approximately several tens of seconds. After improving the speed of the feedback loop, this system might be used in DNA winding experiments.

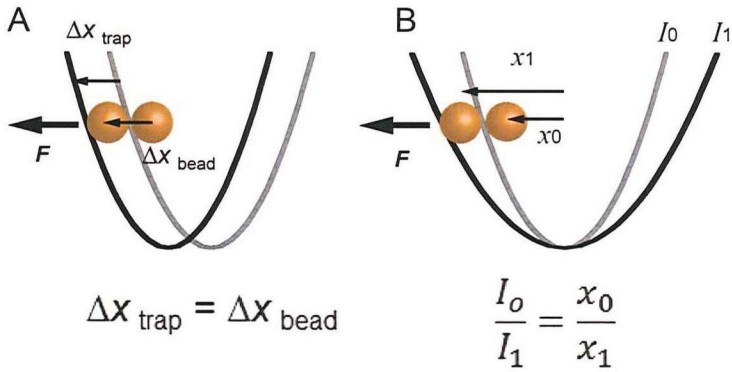


**Figure 5-4 Two types of force clamp.** (A) Force clamp based on beam deflection or stage movement. (B) Force clamp based on intensity modulation.

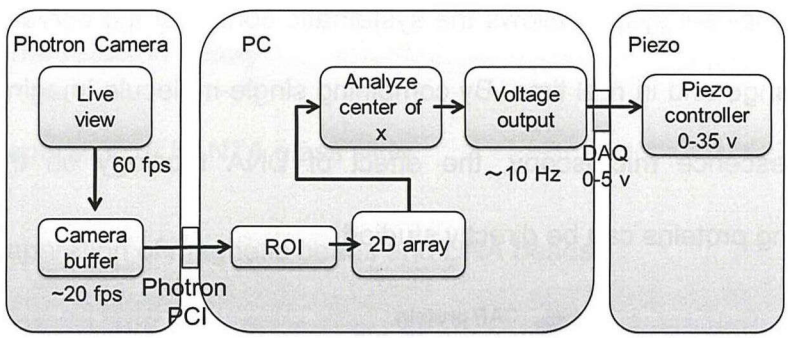


**Figure 5-5 Program flow chart.** This program was built based on LabVIEW.

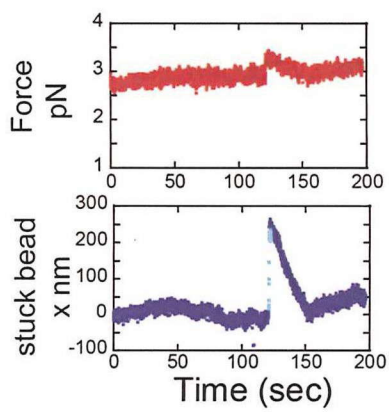


**Figure 5-6 Test of feedback system.** A polystyrene bead was anchored to glass surface through a 3 μm length of DNA. By moving the stage, force was applied to the tethered bead. The stage movements were monitored by bead that was adhered on the glass surface. The force was increased by moving the stepping motor in 110 s (Cyan). The stage was moved by piezo to keep the force as constant at 150 s.

### 5.2.2 Curvature dependence in the affinity of DNA-associating protein

The binding affinity of transcription factor is related to the bending energy of DNA. An experimental demonstration of the curvature dependent affinity was conducted by creating a pre-bent DNA minicircle (79). When a binding sequence for transcription factor was pre-bent in the same direction as the transcription factor induced bending, the affinity of the transcription factor for the binding site was 300-fold higher relative to pre-bending in the opposite direction.

Our nano-reel system allows the systematic control of the curvature of wound DNA in wide range and in real time. By combining single-molecule imaging techniques such as fluorescence microscopy, the effect of DNA topology on the affinity of DNA-associating proteins can be directly studied.

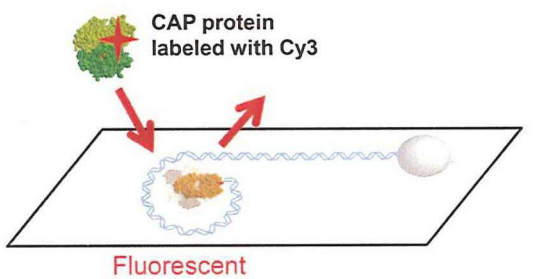


**Figure 5-7 Real time imaging of DNA-associating protein and study of the curvature enhancement of binding affinity**

# Appendix1 Protocols for experiments

## Preparation of $F_1$ and DNA sample

-Protocol 1 Preparation of labeled DNA by PCR

-Protocol 2 Purification of $F_1$ protein from E.coli

-Protocol 3 ATPase activity analysis of $F_1$-ATPase

-Protocol 4 Crosslink reaction

## Single-molecule rotation assay

-Protocol 5 Preparation of Ni-NTA glass slide

-Protocol 6 Preparation of magnetic beads and DNA beads

-Protocol 7 Rotation assay and DNA winding experiment

## Single-molecule fluorescence observation

- Protocol 8 Fluorescence observation of DNA or Cy3 labeled protein

## Optical tweezers and Magnetic tweezers

-Protocol 9 Arrangement of optics for single-beam optical tweezers

-Protocol 10 Calibration of optical tweezers stiffness

-Protocol 11 Calibration of magnetic tweezers

## A.1.1 Preparation of $F_1$ and DNA sample

***-Protocol 1: Preparation of labeled DNA by PCR***

**-5'-biotin and 5'-digoxigenin labeled DNA**

**MATERIALS**

- Extaq DNA polymerase (#RR001A, TaKaRa, Japan),
- Wizard® SV Gel and PCR Clean-Up System (#9280,Promega, USA)
- pRA100 plasmid (purified from E.coli)
- 5'-biotin prime, 5'-digoxigenin (DIG) primer (Sigma Genosys, USA)

**METHODS**

**1. PCR reaction** (96 tube = 9.6 mL)

| | | | |
|---|---|---|---|
| Takara Ex taq(5U/ul) | 0.5 µl | 24 µl | 48 µl |
| 10X Extaq buffer | 10 µl | 480 µl | 960 µl |
| dNTP(2.5mM) | 8 µl | 384 µl | 768 µl |
| template pRA100 | 0.5 µl | 24 µl | 48 µl |
| 5' Biotin Primer (100µM) | 0.5 µl | 24 µl | 48 µl |
| 5` Dig Primer (100µM | 0.5 µl | 24 µl | 48 µl |
| Sterilized milliQ | up to 100 ul | Up to4.8 mL | Up to 9.6 mL |

Program:
98°C 1 min
(98°C 10 sec, 55°C 30 sec, 72°C 1 min/kb) 40 cycle
72°C 5 min (< 3kb) 10 min (3 kb-9 kb)
4°C ∞

**2. Purification of PCR product**

↓ Use Wizard system (Max 40 µg DNA per tube). Add equal volume of membrane binding solution, 800 µl per tube.

↓ Check PCR product by 1% agarose gel. Measure DNA concentration by 260 nm absorbance (Abs260).

↓ [DNA ng] = Abs260 X 50 ng/μl, [DNA molar concentration]= [DNA ng]/ MW

↓ *ds DNA MW = 660/bp; ssDNA MW=330.

↓ 1.5 kbp DNA MW= $0.99*10^6$, 3446 bp = $2.29*10^6$, 6362 bp = $4.2*10^6$, 8688 bp = $5.73*10^6$

*0.6~0.8 μg/μl DNA can be purified. For 500 bp, ~2 μM DNA can be purified. For 6 kbp, ~0.2 μM DNA can be purified.

**- Using thiol group labeled primer (DTT treatments)**

DTT treatment of primer (200 μM 100 μl for 9.6 mL PCR reaction, two times)
5' thiol-primer 200 μM 100 μl
DTT 0.12 M 66 μl
KPi 0.5 M (pH8.0) 33 μl
RT 16 hour.
Nap5 equilibrate with TE or milliQ (10 mL). Add primer200 μl. Add 300 μl buffer. Elute with 750 μl TE buffer.
[Oligo]=Abs 260/ε-primer (For 567-SH ε =0.314 $\mu M^{-1}$)
Store at -20°C.
*After DTT treatment, primer can store at -20°C for one month. For longer time, thiol group will be oxidized.
*PCR reaction condition is as same as 5'-biotin and 5'-digoxigenin

| Box: Extinction coefficient for primer |
|---|
| $A_{260}$=0.89[A×15480+C×7340+G×11760+T×8850] |

***-PCR use Rhodamin or Dig-dUTP to label DNA (dTTP/dUTP=1/80)***

| | | | |
|---|---|---|---|
| Takara Ex taq(5 U/ul) | 0.5 μl | 24 μl | 48 μl |
| 10X Extaq buffer | 10 μl | 480 μl | 960 μl |
| dNTP(ATCG2.5 mM) | 8 μl | 384 μl | 768 μl |
| Rhodamine-dUTP 1mM | 0.25 μl | 12 μl | 24 μl |
| template pRA100 | 0.5 μl | 24 μl | 48 μl |
| 5' Biotin Primer (100 μM) | 0.5 μl | 24 μl | 48 μl |
| 5` Dig Primer (100 μM | 0.5 μl | 24 μl | 48 μl |
| Sterilized milliQ | up to 100 ul | Up to4.8 mL | Up to 9.6 mL |

*Rhodamine-dUTP (Roche #11534378910) 1 mM 25 µl

PCR Program:
98°C 1 min
(98°C 10 sec, 55°C 30 sec, 72°C 1.5 min/kb) 40 cycle
* for Rhodamine-dUTP, use longer extension time than normal
72°C 5min ( < 3kb) 10min(3kb-9kb)
4°C ∞
*Rhodamine: ε551nm=65000$cm^{-1}M^{-1}$
*For PCR 9kb, dTTP/dUTP=1/40, the label efficiency is about 100 rhodamin per DNA molecule.

***-Protocol 2: Purification of $F_1$ protein from E.coli***

**-Mutagenesis and purification of $TF_1$**

Expression system for thermophilic Bacillus $\alpha_3\beta_3\gamma$ complex in E.coli was constructed in 1995(80). $TF_1$ was expressed in JM103 strain *E. coli* (ΔuncB-uncD). Expression plasmid was drive from pKK223-3. Our modification of mutant and purification methods are all based on their work.

**-Expression and purification of $TF_1$**

$F_1$ purification was based on histidine-tagged protein purification methods. Histidine modified N-terminus of α and β have high selective affinity for $Ni^{2+}$ metal ion. Nichel nitrilotriacetic acid (Ni-NTA) column was use for purification. After Ni-NTA column, gel filtration column superdex 200 was used in final purification for remove free α and β subunits and other protein.

**MATERIALS**

- Protease Inhibitor Cocktail: Complete, Mini, EDTA-free, EASYpack (#4693159 Roche USA)

- Ni-NTA agarose (#30230, QIAGEN, Germany)
- Superdex 200 10/300GL (#17-5175-01 GE life sciences, USA)
- MILLIPORE, Amicon Ultra-15, Ultracel 10K, 15 mL (UFC901008, Millipore, USA)
- Biotin-$PEAC_5$-maleimide (B299, Dojindo, Japan)

## METHODS

### 1. Culture and expression check

Expression check

↓ Streak the glycerol stock ( in JM103ΔuncB-uncD) on LB agar plate containing 100 μg/mL Ampicillin
↓ Incubate at 37°C for 16 hours (overnight generally)
↓ Pick a single colony from the plate using autoclaved toothpick and add to the LB/ampicilin tube (3 mL 4tube)
↓ Incubate in a shaker at 37°C for at least 8 hours.
↓ Take 200 μl of expression culture and centrifuge at 1,5000 rpm for 1 min (for SDS-PAGE).
↓ Discard the supernatant and suspend the pellet in SDS-sample buffer (milliQ 15 μL, 4*SDS sample buffer 5 μL)
↓ Boil at 95°C for 5 min
↓ SDS-PAGE analysis (30 mA, 50 min)

Main culture

↓ Add 1.25 mL of pre-culture (LB 1% tryptone, 0.5% yeast extract and 1% NaCl)to 1.25 L TB (1.2% tryptone, 2.4% yeast extract, 0.4% glycerol, 1.25% $K_2HPO_4$ and 0.23% $KH_2PO_4$) medium containing 100 μg/mL of Ampicillin
↓ Incubate at 37°C for at least 10 hours (overnight generally)
↓ Centrifuge expression culture at 7000 rpm for 15 min at 4°C and discard the supernatant.
↓ Dispense the cells into the two 50 mL tube
↓ Measure the cell weight
↓ Freeze in liquid nitrogen
↓ Store at -80°C

### 2. *E.coli* cell disruption by sonication

↓ Add 25 ml of E.coli wash buffer [50 mM Tris-HCl, 100 mM NaCl (pH 8.0)].
↓ 7,000 rpm、10 min、4°C.
↓ Suspend in [50 mM Imidazole,100 mM NaCl] 15 ml + Protease Inhibitor Cocktail 1/3 tablet
↓ Sonication 5 min*2 on ice.
↓ Standard Micro Tip, "5", pulse 1 sec, off 0.5 sec
↓ Sample 10 μL for PAGE
↓ Heat treatment at 60°C for 30 min
↓ 60,000 rpm 10 min 4°C
↓ Sup (sampling 10 μL for PAGE)

**3. Purification by Ni-NTA column**

↓ Apply supernatant to Ni-NTA column : flow through fraction.
↓ [50 mM Imidazole,100 mM NaCl] 20 mL wash : 50 mM wash fraction
↓ [100 mM Imidazole,100 mM NaCl] 10 mL wash : 100 mM wash fraction
↓ [200 mM Imidazole,100 mM NaCl] 10 mL wash : 200 mM wash fraction
↓ [500 mM Imidazole,100 mM NaCl] 5 ml×4 times elution : 500 mM elution ①~④ fraction
↓ [800 mM Imidazole,100 mM NaCl] 10 mL wash : 800 mM wash fraction
↓ Sampling each fraction (10 μL for SDS-PAGE、Native-PAGE and 10 μL for BCA analysis)

Analysis fraction by SDS-PAGE and Native-PAGE and stained by Quick CBB (Wako)
SDS-PAGE : 2 gel ( 60 mA ~1hour) (during SDS-PAGE)add DTT to 100~800 mM fraction (final 1 mM DTT) incubate for at least 1 hour at RT.

**4. Purification by Gel filtration HPLC**

↓ HPLC buffer preparation(100mM KPi, 2 mM EDTA pH7.0) and column equilibration
↓ Buffer filter with 0.22 or 0.44 μm filter and degassed
↓ Equilibrate HPLC column (Superdex 200HR 10/30) with 50 mL(2CV) of HPLC buffer(0.5 mL/min).

<Sample condensation>

↓ Ni-NTA purified sample(elution fraction) condense to 1 mL with membrane filter (Amicon Ultra-4 or 15, MW:50K or 100K)

↓ Filtrate with 0.22 μm filter

<Sample loop wash>

↓ Wash the sample loop with 5 mL of water by the syringe
↓ Wash the sample loop with 5 mL of HPLC buffer by syringe
↓ Sample injection
↓ Inject 1 mL of sample to injection valve
↓ Run

**AKTA condition**

| | |
|---|---|
| column name | superdex 200 HR 10/30 |
| wave length 1 | 280 nm |
| wave length 2 | 260 nm |
| Pressure limit | 1.50 MPa |
| Averaging Time | 5.12 |
| Flow Rate | 0.5 mL/min |
| Equilibrate with | 0.1 CV |
| Empty loop with | 5 mL |
| Elution Frac. Size | 1.5 mL |
| Peak Frac. Size | 0.15 mL |
| Peak Start Slope | 100 mAU/min |
| Peak End Slope | 75 mAU/min |
| Minimum Peak width | 1 |
| length elution | 1.5 |

**5. $F_1$ protein quantification and biotinylation**

↓ Collect peak fraction ($\alpha_3\beta_3\gamma$ complex) and measure concentration by UV spectrometer.

OD280nm / 0.154 $uM^{-1}$ = uM

OD280nm * 2.2 = mg/mL

*$F_1$ extinction coefficient ε = 0.154, MW=360000

↓ Prepare 10mM Biotin-$PEAC_5$-maleimide (1mg/17.9 uL DMSO)
↓ Add 10mM Biotin-$PEAC_5$-maleimide to protein solution ($F_1$ : biotin = 1:3).
↓ Incubate at RT for at least 1 hour.
↓ Freeze in liquid nitrogen
↓ Store $F_1$ at -80°C.

### *-Protocol 3 ATPase activity analysis of $F_1$-ATPase*

ATPase activity of $F_1$-ATPase was measured by ATP regeneration system. The mechanism of ATP regenerating system is shown in Figure A-1. When $F_1$-ATPse hydrolyzes one ATP molecule, pyruvate kinase will remove the Pi group from PEP and synthesize one ATP. The LDH will catalyze pyruvate to Lactate. During this reaction, NADH will be converted to $NAD^+$. Since one ATP hydrolysis is coupled with one NADH dehydrogenate, ATP hydrolysis activity can be monitor from the absorbance decrease of NADH at 340 nm.

**MATERIALS**

- PK: Pyruvate Kinase (PK) from rabbit muscle (#10109053001, #10109045001, Roche)
- LDH: L-Lactate Dehydrogenase (#10127221001, #10127230001,Roche)
- PEP: Phospho(enol)pyruvic acid tri(cyclohexylammonium) salt (P7252#, Sigma-Aldrich)
- ATP: Adenosine 5′ -triphosphate disodium salt hydrate (#A3377, Sigma-Aldrich)
- NADH (#10107735001, Roche)
- LDAO
- UV/VIS Spectrometer (VP-550, Jasco)

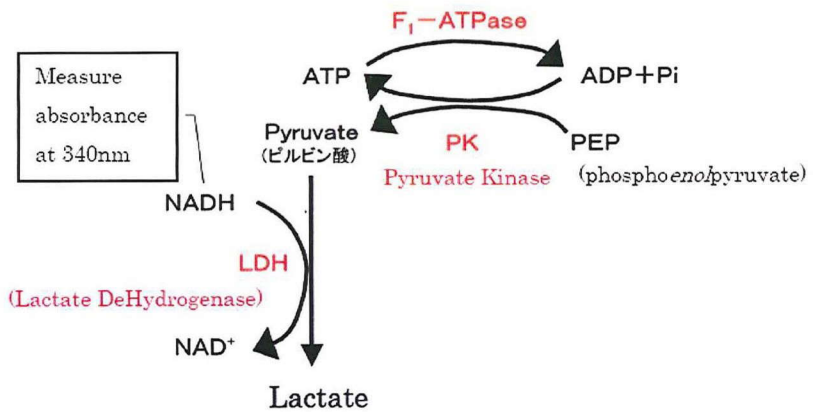


**Figure A-1 ATP regenerating system**

$$\text{ATPase (turn over} \cdot s^{-1}) = \frac{\text{Slope dAbs/dsec } (s^{-1}cm^{-1})}{6200\ (cm^{-1}M^{-1}) \cdot F_1\ \text{conc(M)}}$$

**METHODS**

↓ Prepare 20 mM NADH solution: 2 mg NADH to 141 µl milliQ

↓ Prepare 100 mM ATP

↓ Prepare **assay mixture** (5 mL for 3~4 times measurements)

| | Stock solution | volume (in 5 mL) |
|---|---|---|
| 50 mM MOPS-KOH (pH7.0). | 1 M | 250 µL |
| 50 mM KCl | 2 M | 125 µL |
| 2 mM MgCl2 | 1 M | 10 µL |
| 0.2 mM NADH | 20 mM | 50 µL |
| 200 µg/mL PK | 10 mg/mL | 100 µL |
| 50 µg/mL LDH | 10 mg/mL | 25 µL |
| 2.5 mM PEP | 100 mM | 125 µL |
| MilliQ | | 4315 µL |

↓ Set the cell-holder and circulate temperature controlled water (25°C) to the cell-holder.

↓ Place the cell into the cell-holder.

↓ Auto-zero calibration

**Measurement condition**

| | |
|---|---|
| バンド幅(band width) | 2.0 nm |
| レスポンス(response) | Medium |
| 測定範囲(time range) | 0-600 sec |
| データ取り込み間隔(data acquisition interval) | 0.5 sec |
| 測定波長(wavelength) | 340 nm |

↓ Add 1.2 mL of assay mixture and magnetic stirring bar.

↓ **Start** measurement with stirring.

↓ Add ATP stock solution (final 1 mM) at 30 sec.

↓ Add $F_1$-ATPase (final 5 nM) at 60 sec.

↓ Add LDAO (final 0.3%) at 300 sec.

↓ **End** measurement (after 600 sec)

↓ Repeat measurement 3-times.

↓ Calculate ATPase activity from the slope (initial, steady state, after LDAO)

*During measurement, if all NADH was converted to NAD+, add additional 12 µL of 20 mM NADH

***Protocol 4 Crosslink reaction***

**MATERIALS**

Cy3 Mono reactive Dye (PA23001, GE life sciences, USA)

Nap 10 column (17-0853-02, GE life sciences, USA)

Nap 5 column (17-0854-02, GE life sciences, USA)

Biospin 30 column (#732-6231, Life Science Research, USA)

EZ-Link Sulfo-NHS-Biotin, No-Weigh Format (#21326, Thermo Fisher Scientific, USA)

SPDP (#21857, Thermo Fisher Scientific, USA)

Anti-digoxigenin (DIG) Fab fragment from sheep (#11093274910 Roche, Switzerland)

KPi buffer: 10 mM KPi (pH7.0).

**1 Biotinylation of Fab fragments**

↓ Anti Dig Fab 1 mg/ml (40 µM) in 100 mM KPi (pH7.0) 2 mM EDTA

↓ Fab: biotin-PEG-NHS=1:20

40 µM Fab 500 µl

20 mM NHS-PEG-biotin 20 µl (final 800 µM)

↓ RT 1.5 hour

↓ Remove NHS-PEG-Biotin by Nap5 column. 500 µl-> 1 mL, Kpi buffer (pH 7.0)

**2. Crosslink reaction of Fab and $F_1$-ATPase**

↓ Biotin labeled anti-dig Fab (Roche) (1 mg/ml = 40 uM) in 100 mM KPi (pH7.0) 2 mM EDTA

↓ 2 mg SPDP (thermo) to 320 µl DMSO (20 mM) 10X dilute to 2 mM 100 mM KPi (pH7.4)

1:10 Fab 20 µM 225 µl

SPDP 2 mM 15 µl (final 100uM)

KPi (pH8.0) 0.5 M 60 µl

↓ RT 30 min

↓ Quench by 1 M Tris-HCl (pH8.0) 6 µl (final 20 mM) RT 10 min

↓ BioSpin 30 column

↓ Mix Fab 10 µM 300 µl and XP 18.7 µM 50 µl (Fab:XP=3:1)

↓ RT overnight

### 3. Cy3 labeling of proteins

↓ Dissolve protein to 2 mg/mL (around 500 µl) in 100mM KPi buffer(pH 7.0).
↓ Add the protein solution to the dye vial, cap the vial, and mix thoroughly.
↓ Incubate the reaction at room temperature for **30 minutes** with additional mixing approximately every 10 minutes.
↓ !Care should take to prevent foaming of the protein solution.
↓ Remove of free dye from protein by Nap5 column, 500 µl to 1 mL
↓ Two pink bands should develop during elution. The faster moving band is Cy3-labelled protein while the slower band is free dye.
↓ Estimation of final dye/protein ratio

[Cy3]=$A_{552nm}$/ 150 000 (extinction coefficients of Cy3 is 150 000 $M^{-1}cm^{-1}$)

[Protein] = ($A_{280nm}$-0.08•A552nm) / $\varepsilon_{protein}$

## A1.2 Single-molecule rotation assay

### *-Protocol 5 Preparation of Ni-NTA glass slide*

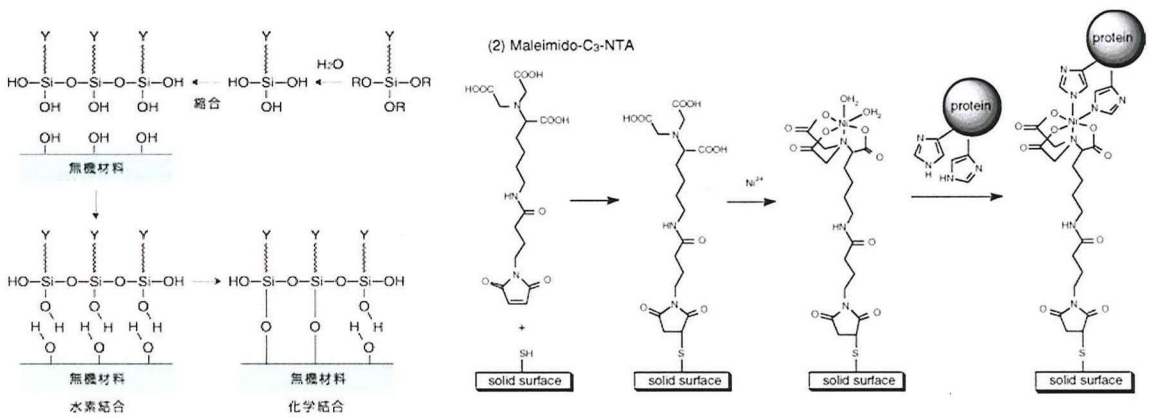


**Figure A- 2 Silanization and coupling with NTA-C3-Maleimide**

**MATERIALS**

- Glass coverslips 24X32mm (Matsunami)
- Glass holder and PMP beaker.
- Mercaptopropyltrimetoxysilane (LS-1390,)
- NTA-$C_3$-maleimide (Dojindo)

- DTT, KOH, chloroform, toluene, ethanol (Wako).

**METHODS**

Cleaning glass coverslips (chemical cleaning)

↓ Put 24 X 32 mm glass coverslips on a glass holder and place into 10N KOH solution overnight. (To form hydroxyl groups on the glass surface)

↓ Remove the glass with the glass holder from the KOH solution and sonicated in MilliQ water to clean the surface

↓ Wash glass in milliQ over 6 times.

Cleaning glass coverslips (plasma cleaning)

↓ Put the coverslips on a glass slide holder and place into the Teflon beaker containing 250 ml of ethanol.

↓ Sonicate the substrates in a bath sonicator for 15 min (repeat this wash-step 2 times).

↓ The substrates are dried under nitrogen stream.

↓ Place the substrates into the reactive ion etcher.

↓ Perform $O_2$ plasma treatment (10 min).

*Both chemical cleaning and plasma cleaning method can be used for clean the glass.

Silanization (Ethanol method)

↓ Remove water on cover glass by air blow, and rinse by ethanol two times in order to remove remained water completely.

↓ Immerse coverslips in 100 mL of ethanol.
*Each coverslips should be separated and the surface should be exposed to the reaction solution.

↓ Add 100 µL 3-mercapto-propyltrimethoxysilane with stirring. React for 30 min at RT with stirring.

↓ Pick up coverslips from silanization solution. Blow away reaction solution; wash with ethanol two times and then wash with MilliQ water 6 times.

Coupling with NTA-$C_3$-Maleimide

↓ Put the coverslips into the beaker containing 100 ml of DTT solution (10 mM DTT in milliQ) and incubate for at least 1 hour at room temperature.

↓ Wash 5 times by milliQ.

↓ Immerse coverslip one by one to 1 mL of 10 mg/ml maleimide-C3-NTA solution (in 50 mM MOPS/KOH, pH 7.0, 50 mM KCl Buffer) for over 3 hour

*Maleimide-C3-NTA is expensive. Reduce reaction volume as far as possible. 1mL solution is enough for prepare 15 coverslips.

*Other buffer at pH 7.0 can be used instead of MOPs

$Ni^{2+}$

↓ Prepare 1 ml of NTA solution (50 mM MOPs buffer pH7.0, 5 mg/ml maleimide-C3-NTA) and 80 µl of solution was coated on a substrate at room temperature for at least 1 hour.

↓ Wash with milliQ six times and then immersed into the nickel solution (20mM nickel sulfate in water).

↓ Stored at 4°C to suppress fluorescent background.

***-Protocol 6 Preparation of magnetic beads and DNA beads***

**1. Magnetic beads preparation**

Before infusing the beads into flow cell, beads solution is sonicated for few second and centrifuged by capsulefuge (chibitan) for few second. Then sup (thin brown color solution) is available. (When there are many aggregated beads in the solution, beads are difficult to bind) Depending on the volume of the flow cell, <8 µL beads solution is sufficient for experiment when 3 flow cells were made on one glass (34 x 24 mm).

**MATERIALS**

Sera-Mag magnetic beads (#30152105010150, Thermo Scientific, USA)

**METHODS 1**

↓ 10 µL magnetic beads

↓ sonication for few second

↓ fill milliQ up to 1 mL

↓ 3000 rpm for 1 min

↓ Take the supernatant (800~900 μL)
↓ 15000 rpm for 1 min
↓ Discard the supernatant (avoid as practically as possible to discard pellet)
↓ Suspend pellet in 20 μL buffer (50 mM MOPS/KOH, pH 7.0, 50 mM KCl). Beads solution is available for several days.

**2. DNA beads preparation**

**MATERIALS**

- Streptavidin coated microspheres (#CP01N, 0.5 μm diameter, 1% w/v, Bangs Laboratories, USA)
- 9 kb DNA (prepared as protocol 1)

**METHODS**

↓ 50 μL beads (streptavidin coated microspheres)
↓ Wash beads with 450μL KPi buffer (100 mM KPi, pH7.0, 2 mM EDTA).
↓ 15000 rpm for 5 min
↓ Add 9 kb DNA and KPi buffer up to 500μL. Mixed at RT overnight.
↓ 15000rpm for 5 min, discard supper.
↓ Wash beads with 1 mL KPi buffer
↓ 15000 rpm for 5 min, discard supper. 6 Times
↓ Suspend pellet in 50 μL buffer (50 mM MOPS/KOH, pH 7.0, 50 mM KCl).Store at 4°C. Beads solution is available for months.

***-Protocol 7 Rotation assay and DNA winding experiments***

**MATERIALS**

- Ni-NTA coverslip
- Cover glass 18X18mm (MATSUNANI)
- Silicone grease (DOW CORNING)
- Mops buffer: 50 mM MOPS-KOH pH 7.0, 50 mM KCl)
- BSA buffer: 5 mg/ml BSA (Wako), 50 mM MOPS-KOH pH 7.0, 50 mM KCl. (5 mg BSA+1 mL MOPS buffer)
- ATP buffer:

| | | |
|---|---|---|
| Pyruvate kinase (PK) 10μg/μl | 5 μl | Final 0.1 μg/μl |

| | | |
|---|---|---|
| Phosphoenolpyruvate (PEP) 100mM | 10 µl | Final 2 mM |
| ATP 200mM | 5 µl | Final 2 mM |
| Mops-Buffer | Up to 500 µl | |

*Prepare ATP stock and measure the concentration by Abs260, stored at -30°C.

*Prepare 1 mM phosphoenlpyruvate, stored at -30°C.

**METHODS**

**1. Preparing flow chamber**

↓ Wash Ni-NTA glass by milliQ, dry it in air.

↓ Cut the paper of parafilm into 2.5 X 25 mm slice; spread with grease; put it on Ni-NTA glass.

↓ Put a cover glass (18X18 mm) over the slide. Push and make sure the cover glass attach to slide. Then a 10-20 µl volume sample chamber formed.

**2. Rotation assay (driven by ATP)**

↓ Add BSA buffer to flow cell, incubate 5 min.

↓ Add 10 pM~100 pM $F_1$ (dilute by Mops buffer), incubate 15 min, wash by 100 µl BSA buffer to remove the unbound $F_1$.

↓ Add Magnetic beads, incubate 30 min (For low $F_1$ concentration 10 pM, increase the incubation time to 1 hour)

↓ Wash by 100 µl BSA buffer to remove the unbound magnetic beads.

↓ Add 200 µl ATP buffer, observation.

*Add BSA in all step for reduce the non-specific binding.

*Dilute of $F_1$ before use. $F_1$ cannot store at low concentration maybe due to the dissociation of complex.

**3. Winding DNA (use magnetic tweezers)**

↓ Infuse DNA-coated polystyrene beads (0.5 µm) in flow chamber. Beads was 1/50 dilute in BSA buffer containing 2 mM ATP and 5 mM Biotin-PEG-NH2 (MW3400, Creative PEG Works, USA).

*Biotin-PEG-NH2 was used to block the nonspecific binding of DNA to magnetic bead.

↓ Find rotating magnetic beads

↓ Capture a floating DNA-coated bead with optical tweezers

↓ Move DNA-coated bead towards the rotating magnetic bead until the DNA-coated bead inhibited the rotation of $F_1$ through steric hindrance.

↓ Stretch DNA by horizontally moves the microscope stage using a stepping motor.

*For smoothly move the stage, I used ActOperator software (Sigma Koki) and set division=5, the speed as S1F1S1.

↓ Check if the rotation was stopped by external force.

↓ Held the system for several seconds to minimize stage drift.

↓ Rotate the magnetic tweezers by Celery software. The rotation rate is set as 0.1 rps.

## A1.3 Single-molecule fluorescence observation

***-Protocol 8 Fluorescence observation of DNA or Cy3 labeled proteins***

**MATERIALS**

- 532-nm diode-pumped Nd:YVO4 laser (CL-2000, CrystaLaser,USA )
- Image intensifier (VS4-1845, Video scope, USA)
- Monochrome CCD camera (WAT-120N, Watec, Japan)

**EXPERIMENT CONDITION FOR DNA**

- 532 nm laser Power=20.4 μw / 100 $\mu m^2$
- Intensifier gain: 600
- Camera: Frame = 2, gain = Hi

**EXPERIMENT CONDITION FOR CY3-PROTEINS**

- 532nm laser Power = 180 μw / 100 $\mu m^2$
- Intensifier gain 500
- Camera: Frame = 2, gain = Hi

## A1.4 Optical tweezers and magnetic tweezers

***-Protocol 9 Arrangement of optics for single-beam optical tweezers***

**MATERIALS**

Microscopy

- Inverted microscope (IX71, Olympus, Japan)

- 100× objective lens (PlanSAPO NA1.3, Olympus, Japan)
- Microscopy stage (KS-0,Japan)
- Optical table: TDI high-performance three-dimensional six-degree-of-freedom Vibration Isolation System (TDIS-168LA, Herz, Japan)
- Stepping motors (SGSP-13ACTR, Sigma Koki, Japan)
- Stage controller (SHOT-202, Sigma Koki, Japan), DMINIS cable (DMINIS-CA-2, Sigma Koki, Japan)

Optical trap

- Infrared(IR) laser (1047 nm, Nd:YLF, 1 W, IPG Photonics, USA)
- Laser power meter (#407A, Newport,USA)
- Infrared(IR) viewer (Electroviewer 7215, Electrophysics, USA)
- 1064 nm polarizing beamspliter cube (PBS) (#PBS253, Thorlabs, USA)
- Half wave plate (λ/2)
- Side port for introduction of an external laser beam (IX2-RFACB2-R, Olympus, Japan)
- Lens: achromatic doublets (DLB-15-50PM, Sigma Koki, Japan)
- Filter (Chroma technology)
- Mirror (TFMHP-2633R03-1064)
- Other optics form Thorlabs: C mount adapter (SM1A10, SM1A9),Stackable lens tube forlin (SM1L05, SM1L20), Lens tubes couplers(SM1T1, SM1T2), Threaded cage plate (CP02/M), Right angle kinematic cage block (KCB1), 25.4 mm dia round mirror 3.2 mm Thick (ME-P01), Extension Rod 6 in (ER6)

Camera

- High-speed camera (FASTCAM-1024PCI, Photron, USA)
- IR cut filter: short pass Filter/IR 900 nm φ25 mm (Asahi Spectra, Japan)

## METHODS

! CAUTION: always use laser safety goggles when you use the optical tweezers. Never use the microscope oculars for direct viewing with the naked eye when the optical tweezers is in use.

**1. Place and adjust the laser collimator:**

↓ Place the optical ray,

↓ Set the height of the laser collimator at 10-15 cm above the optical bench.

↓ Place an adjustable diaphragm in the optical ray and close to the laser set the height is as same as the laser collimator.

↓ Move the diaphragm along the optical ray to ensure that the collimated beam runs parallel to the surface of the optical bench.

↓ Place mirror M2 in the optical ray. Adjust the direction of M2 by use the diaphragm.

**2. Control of the power**

↓ To control the power of the single-beam optical trap, insert a half wave plate (λ/2) in front of a rotation mount and a PBS after laser. Rotating the λ/2 wave plate will change the polarization direction of the linearly polarized input beam and thus result in a change in the relative power in each output arm of the PBS.

**3. Adjust lenses**

↓ Use two lenses (L1 and L2) to expand the laser beam.
*The beam is expand to overfill the back aperture of the object by around 10%.We use lenses L1 and L2 to form a beam expander that expander the collimated laser beam.

↓ For align the lenses, insert only L1 first, and observe the output laser (Fig. A-3 B)

↓ Insert L2 and put it f1+f2 distant from L1. Adjust the height and center of L2 by use a thin paper put on the top of objective. For more careful adjustment of L2, put a coverslip on the top objective. Adjust the focus of objective to make sure the coverslip is at focal plane. Observe the reflected laser light from CCD camera.

**4. Adjust the z-axial position**

↓ Adjust the z-axial position of an optical tweezers by move the L2 (Figure A-3).

*In my experiment, I want to focus on the rotation of magnetic bead at h = 0.2-0.4 μm from glass surface by using halogen lamp. The trapping position at h = 0.5 μm. We also need consider that different wavelength of light have different focal lengths due to the chromatic aberration of lens. So the adjustment is conducted by observe both beads stuck on glass surface and trapped bead.

**5. Imaging from high speed CCD camera**

↓ Put the IR cut filter in front of CCD camera.

↓ Set Olympus condenser at bright field mode. (No1 or No5)

↓ Set the camera gain = 8, gamma = 1

* This setup is for calibration of optical trap stiffness. The Maximum frame rate for observing 0.5μm bead is around 27000fps.

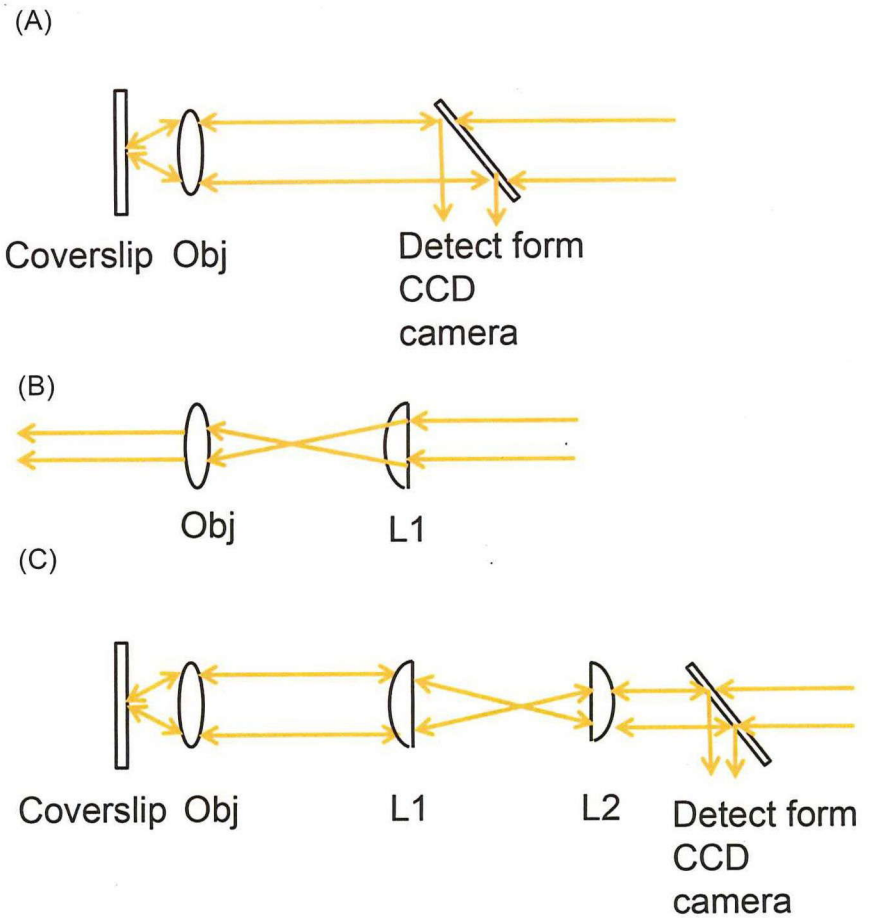


**Figure A-3** (A) Insert only Objective and adjust the optical ray B) Insert lens L1, adjust by observe the laser beam pass through objective lens. (C) Insert lens L2, adjust the position of L2 by observe the reflected laser light on CCD camera.

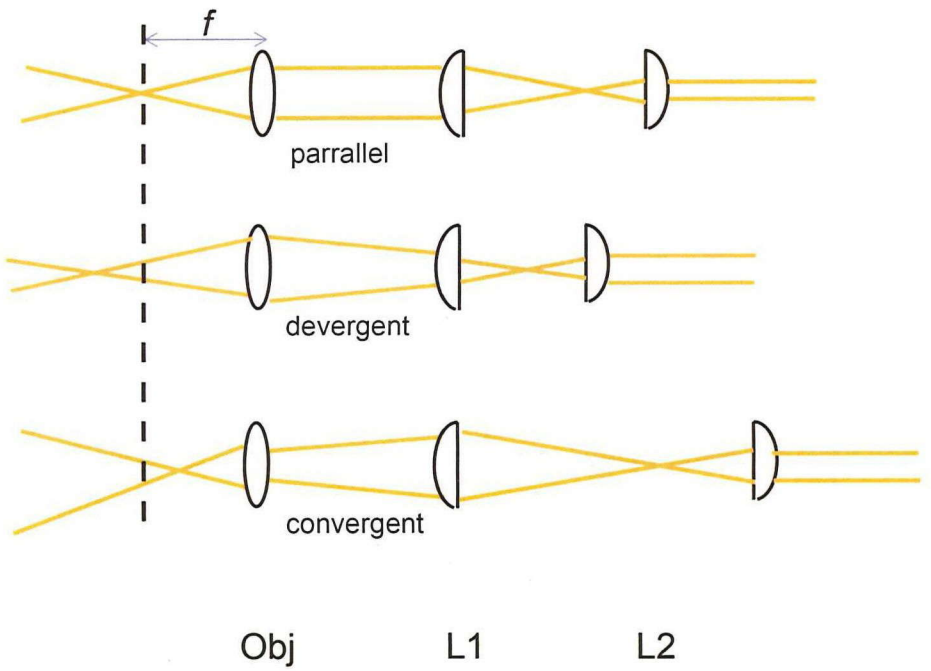


**Figure A- 4 Adjustment of the axial position of an optical tweezers by change L2 position.** Adjustment of the collimation of the input laser changes the position of the focus relative to the image plane (dashed line).

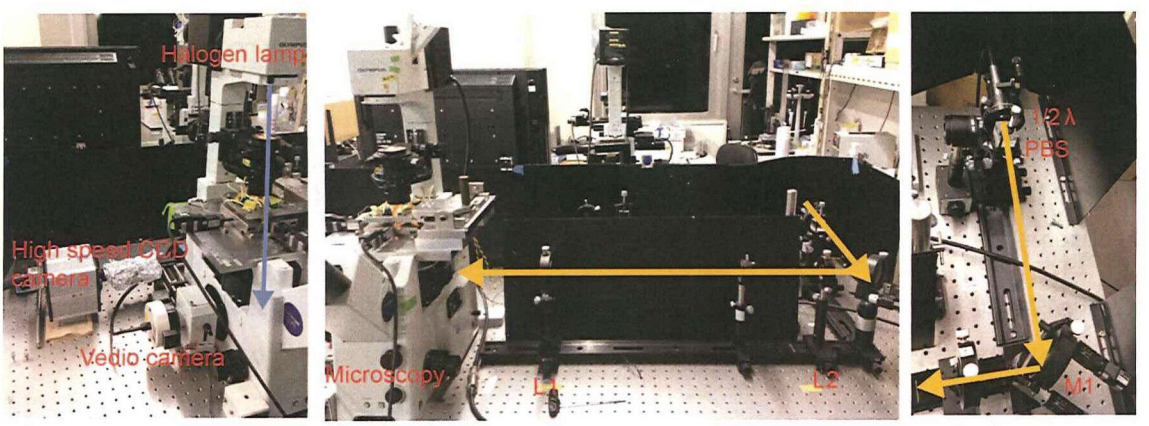


**Figure A- 5 Microscopy.** Diagram of optics was presented in Figure 2-5.

***-Protocol 10 Calibration of optical tweezers stiffness***

**1. Drag force methods (Stock's law)**

Viscous force $F = 6\pi\eta r v$

Stiffness $k = \frac{6\pi\eta r v}{\Delta x}$

If the beads are very close to glass surface, the drag force will increase by glass surface.

$$\beta = \frac{6\pi\eta r v}{1 - \frac{9}{16}\left(\frac{a}{h}\right) + \frac{1}{8}\left(\frac{a}{h}\right)^3 - \frac{45}{256}\left(\frac{a}{h}\right)^4 - \frac{1}{16}\left(\frac{a}{h}\right)^5}$$

, where r is beads radius, h is the distance from surface. From the h/a, β can calculated using Table A-1.

Table A-1 Drag on a sphere near a planar surface (Faxen's Law)

| (h/a) | β ($F_h'/F_0$) |
|---|---|
| 1.01 | 2.97 |
| 1.10 | 2.36 |
| 1.25 | 1.92 |
| 1.50 | 1.62 |
| 1.75 | 1.47 |
| 2 | 1.39 |
| 3 | 1.23 |
| 4 | 1.16 |
| 5 | 1.10 |
| 10 | 1.06 |
| 50 | 1.01 |
| ∞ | 1.00 |

*Variables: $h$, distance above surface of center of sphere; $a$, sphere radius. The drag on the sphere at $h = \infty$ is given by Stokes' Law, $\beta = 6\pi r a$.

*For 500nm diameter beads, move stage as speed 200um/s (the speed of stage measured by 10X lens or by stuck beads),

$F = 6\pi \times 10^{-3} Pas \times 0.25\ um \times 200\ um/s$ = 0.94 pN, Δx= 1.5 pixels = 126nm,

Thus, k = 0.007 pN/nm.

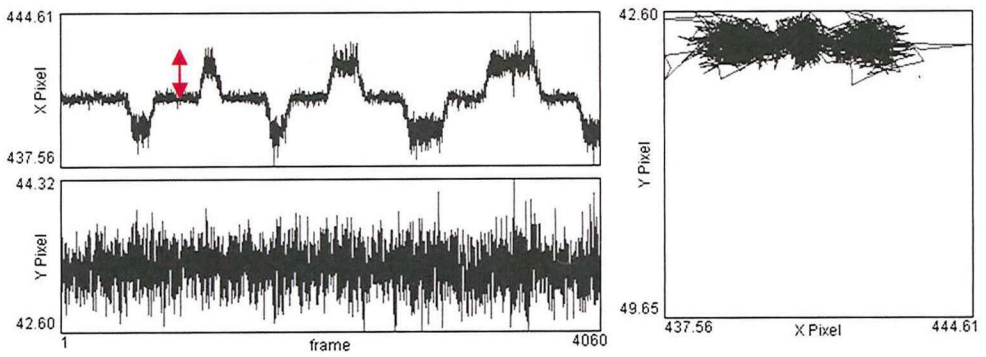


**Figure A- 6** Trajectory of trapped beads. Flow was applied by moving the stage. Red arrow showed the Δx. Data analyzed by Image J, centra3.

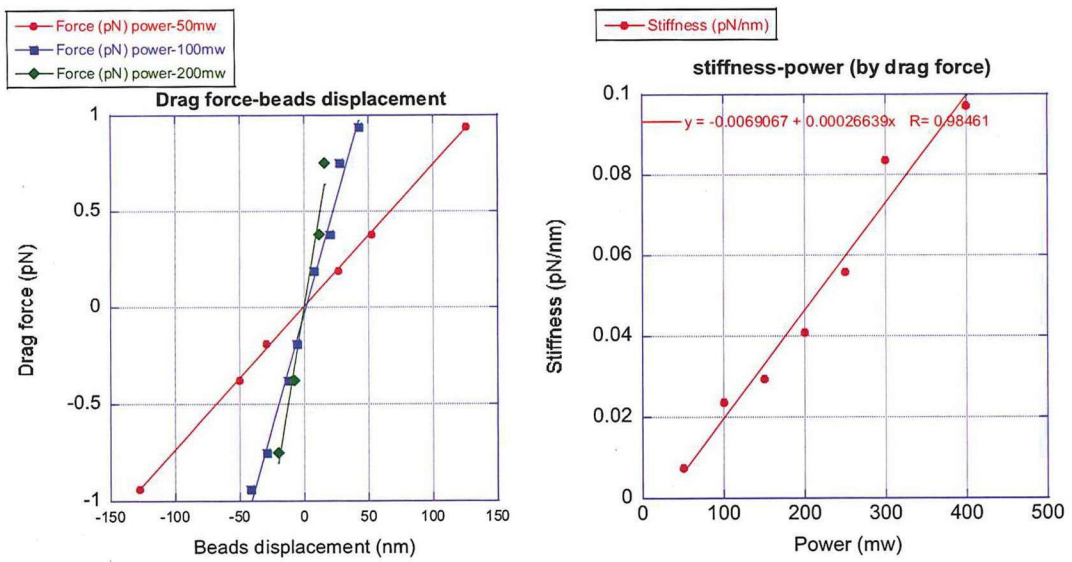


**Figure A- 7** (A). Stiffness measured by moving stage at different speed: 40 μm/sec, 80 μm/sec, 160 μm/sec, 200 μm/sec (B) Stiffness measured at different power. (50 mw, 100 mw, 200 mw results from fitting. 250 mw, 300 mw and 400 mw only measured by moving stage at 200 μm/sec)

## 2. Equipartition theorem methods

$$\frac{1}{2}k_BT = \frac{1}{2}k < x^2 > \quad (4)$$

At room temperature, $1k_BT = 4.14\,pN \cdot nm$, $k = 4.14\,pN \cdot nm/< x^2 >$

Here, $< x^2 >$ can be calculated from the trajectory of trapped bead (Fig.A-8). Use kaleidaGraph program, Statistics->Std deviation. When $\Delta x$ = 2 nm, stiffness $k$ = 1 pN/nm; $\Delta x$ = 6.4 nm, $k$ = 0.1 pN/nm; $\Delta x$ = 20 nm, $k$ = 0.01 pN/nm.

Table A-2 Spatial resolution of stuck beads.

| | | SD $x$ | SD $y$ |
|---|---|---|---|
| Ultrahigh speed camera | 1000 fps | 5.61 nm | 5.36 nm |
| High speed camera | 250 fps | 3.2 nm | 5.4 nm |
| | 400 fps | 4.0 nm | 5.7 nm |
| | 1000 fps | 3.8 nm | 8.6 nm |
| Normal camera | 30 fps | 2.8 nm | 3.4 nm |

**3. Measure form trap potential**

$$P(x) = \frac{1}{z}\exp\left(\frac{-U(x)}{k_B T}\right) = \frac{1}{z}\exp\left(\frac{-kx^2}{2k_B T}\right)$$

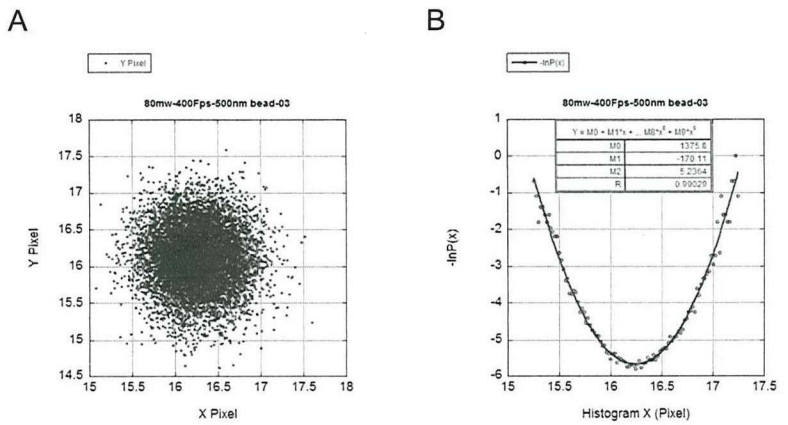


**Figure A- 8** (A) xy trajectory of a bead in the trap center. (B) x axis histogram of trapped bead

**4. Power spectrum methods**

$$\Phi(f) = \frac{\Phi(0)}{1 + (\frac{f}{fc})^2}$$

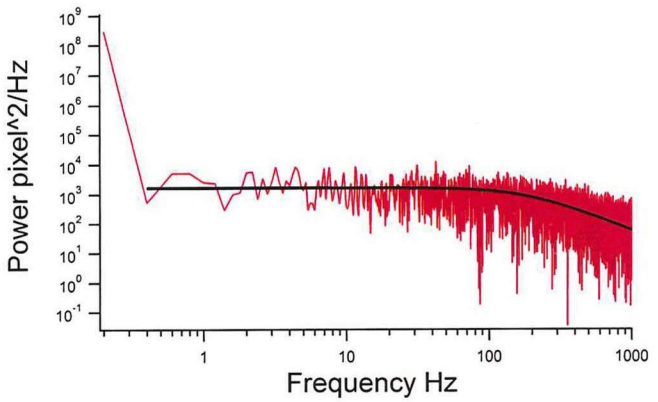


**Figure A- 9 power spectral of trapped beads.**

***- Protocol 11 Calibration of magnetic tweezers***

**MATERIALS**

- Gaussmeter Lakeshore 421 Probe : XMNT-1341
- BNC cable
- Power supply

**METHODS**

1. Calibrate the output voltage of PC and angle (Figure A-1.A).
2. Calibrate the output voltage of PC and PWR (Figure A-1.A).
3. Calibrate the magnetic flux versus angle using gaussmeter.

↓ Put gaussmeter probe on the top of objective lens (Figure A-1.B)

↓ Set the angle of magnetic tweezers using cerely program.

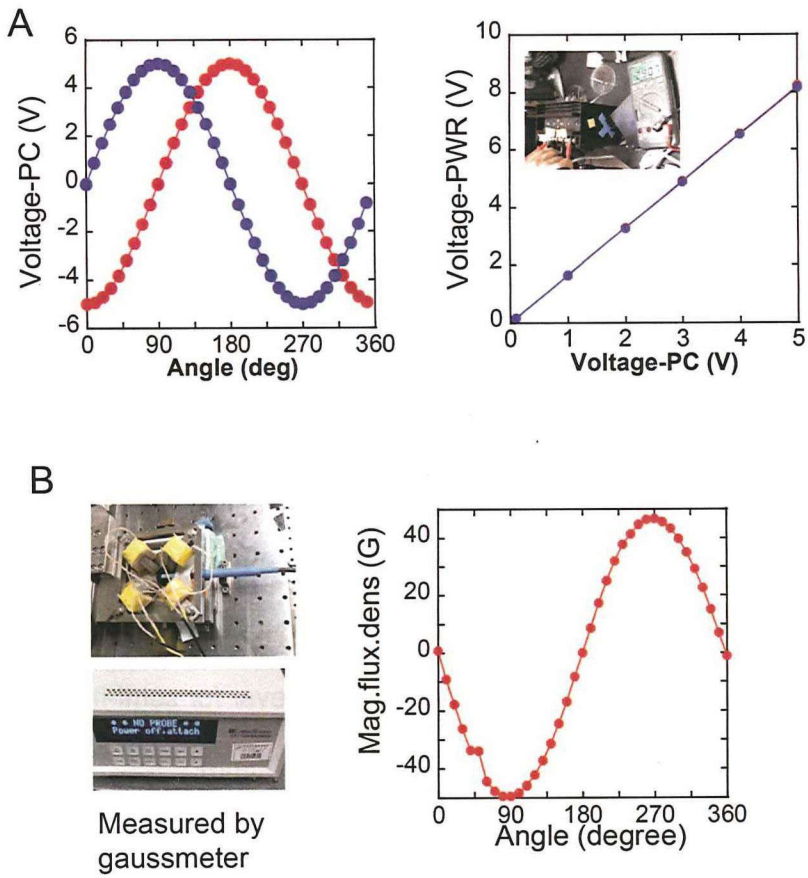


**Figure A- 10. (A) Calibration of the output voltage of PC and angle (left). Calibration of the output voltage of PC and PWR (right). (B) Calibrate the magnetic flux by gauss meter.**

# Appendix2: Derivations and calculations

## A.2.1 Freely jointed chain model

The freely jointed chain model (FJC model) is the first and the simplest mechanical model described the behavior of polymers (3-5). The FJC model treats the polymer as a chain composes of *n* statically independent segments with a fixed length. The segment length *b* called the Kuhn length is a parameter relates to DNA's flexibility. A significant conclusion in this model is that the mean-square end-to-end distance of the chain (variance of the end-to-end length) is proportional to the number of the independent segment $\langle R^2 \rangle = nb^2$. For flexible polymers, the Kuhn length is same order as chemical bonds, ~$\sqrt{2}a$, ($a$ is the length of chemical bond). However for semi-flexible polymer like DNA, the Kuhn length is hundreds base pair, around 100 nm.

**The force–extension relationship of FJC model**

The FJC model assumes that the elastic restoring force of the polymer results from the entropy change. Force (*F*) required for extending the chain to an averaged distance $\langle z \rangle$ is

$$\frac{\langle z \rangle}{L_0} = L\left(\frac{Fb}{k_B T}\right) \qquad \textbf{[25]}$$

, where *z* is the extension of polymer, *L*o is the counter length of polymer, and $L(\frac{Fb}{k_B T})$ is the **Langevin function**.

The equation [25] described the force-extension relationship of DNA measured in single-molecule stretching experiments(31) in the small forces regime (F < 0.08pN) with a good accuracy. In this regime, DNA act as a spring with an effective spring constant $\frac{3k_B T}{bL_0}$. However, the FJC model was failed at intermediate force range.

Deviations in intermediate force regime suggest that DNA has significant local curvature in solution.

Equation [25] can be derived as follow:

1. The potential energy of the free jointed chain is

$$U(\theta) = -Fb\cos\theta$$

2. The probability of finding a segment of the polymer making an angle between θ and θ+dθ is

$$p\,(\theta)d\theta = \frac{1}{Z}\exp\left(-\frac{U(\theta)}{k_{\mathrm{B}}T}\right)\sin\theta d\theta$$

, where $Z$ is the partition function

$$\mathrm{Z} = \int_0^{\pi} p\,(\theta)\cdot d\theta$$

3. $\langle\cos\theta\rangle$ can be calculated using the partition function

$$\langle\cos\theta\rangle = \langle\frac{z}{L_0}\rangle = \int_0^{\pi}\cos\theta\cdot p(\theta)\cdot d\theta = \frac{1}{Z}\int_0^{\pi}\cos\theta\cdot\exp\left(\frac{Fb}{k_{\mathrm{B}}T}\cos\theta\right)\sin\theta\cdot d\theta$$

$$= \frac{\int_{-1}^{1} y\exp(xy)\cdot dy}{\int_{-1}^{1}\exp(xy)\,dy} = \frac{e^{x}+e^{-x}}{e^{x}-e^{-x}} - \frac{1}{x} \equiv L(Fb/k_{\mathrm{B}}T)$$

, where $x \equiv \frac{Fb}{k_{\mathrm{B}}T}, y \equiv \cos\theta.$

This equation can be inverted to give:

$$F = \frac{k_{\mathrm{B}}T}{b}L^{-1}(\frac{\langle z\rangle}{L_0})$$

For small force, $\frac{e^x+e^{-x}}{e^x-e^{-x}} \approx \frac{1}{x}+\frac{x}{3}-\cdots$, so $L(Fb/k_BT) \cong Fb/3k_BT$,

$$F = \frac{3k_BT}{L_0 b}\langle z\rangle$$

For large force, $\frac{e^x+e^{-x}}{e^x-e^{-x}} \approx 1$, $\frac{\langle z\rangle}{L_0} = 1-\frac{1}{x}$, $F = \frac{k_BT}{b}\cdot\frac{1}{1-\frac{z}{L_0}}$, so $z \propto 1/F$.

**End to end distance**

The end-to-end distance of FJC obeys Gaussian statistics, so this FJC also called **Gaussian chain.** The probability density function is

$$P_n(R) = (\frac{3}{2\pi nl^2})^{\frac{3}{2}}\cdot \exp(-\frac{3R^2}{2nl^2})$$

The end-to end distance of free jointed chain at zero force is $\langle R^2\rangle = nb^2 = L_0 b$. In the WLC, the end to end distance is $\langle R^2\rangle = 2L_pL_0$. so $b = 2L_p$. These two parameters were both used for described DNA bending property.

**The relationship of WLC model and FJC model**

The WLC model can be considered as a modified FJC model in restricted condition. The persistence length $L_p$ is considered to be one half of the Kuhn length *b*. We assume a freely joined chain composed of *n* segment of lengths *b* with fixed bond angles *θ*. The end to end vector of the chain is ***R.***

Then the average of the projection of ***R*** to the first vector is

$$\langle \boldsymbol{R}\cdot\boldsymbol{t}_1\rangle = \frac{1}{b}\sum_1^{n-1}\langle \boldsymbol{t}_1\cdot\boldsymbol{t}_i\rangle \qquad \textbf{[26]}$$

For two vector, $\boldsymbol{t}_1$ and $\boldsymbol{t}_2$ is $\langle \boldsymbol{t}_1 \cdot \boldsymbol{t}_2 \rangle = b^2 \cos\theta$. Similarly to this, the average projections of each of the segment vectors on the first segment vector is $\langle \boldsymbol{t}_1 \cdot \boldsymbol{t}_i \rangle = b^2 (\cos\theta)^{i-1}$. Therefore, using the formula of geometric series, we have

$$\langle \boldsymbol{R} \cdot \boldsymbol{t}_1 \rangle = \frac{1 - (cos\theta)^n}{1 + cos\theta} \qquad \textbf{[27]}$$

Considering $n \to \infty, b \to 0$, and $\theta \to 0$, ($cos\theta$ approaches 1) and assuming the contour length of $L_0$ held as constant.

$$\lim_{n\to\infty} \langle \boldsymbol{R} \cdot \boldsymbol{t}_1 \rangle = \frac{b}{1 + cos\theta} = \frac{b}{2} = Lp \qquad \textbf{[28]}$$

The persistence length equals the average projection of the end-to-end vector on the tangent to the chain contour at a chain end in the limit of infinite chain length.

## A.2.2 Relationship between persistence length and bending stiffness

Derivation of the **equation [6]**:

Let $f(s) = \langle cos[\theta(s)] \rangle$

$$\frac{df}{ds}\Delta s \cong f(s + \Delta s) - f(s) = \langle \cos[\theta(s + \Delta s)] - \cos[\theta(s)] \rangle$$

$$= \langle \cos[\Delta\theta + \theta(s)] \rangle - \langle \cos[\theta(s)] \rangle$$

Where $\Delta\theta = \theta(s + \Delta s) - \theta(s)$

$$\frac{df}{ds}\Delta s \cong \langle \cos[\theta]\cos[\Delta\theta] - \sin\theta \sin[\Delta\theta] \rangle - \langle \cos[\theta] \rangle$$

$$= \langle \cos[\theta] \rangle \cdot \{ \langle \cos[\Delta\theta] \rangle - 1 \}$$

$$\frac{df}{ds} \cong \frac{\langle cos[\Delta\theta] - 1 \rangle}{\Delta s} f(s) \cong -\frac{1}{2}\left\langle \frac{\Delta\theta^2}{\Delta s} \right\rangle f(s) = -\frac{1}{2}\left\langle \left(\frac{\Delta\theta}{\Delta s}\right)^2 \Delta s \right\rangle f(s) = -\frac{\langle \Delta U \rangle}{EI} \cdot f(s)$$

Here, we used the **elastic energy calculated from beam equation** $\frac{dU}{ds} = \frac{1}{2} EI(\frac{d\theta}{ds})^2$, and **equipartition of energy** $\langle \Delta U \rangle = \kappa_B T$ (3D), thus

$$\frac{df}{ds} = -\frac{1}{2}\frac{k_B T}{EI} f(s)$$

Solving the differential equation give

$$\langle cos[\theta(s) - \theta(0)] \rangle = \exp(-\frac{k_B T s}{2EI})$$

Use the definition of $L_p$

$$\langle cos[\theta(s) - \theta(0)] \rangle = \exp(-\frac{L_p}{s})$$

$$L_p = \frac{EI}{k_B T} = \frac{\kappa}{k_B T}$$

## A.2.3 Force-extension curve calculated by WLC model

The Marko-siggia WLC model introduced in chapter 1.3.2 is the most common used form of the force-extension curve. Here we will introduce more detailed about the deviation of **equation [11]**.

$$F = (\frac{k_B T}{L_p})[\frac{1}{4\left(1 - \frac{z}{L_0}\right)^2} - \frac{1}{4} + \frac{z}{L_0}]$$

1. Potential energy of the chain in the absent of force is

$$U = \frac{1}{2}\kappa \int_0^L ds\, (\frac{d\theta}{ds})^2$$

2. Potential energy resulting from a force $F$ to the end of the molecular chain is

$$U = \int_0^L ds(\frac{\kappa}{2}(\frac{d\theta}{ds})^2 - F\cos\theta\,(s))$$

It is difficult to calculate the force-extension relation for the WLC chain analytically. The approximation formula was calculated as follow:

At low force, extension follows Hooke's law,

$$\langle \frac{z}{L_0} \rangle = \frac{FL_p}{k_B T}$$

At large force, $\langle z \rangle \approx L_0$

$$\langle \frac{z}{L_0} \rangle = 1 - 1/(\frac{4FL_p}{k_B T})^{1/2}$$

$z \propto 1/\sqrt{F}$ for WLC model at large force, this is different from FJC model. For the WLC, when DNA extension is close to the counter length of DNA, larger force required to extend the DNA.

$$\frac{FL_p}{k_B T} = \frac{1}{4\left(1 - \frac{z}{L_0}\right)^2}$$

Summarizing these results, an approximate interpolation formula was obtained for force-extension relationship.

$$\frac{FL_p}{k_B T} = \frac{1}{4\left(1 - \frac{z}{L_0}\right)^2} - \frac{1}{4} + \frac{z}{L_0}$$

### A.2.4 Elastic energy and restoring force calculated from the WLC model and SEC model.

In the classic WLC model, the energy required to bend a thin flexible rod into an arc of circle of diameter *D* is given by;

$$U_{\mathrm{WLC}}(\theta) = \frac{L_{\mathrm{p}} k_{\mathrm{B}} T}{2L} \theta^2 = \frac{2L_{\mathrm{p}} k_{\mathrm{B}} TL}{D^2}$$

, where $\theta$ is the bending angle, $L$ is the total length of wound dsDNA. $L_{\mathrm{p}}k_{\mathrm{B}}T$ is the bending stiffness, also called flexural rigidity. The elastic energy per unit length is $\frac{U_{\mathrm{WLC}}}{L} = \frac{2L_{\mathrm{p}}k_{\mathrm{B}}T}{D^2}$ . Wind a segment of length $\Delta L$ DNA against force $F$, the change of elastic energy is $\Delta U_{\mathrm{WLC}} = \Delta L \frac{2L_{\mathrm{p}}k_{\mathrm{B}}T}{D^2}$, the force applied on the DNA rod can be calculated as:

$$F = \frac{\Delta U_{\mathrm{WLC}}}{\Delta L} = \frac{2L_{\mathrm{p}} k_{\mathrm{B}} T}{D^2}$$

Therefore, $F$ is proportional to $D^{-2}$

In the LSEC model(49), the elastic energy $E$ is linearly proportional to the bending angle;

$$U_{\mathrm{LSEC}}(\theta) = \alpha|\theta| k_{\mathrm{B}} T = \alpha \frac{2L}{D} k_{\mathrm{B}} T$$

$$F = \frac{\Delta U_{\mathrm{LSEC}}}{\Delta L} = \frac{2\alpha k_{\mathrm{B}} T}{D} = \frac{\beta}{D}$$

, where $\alpha$ and $\beta$ are constant. Therefore, $F$ is proportional to $D^{-1}$.

## A 2.5 Torsional stiffness of DNA

In chapter 1.3.1, we mentioned about the torsional stiffness of DNA in cyclization experiment. The torsional stiffness of spring can be calculated with equipartition theorem:

$$\kappa_\theta = \frac{\kappa_{\mathrm{B}} T}{{\sigma_\theta}^2}$$

The torsional stiffness of dsDNA is related to its counter length:

$$\sigma_\theta{}^2 = \frac{Lc \cdot \kappa_B T}{C}$$

, where *Lc* is the counter length of DNA. C is the effective torsional persistence length. C has the unit of pN·nm$^2$.

$$\kappa_{\theta,\mathrm{DNA}} = \frac{C}{Lc}$$

## Appendix3: sequence of DNA used in winding experiments

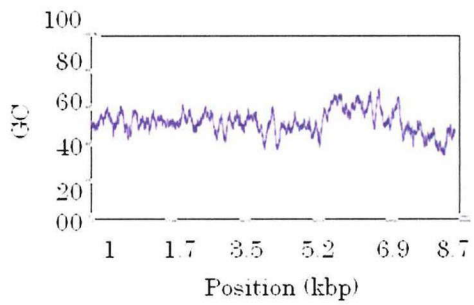


**The sequence in the wounded end:**

TTGGAGTCGGTCATTTCGTGGTAGAAGTCGTTACCCTCACGAGTACGTTCACCTA
CGCCCGCAAACACAGAGTAACCGGAGTGCTCGATCGCGATGTTACGAATGAGCT
CCATCATGTTTACGGTTTTACCTACACCCGCACCACCGAACAGACCAACTTTACCG
CCCTTAGCGAACGGACACATCAGGTCGATAACTTTGATACCGGTTTCCAGCAGTT
CCTGAGAGTTTGACAGCTCTTCGTAGGAAGGTGCTGCGCGGTGAATCGCCCAAC
GCTCTTCTTCACCGATCTCGCCTTTC

## List of publication

1 Huijuan You, Ryota Iino, Rikiya Watanabe, Hiroyuki Noji (2012). Winding single-molecule double-stranded DNA on a nanometer-sized reel. *Nucleic Acids Research*, 2012 doi: 10.1093/nar/gks651

## References


1. Watson, J.D. and Crick, F.H.C. (1953) Molecular Structure of Nucleic Acids - a Structure for Deoxyribose Nucleic Acid. *Nature*, **171**, 737-738.
2. Zahn, K. and Blattner, F.R. (1987) Direct Evidence for DNA Bending at the Lambda Replication Origin. *Science*, **236**, 416-422.
3. Howard, J. (2001) *Mechanics of motor proteins and the cytoskeleton*. Sinauer Associates, Publishers, Sunderland, Mass.
4. Mark, J.E. (2007) *Physical properties of polymers handbook*. Springer Verlag.
5. Yamakawa, H. (1971) *Modern theory of polymer solutions*. Electronic Edition. Harper & Row.
6. Kratky, O. and Porod, G. (1949) Röntgenuntersuchung gelöster fadenmoleküle. *Recueil des Travaux Chimiques des Pays-Bas*, **68**, 1106-1122.
7. Fixman, M. and Kovac, J. (1973) Polymer conformational statistics. III. Modified Gaussian models of stiff chains. *The Journal of Chemical Physics*, **58**, 1564.
8. Marko, J.F. and Siggia, E.D. (1995) Stretching DNA. *Macromolecules*, **28**, 8759-8770.
9. Bustamante, C., Marko, J.F., Siggia, E.D. and Smith, S. (1994) Entropic elasticity of lambda-phage DNA. *Science*, **265**, 1599-1600.
10. Hagerman, P.J. (1988) Flexibility of DNA. *Annu Rev Biophys Biophys Chem*, **17**, 265-286.
11. Jolly, D. and Eisenberg, H. (1976) Photon Correlation Spectroscopy, Total Intensity Light-Scattering with Laser Radiation, and Hydrodynamic Studies of a Well Fractionated DNA Sample. *Biopolymers*, **15**, 61-95.
12. Hays, J.B., Magar, M.E. and Zimm, B.H. (1969) Persistence Length of DNA. *Biopolymers*, **8**, 531-536.
13. Kovacic, R.T. and Vanholde, K.E. (1976) Transition from Rigid Rod to Stiff Coil Behavior - Conformation of Small Double Stranded DNA-Molecules in Solution. *Biophysical Journal*, **16**, A60-A60.
14. Hagerman, P.J. (1981) Investigation of the Flexibility of DNA Using Transient Electric Birefringence. *Biopolymers*, **20**, 1503-1535.
15. Frontali, C., Dore, E., Ferrauto, A., Gratton, E., Bettini, A., Pozzan, M.R. and Valdevit, E. (1979) Absolute Method for the Determination of the Persistence Length of Native DNA from Electron-Micrographs. *Biopolymers*, **18**, 1353-1373.
16. Bettini, A., Pozzan, M.R., Valdevit, E. and Frontali, C. (1980) Microscopic Persistence Length of Native DNA - Its Relation to Average Molecular Dimensions. *Biopolymers*, **19**, 1689-1694.

17. Rivetti, C., Guthold, M. and Bustamante, C. (1996) Scanning force microscopy of DNA deposited onto mica: equilibration versus kinetic trapping studied by statistical polymer chain analysis. *J Mol Biol*, **264**, 919-932.
18. Shore, D., Langowski, J. and Baldwin, R.L. (1981) DNA Flexibility Studied by Covalent Closure of Short Fragments into Circles. *Proc Natl Acad Sci U S A*, **78**, 4833-4837.
19. Kam, Z., Borochov, N. and Eisenberg, H. (1981) Dependence of Laser-Light Scattering of DNA on Nacl Concentration. *Biopolymers*, **20**, 2671-2690.
20. Wiggins, P.A., van der Heijden, T., Moreno-Herrero, F., Spakowitz, A., Phillips, R., Widom, J., Dekker, C. and Nelson, P.C. (2006) High flexibility of DNA on short length scales probed by atomic force microscopy. *Nat Nanotechnol*, **1**, 137-141.
21. Peters, J.P., Becker, N.A., Rueter, E.M., Bajzer, Z., Kahn, J.D. and Maher, L.J., 3rd. (2011) Quantitative methods for measuring DNA flexibility in vitro and in vivo. *Methods Enzymol*, **488**, 287-335.
22. Cloutier, T.E. and Widom, J. (2005) DNA twisting flexibility and the formation of sharply looped protein-DNA complexes. *Proc Natl Acad Sci U S A*, **102**, 3645-3650.
23. Shimada, J. and Yamakawa, H. (1984) Ring-Closure Probabilities for Twisted Wormlike Chains - Application to DNA. *Macromolecules*, **17**, 689-698.
24. Geggier, S. and Vologodskii, A. (2010) Sequence dependence of DNA bending rigidity. *Proc Natl Acad Sci U S A*, **107**, 15421-15426.
25. Shore, D. and Baldwin, R.L. (1983) Energetics of DNA Twisting .1. Relation between Twist and Cyclization Probability. *Journal of Molecular Biology*, **170**, 957-981.
26. Cloutier, T.E. and Widom, J. (2004) Spontaneous sharp bending of double-stranded DNA. *Mol Cell*, **14**, 355-362.
27. Du, Q., Smith, C., Shiffeldrim, N., Vologodskaia, M. and Vologodskii, A. (2005) Cyclization of short DNA fragments and bending fluctuations of the double helix. *Proc Natl Acad Sci U S A*, **102**, 5397-5402.
28. Bustamante, C., Smith, S.B., Liphardt, J. and Smith, D. (2000) Single-molecule studies of DNA mechanics. *Curr Opin Struct Biol*, **10**, 279-285.
29. Bustamante, C., Bryant, Z. and Smith, S.B. (2003) Ten years of tension: single-molecule DNA mechanics. *Nature*, **421**, 423-427.
30. Yanagida, M., Hiraoka, Y. and Katsura, I. (1983). Cold Spring Harbor Laboratory Press, Vol. 47, pp. 177-187.

31. Smith, S.B., Finzi, L. and Bustamante, C. (1992) Direct mechanical measurements of the elasticity of single DNA molecules by using magnetic beads. *Science*, **258**, 1122-1126.
32. Smith, S.B., Cui, Y.J. and Bustamante, C. (1996) Overstretching B-DNA: The elastic response of individual double-stranded and single-stranded DNA molecules. *Science*, **271**, 795-799.
33. Cluzel, P., Lebrun, A., Heller, C., Lavery, R., Viovy, J.L., Chatenay, D. and Caron, F. (1996) DNA: An extensible molecule. *Science*, **271**, 792-794.
34. Zlatanova, J., Lindsay, S.M. and Leuba, S.H. (2000) Single molecule force spectroscopy in biology using the atomic force microscope. *Prog Biophys Mol Bio*, **74**, 37-61.
35. Garcia, H.G., Grayson, P., Han, L., Inamdar, M., Kondev, J., Nelson, P.C., Phillips, R., Widom, J. and Wiggins, P.A. (2006) Biological consequences of tightly bent DNA: the other life of a macromolecular celebrity. *Biopolymers*, **85**, 115-130.
36. Luger, K., Mader, A.W., Richmond, R.K., Sargent, D.F. and Richmond, T.J. (1997) Crystal structure of the nucleosome core particle at 2.8 A resolution. *Nature*, **389**, 251-260.
37. Richmond, T.J. and Davey, C.A. (2003) The structure of DNA in the nucleosome core. *Nature*, **423**, 145-150.
38. Widom, J. (2001) Role of DNA sequence in nucleosome stability and dynamics. *Q Rev Biophys*, **34**, 269-324.
39. Jiang, W., Chang, J., Jakana, J., Weigele, P., King, J. and Chiu, W. (2006) Structure of epsilon15 bacteriophage reveals genome organization and DNA packaging/injection apparatus. *Nature*, **439**, 612-616.
40. Smith, D.E., Tans, S.J., Smith, S.B., Grimes, S., Anderson, D.L. and Bustamante, C. (2001) The bacteriophage straight phi29 portal motor can package DNA against a large internal force. *Nature*, **413**, 748-752.
41. Lia, G., Bensimon, D., Croquette, V., Allemand, J.F., Dunlap, D., Lewis, D.E., Adhya, S. and Finzi, L. (2003) Supercoiling and denaturation in Gal repressor/heat unstable nucleoid protein (HU)-mediated DNA looping. *Proc Natl Acad Sci U S A*, **100**, 11373-11377.
42. Seeman, N.C. (2003) DNA in a material world. *Nature*, **421**, 427-431.
43. Hamdi, M. and Ferreira, A. (2008) DNA nanorobotics. *Microelectron J*, **39**, 1051-1059.

44. Muscat, R.A., Bath, J. and Turberfield, A.J. (2011) A programmable molecular robot. *Nano Lett*, **11**, 982-987.
45. Zocchi, G. (2009) Controlling proteins through molecular springs. *Annu Rev Biophys*, **38**, 75-88.
46. Yan, J. and Marko, J.F. (2004) Localized single-stranded bubble mechanism for cyclization of short double helix DNA. *Phys Rev Lett*, **93**, 108108.
47. Wiggins, P.A., Phillips, R. and Nelson, P.C. (2005) Exact theory of kinkable elastic polymers. *Phys Rev E Stat Nonlin Soft Matter Phys*, **71**, 021909.
48. Browne, W.R. and Feringa, B.L. (2006) Making molecular machines work. *Nature Nanotechnology*, **1**, 25-35.
49. Wiggins, P.A. and Nelson, P.C. (2006) Generalized theory of semiflexible polymers. *Phys Rev E Stat Nonlin Soft Matter Phys*, **73**, 031906.
50. Bustamante, C., Chemla, Y.R., Forde, N.R. and Izhaky, D. (2004) Mechanical processes in biochemistry. *Annu Rev Biochem*, **73**, 705-748.
51. Shroff, H., Reinhard, B.M., Siu, M., Agarwal, H., Spakowitz, A. and Liphardt, J. (2005) Biocompatible force sensor with optical readout and dimensions of 6 nm3. *Nano Lett*, **5**, 1509-1514.
52. Shroff, H., Sivak, D., Siegel, J.J., McEvoy, A.L., Siu, M., Spakowitz, A., Geissler, P.L. and Liphardt, J. (2008) Optical measurement of mechanical forces inside short DNA loops. *Biophysical Journal*, **94**, 2179-2186.
53. Abrahams, J.P., Leslie, A.G., Lutter, R. and Walker, J.E. (1994) Structure at 2.8 A resolution of F1-ATPase from bovine heart mitochondria. *Nature*, **370**, 621-628.
54. Boyer, P.D. (1993) The binding change mechanism for ATP synthase--some probabilities and possibilities. *Biochim Biophys Acta*, **1140**, 215-250.
55. Noji, H., Yasuda, R., Yoshida, M. and Kinosita, K., Jr. (1997) Direct observation of the rotation of F1-ATPase. *Nature*, **386**, 299-302.
56. Hirono-Hara, Y., Ishizuka, K., Kinosita, K., Jr., Yoshida, M. and Noji, H. (2005) Activation of pausing F1 motor by external force. *Proc Natl Acad Sci U S A*, **102**, 4288-4293.
57. Rondelez, Y., Tresset, G., Nakashima, T., Kato-Yamada, Y., Fujita, H., Takeuchi, S. and Noji, H. (2005) Highly coupled ATP synthesis by F1-ATPase single molecules. *Nature*, **433**, 773-777.
58. Watanabe, R., Okuno, D., Sakakihara, S., Shimabukuro, K., Iino, R., Yoshida, M. and Noji, H. (2012) Mechanical modulation of catalytic power on F1-ATPase. *Nat Chem Biol*, **8**, 86-92.

59. Okuno, D., Iino, R. and Noji, H. (2010) Stiffness of gamma subunit of F(1)-ATPase. *Eur Biophys J*, **39**, 1589-1596.
60. Ashkin, A., Dziedzic, J.M., Bjorkholm, J.E. and Chu, S. (1986) Observation of a Single-Beam Gradient Force Optical Trap for Dielectric Particles. *Opt Lett*, **11**, 288-290.
61. Greenleaf, W.J., Woodside, M.T. and Block, S.M. (2007) High-resolution, single-molecule measurements of biomolecular motion. *Annu Rev Biophys Biomol Struct*, **36**, 171-190.
62. Moffitt, J.R., Chemla, Y.R., Smith, S.B. and Bustamante, C. (2008) Recent advances in optical tweezers. *Annu Rev Biochem*, **77**, 205-228.
63. Svoboda, K. and Block, S.M. (1994) Biological Applications of Optical Forces. *Annu Rev Bioph Biom*, **23**, 247-285.
64. Pierce, T.S. (2009), *Thermo Fisher Scientific, Rockford, IL, USA*.
65. O'Hare, H.M., Johnsson, K. and Gautier, A. (2007) Chemical probes shed light on protein function. *Curr Opin Struct Biol*, **17**, 488-494.
66. Bell, G.I. (1978) Models for the specific adhesion of cells to cells. *Science*, **200**, 618-627.
67. Merkel, R., Nassoy, P., Leung, A., Ritchie, K. and Evans, E. (1999) Energy landscapes of receptor-ligand bonds explored with dynamic force spectroscopy. *Nature*, **397**, 50-53.
68. Neuert, G., Albrecht, C., Pamir, E. and Gaub, H.E. (2006) Dynamic force spectroscopy of the digoxigenin-antibody complex. *FEBS letters*, **580**, 505-509.
69. Peneva, K., Mihov, G., Herrmann, A., Zarrabi, N., Borsch, M., Duncan, T.M. and Mullen, K. (2008) Exploiting the nitrilotriacetic acid moiety for biolabeling with ultrastable perylene dyes. *J Am Chem Soc*, **130**, 5398-+.
70. Kienberger, F., Kada, G., Gruber, H.J., Pastushenko, V.P., Riener, C., Trieb, M., Knaus, H.G., Schindler, H. and Hinterdorfer, P. (2000) Recognition Force Spectroscopy Studies of the NTA - His6 Bond. *Single Molecules*, **1**, 59-65.
71. Aggeler, R., Chicas-Cruz, K., Cai, S.X., Keana, J.F. and Capaldi, R.A. (1992) Introduction of reactive cysteine residues in the epsilon subunit of Escherichia coli F1 ATPase, modification of these sites with tetrafluorophenyl azide-maleimides, and examination of changes in the binding of the epsilon subunit when different nucleotides are in catalytic sites. *Biochemistry*, **31**, 2956-2961.

72. Cecconi, C., Shank, E.A., Bustamante, C. and Marqusee, S. (2005) Direct observation of the three-state folding of a single protein molecule. *Science*, **309**, 2057-2060.

73. Cecconi, C., Shank, E.A., Dahlquist, F.W., Marqusee, S. and Bustamante, C. (2008) Protein-DNA chimeras for single molecule mechanical folding studies with the optical tweezers. *Eur Biophys J Biophy*, **37**, 729-738.

74. Bouchiat, C., Wang, M.D., Allemand, J.F., Strick, T., Block, S.M. and Croquette, V. (1999) Estimating the persistence length of a worm-like chain molecule from force-extension measurements. *Biophysical Journal*, **76**, 409-413.

75. Wang, M.D., Yin, H., Landick, R., Gelles, J. and Block, S.M. (1997) Stretching DNA with optical tweezers. *Biophys J*, **72**, 1335-1346.

76. Ortiz, V. and de Pablo, J.J. (2011) Molecular origins of DNA flexibility: sequence effects on conformational and mechanical properties. *Phys Rev Lett*, **106**, 238107.

77. Segal, E., Fondufe-Mittendorf, Y., Chen, L.Y., Thastrom, A., Field, Y., Moore, I.K., Wang, J.P.Z. and Widom, J. (2006) A genomic code for nucleosome positioning. *Nature*, **442**, 772-778.

78. Visscher, K. and Block, S.M. (1998) Versatile optical traps with feedback control. *Molecular Motors and the Cytoskeleton, Pt B*, **298**, 460-489.

79. Parvin, J.D., McCormick, R.J., Sharp, P.A. and Fisher, D.E. (1995) Pre-bending of a promoter sequence enhances affinity for the TATA-binding factor. *Nature*, **373**, 724-727.

80. Matsui, T. and Yoshida, M. (1995) Expression of the wild-type and the Cys-/Trp-less alpha 3 beta 3 gamma complex of thermophilic F1-ATPase in Escherichia coli. *Biochim Biophys Acta*, **1231**, 139-146.

## Acknowledgements

My foremost thanks go to my adviser Dr. Hiroyuki Noji and Dr. Ryota Iino for their guidance in every aspect of my study. When I looked back to myself and the research I had done in the past six years, I noticed that Dr. Noji had so much patience with my growing up in research. He was always encouraging students to challenge authorities and generate new ideas even though in many instances they turned to be worthless. However, without those trials and errors, I would have never started the study of DNA, a completely new topic in Noji lab. This provided me a great opportunity to experience the most exciting parts of research: designing a new experiment and answering a valuable question. Dr. Iino taught me how to manage a project and support me a lot during my study. I gained a variety of knowledge and techniques from him, from microscopy to crosslink chemistry, from presentation skill to scientific writing.

I am also very grateful to my thesis's supervisor Dr. Masahiro Kino-oka for his encouragement and helpful advices.

This thesis could not have been completed without inspiring discussions and assistance from my colleagues. I must thank Dr. So Nishikawa for the support in LabVIEW program and construction of the force-constant feedback system. It was very enjoyable for me to work with him. To Dr. Rikiya Watanabe, I thank for his valuable comments and countless advices in experiments of $F_1$-ATPase. He demonstrated me the way of single-molecule experiment. Thanks also give to Dr. Kumiko Hayashi for advices in physics and optical tweezers. Her passion in science is always a huge inspiration to me.

To Ms.Yuko Ito, Ms.Rie Hasegawa and Dr. Hiromi Imamura, for the assistance in biochemistry and gene manipulation of $F_1$, and to Dr. Daichi Okuno, for helping me in

single-molecule rotation assay of $F_1$, To Dr. Sawako Enoki for assisting me in microscopy. To Ms. Naciye Esma Tirtom for studying the polymer mechanics together with me and helps with my writing. To Dr. Shoichi Sakakihara for consulting me about the physics of bending and other helps in experiments. And to Dr. Liza Lam, for her helps in the fluorescent imaging of DNA.

To all the current and former members of Noji lab: Kazuhito V. Tabata, Hiroshi Ueno, Masahiro Nakano, Liza Lam, SH Kim, Ikeda, Mizue Tanigawara, Yaginuma, Huynh Nhat Phuong Kim, Sintawee Sulaiman, Jotaro Ito. Thank you for the interesting scientific discussions and assistance in experiments. To Ms.Sakai and Ms.Ohta I present my thanks to them for their patient help with all the official procedures.

I also thank the valuable discussion with Dr Jie Yan, Dr. Maria Manosas about DNA flexibility and sequence dependence of DNA flexibility. I thank Dr. Fan Bai for interesting discussion and encouragement.

Thanks for the Ministry of Education, Culture, Sports, Science and Technology, Japan, for scholarship support.

Thanks all my friends in Osaka University and Tokyo University.

Finally, special thanks to my parents for supporting me through all these years.